Design and fatigue assessment of the hybrid monopile connection details using finite element analysis

M.J. Vogel

July 2018

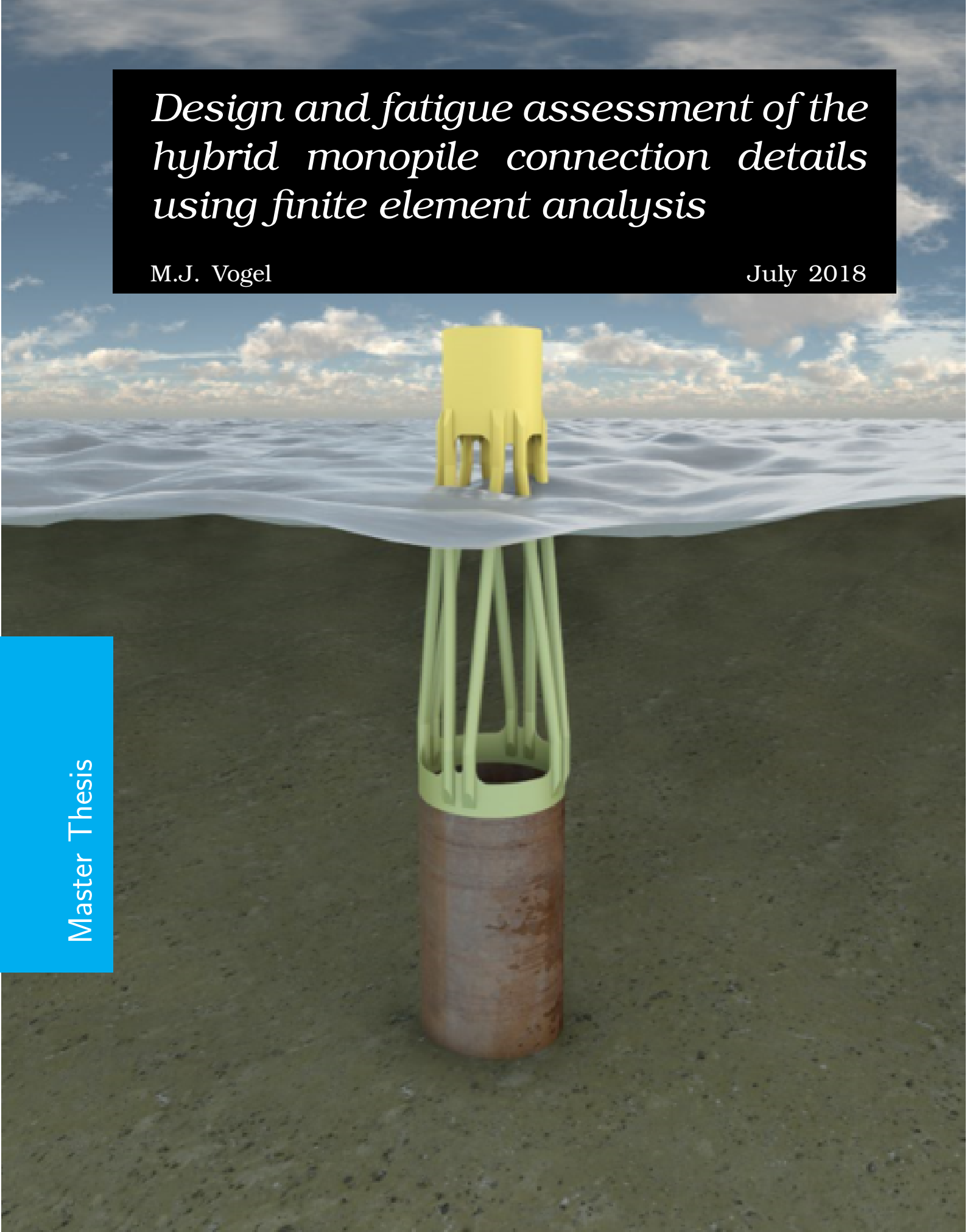

Master Thesis

TU Delft Delft University of Technology

FISTUCA

- This page has been intentionally left blank -

Design and fatigue assessment of the hybrid monopile connection details using finite element analysis

by

Maarten Jacob Vogel

in partial fulfillment of the requirements for the degree of

Master of Science

at the Delft University of Technology

Thesis committee:

Prof. Dr. M.V. Veljkovic	TU Delft – Chairman
Dr. F. Pisanò	TU Delft
Ir. P.C. Meijers	TU Delft
Ir. J.S. Winkes	Fistuca B.V.

Delft. 09 Jul, 2018

Abstract

As the offshore wind industry continues to develop larger turbines, and places them in deeper water, more problems arise with the traditional monopile or jacket support structure. The industry is thus more and more looking to alternatives for those existing methods. One such alternative, the "hybrid monopile", is currently being developed by Fistuca BV. The support structure concept consists of an open braced section situated between two monopile sections.

The advantages of the hybrid monopile with respect to load mitigation is that the open braced zone is in the area where the wave velocities are the largest. This results in a decrease in wave loading on the structure and therefore significant saving on the amount of wave loading and steel to a comparable monopile.

A critical part in the design of the hybrid monopile is the connection between the circular hollow profiles of the hybrid section and the monopile sections. The connection between those two parts should not undo the obtained advantages of the hybrid monopile. Therefore, the connections between those two sections should be relative simple to fabricate and the fatigue life of the connection should long enough. This thesis focuses on the design of the connection of the circular hollow profiles to the monopile.

First the wind and wave loading on the hybrid monopile are calculated. Thereafter several concept designs for the connection are created based on existing solutions. To verify the feasibility of the concepts the maximum Von Mises stress is calculated under the ultimate loading using ANSYS APDL. Then the concept designs are compared with each other and the best concept is selected. The final concept is studied in more detail under ultimate loading. With the design of offshore wind turbines, the dynamic behavior off the total structure is of significant importance. The natural frequencies of the concept design are calculated including the tower and turbine itself. Those natural frequencies should not be in the operating frequencies of the turbine.

Another significant aspect driving the design of offshore structures is the fatigue life of the structural details. To study the fatigue life of the connections in the hybrid monopile first the fatigue class has to be selected. The concept connection consists of several details with each a different class. For each detail the corresponding class is selected using the guidelines prescribed by the DNVGl. Thereafter a finite element analyses in ANSYS APDL is performed with a detailed mesh of the connection. The results of this calculation are exported to Matlab where the stress ranges of the fatigue details are calculated using the hot spot stress methodology. With these stress ranges and the calculated number of cycles during the design life of the structure the total damage and fatigue life is calculated. To reduce the amount of computational time the damage due to wind and wave loading are calculated using different methods. The total damage is then calculated using quadratic superposition of the damage equivalent stresses.

With the hot spot stress methodology, the way the welds are modeled is of significant influence on the stress range, therefore the influence of two methods for modeling the welds using finite element are compared with each other, and the most reliable is used in the final fatigue assessment.

The final result of this thesis is a detailed design of the connection between the circular hollow profiles and the monopile which is strong enough to withstand the ultimate load and has a sufficient design life.

Acknowledgements

I would like to thank some people without whom this project would not have been possible.

First of all I am grateful for the opportunity provided by Fistuca B.V. to work on this project at their office. Thanks to the entire team at Fistuca, even though they are working on completely different projects, for providing me with perspective, interesting ideas and great lunchtimes.

Thanks to my supervisor Jasper Winkes for his enthusiasm, support and guidance throughout the process.

Professor Veljkovic and Peter Meijers for serving as my supervisors from the TU Delft. Thank you for the advice and guidance in the right direction.

Colleague Graduates Koen Creusen, MC Anderson, Lena Bakaloni and most recently Pieter Slingerland with whom I have shared a table in the office, where many software-related frustrations were shared, problems were solved and new ideas came to light.

Finally I would like to thank my family, especially my parents, for there love and support throughout the last fifteen months.

Delft, 9 July 2018 *Maarten Vogel*

Contents

List of Figures

List of Tables

Nomenclature

List of symbols

D	Diameter
E	Youngs modules
t	Steel thickness
ν	Poisson ratio
ρ	Density

List of abbreviations

CHS	Circular Hollow Section
DES	Damage Equivalent Stress
DFF	Design Fatigue Factor
DNVGL	Det Norske Veritas
FLS	Fatigue Limit State
HS	Hot Spot
HSS	Hot Spot Stress
LSE	Linear surface extrapolation
MP	Monopile
PWT	Post weld treatment
SCF	Stress Concentration Factor
TP	Transition Piece
TS	Transition Section
ULS	Ultimate Limit State

Chapter 1: Introduction

1.1 Wind Industry trends

The offshore wind industry is still a relative young industry with the installation of the first offshore windfarm in Denmark in 1991. Since then the industry developed quickly resulting in a total installed capacity of 12,631 MW, from 3,589 grid-connected wind turbines in 10 countries, in the beginning of 2017[5]. With this growth the rated capacity of the wind turbines increased from 450 kW in 1991 to 8 MW in 2016.

Despite the high demand of offshore wind the industry is still dependent of subsidies to make the wind farms cost effective. This subsidies of the industry are caused by EU 2020 climate & energy package[6], which states the following items should be achieved by 2020:

- 20% cut in greenhouse gas emissions (from 1990 levels)
- 20% of EU energy from renewables
- 20% improvement in energy efficiency

This dependency on subsidies is the probably the biggest argument of further development of the offshore wind industry. Therefore DNVGL stated in a manifesto to make this industry cost competitive as soon as possible the cost of offshore wind should be reduced by at least 40% [7]. At least 16%, on average, of the CAPEX is used for the foundation [8], but this is likely to increase in deeper waters. Therefore as cost reduction of the installation of offshore wind turbine foundations is of importance for the reduction of the offshore wind energy costs.

1.2 Current foundation methods

1.2.1 Monopiles

The monopile foundation concept was introduced in the offshore wind park Lely(NL) in 1994. Since then, this substructure has been used for the majority of all projects and is therefore "proven technology". In the early days it was common thought that monopiles where only suitable up to 20-25 meter water dept. But as the industry developed monopiles where installed in up to 37 meter water depth with increasing weight and diameter of more than 800t and 6.5m diameter.

1.2.2 Jackets

Jackets are seen as an alternative to monopiles, especially for increasing water depths the jacket foundation seems to be more suitable. Due to the open braced structure the wave loading is smaller and therefor more suitable for deeper water. A drawback is that the jacket type foundation turned out to be quite expensive [4].

1.2.3 Floating

Floating solutions for offshore wind turbine are being investigated by several companies. Currently a few floating wind turbines are installed and connected to the grid[9], but these are mainly for research into the solution. Large scale floating wind farms are estimated to be at least a decade away [4].

1.3 Developments of monopile substructures

Over the years the offshore wind turbines are moving into deeper waters. Recent studies by Marc Seidel [4] show the importance of wave loading with the design of monopiles increases dramatically in deeper water. Ultimately, in deeper water, the design is dominated by dynamic wave loading. see figure 1.1. This increase in dominance of the wave loading on the design arises from the larger

moment, due the larger arm of the wave load at seabed level, and thus larger fatigue loads at the seabed level. From this problem the idea of the Hybrid monopile arised, by combining the benefits of both the monopile and the jacket this problem could be solved, see further explanation in the next section.

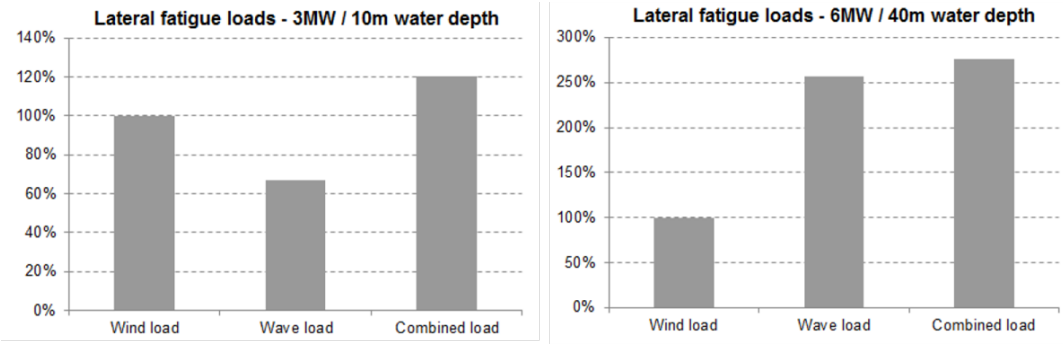

Figure 1.1: Relative importance of fatigue loading for monopiles by Marc Seidel[4]

1.4 Hybrid monopile

The hybrid monopile is a combination of monopile and jacket, hence the name. The philosophy of the design is to combine the advantages of a monopile with respect to fabrication, transport and installation with the advantages of a jacket structure, i.e. relative low wave and current induced loading pattern and no risk for ringing phenomenon. The open section around the water line ensures a decrease in wave loading compared to a similar monopile. Due to the monopile sections above and below the open section the installation is similar to that of a monopile. Therefore the installation can, for example, be done with a BLUE hammer[29].

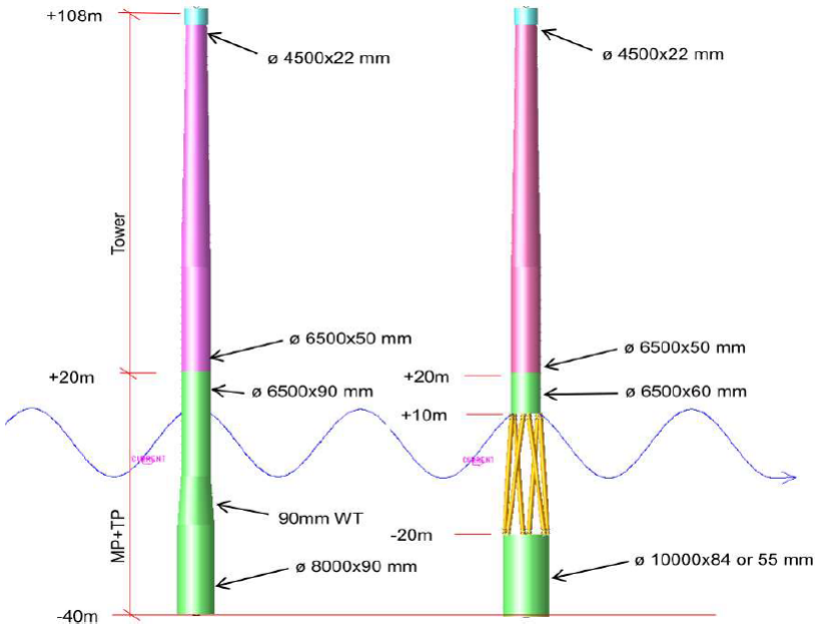

Figure 1.2: Monopile base case(left), and hybrid monopile(right)

1.4.1 Previous studies

Study by Enersea

The first idea for the hybrid monopile concept came forth from a back of the envelope sketch. A first concept feasibility study was done by Enersea[1] and showed promising results. A base case monopile was compared to a hybrid monopile with different configurations of the hybrid sections and shell thickness, see figure 1.2.

The main conclusion from this report are:

- Reduced stress in the base diameter. Furthermore, the hybrid monopile does attract less wave loading, especially for smaller fatigue waves. As a result, significant reduction of MP shell thickness below the hybrid section seems feasible. A shell thickness of 55 mm was checked for the Ultimate Limit State, further referred to as ULS, and Fatigue Limit State, further referred to as FLS, (wave fatigue only) and results were found acceptable.
- Because of the large diameter less embedment dept will be required to pass stability and stiffness limits.
- Configuration with tree times two vertical members is preferred because this result in a reasonable batter angle which has still the ability to transfer shear and torsion.
- A weight saving, compared to base case monopile, of 35% seems feasible.

Study Huisman Equipment

A more detailed concept feasibility study regarding the mechanical feasibility of the concept was done by Huisman, with the geometry and loading input from the Enersea report. Alterations with respect to the initial design are the added horizontal braces at the bottom of the hybrid sections, for maintaining the circular shape of the monopile section. The connection of the Circular Hollow Section, further referred to as CHS, profiles to the monopile section is through vertical shear welds. This requires a knot in the CHS profiles to create a straight connection. See figure 1.3 for a visualization of the initial design. Conclusions regarding this study where:

- Analysis of the ultimate limit state(ULS) showed promising result.
- Fatigue analysis regarding the CHS profiles connection welds to the monopile parts showed promising results.
- A boat landing resulting in a load of 35t at the middle of a brace will lead to extra stress. This should be added to normal operating conditions.

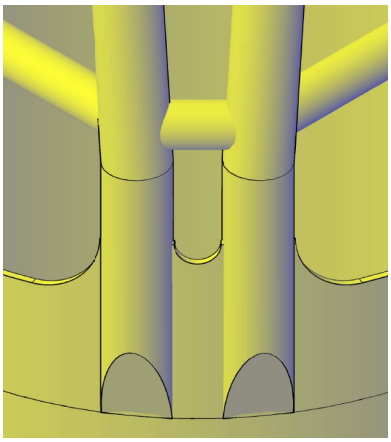

Figure 1.3: Visualization of the connection as designed by Huisman

Study Fistuca

Further study by Fistuca[3] optimized the design with respect to wind and wave loading, which resulted in a hybrid section height of 22 meter and a configuration with eight CHS profiles in the hybrid section. This study focused on the global design, thus the question remained if the structural details would be strong enough.

In figure 1.4 a sketch of the hybrid section of the foundation including the overall dimensions. The monopile sections above and below the hybrid part have an outer diameter of 6.5 meter and 10 meter and a thickness of 55 millimeter. The hybrid part of the foundation consist of four times two tubular members with an outer diameter of 0.85 meter and a thickness of 42 millimeter, the height of the hybrid section is 22 meter. These members are connected to two small MP sections of 100mm thick at the top and 90mm at the bottom.

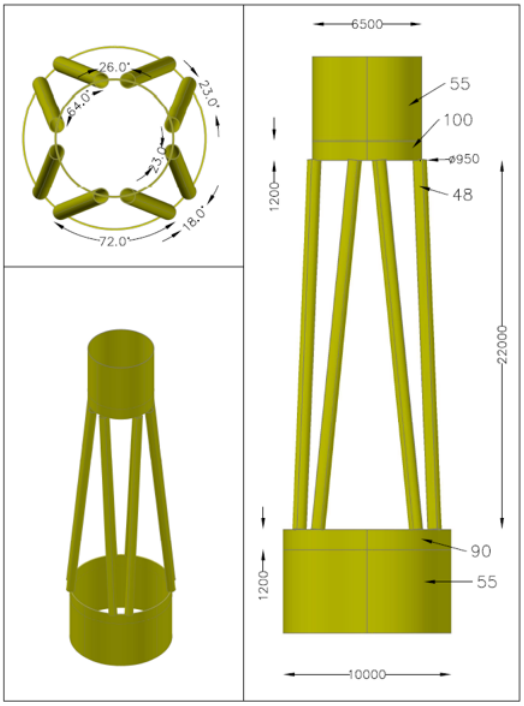

Figure 1.4: Sketch of the global design by Fistuca of the hybrid MP

1.5 Problem statement

Previous studies of the hybrid monopile already showed the feasibility of the global design. A critical part in the design of the hybrid monopile is the connection between the CHS profiles of the hybrid section to the monopile sections. The connection between those two parts should not undo the obtained advantages of the hybrid monopile. Therefore the connections between those two sections should be relative simple to fabricate and the fatigue life of the connection should long enough. Thus the focus of this thesis is on the two transition sections between the three overall sections, see figure 1.5.

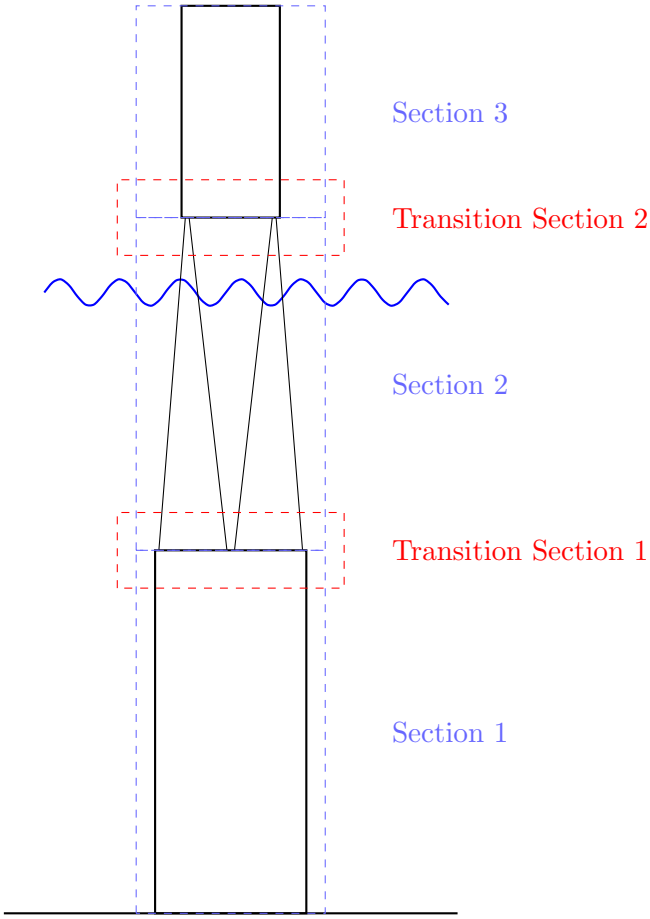

Figure 1.5: Optimization areas

In monopile foundation structures the largest stresses are located at the mudline, but with the hybrid monopile concept the largest stresses occur at the location of the CHS profiles. A simple calculation was carried out, by representing the hybrid MP as a cantiliver beam and only using the areas of the cross section and the distance to the center by appling the Steiner theorem. An ULS load from Anderson[3] was applied and the maximum stresses are calculated. The result is shown in figure 1.6, the largest stresses occur in the hybrid section and a shift in max stress at the transitions section.

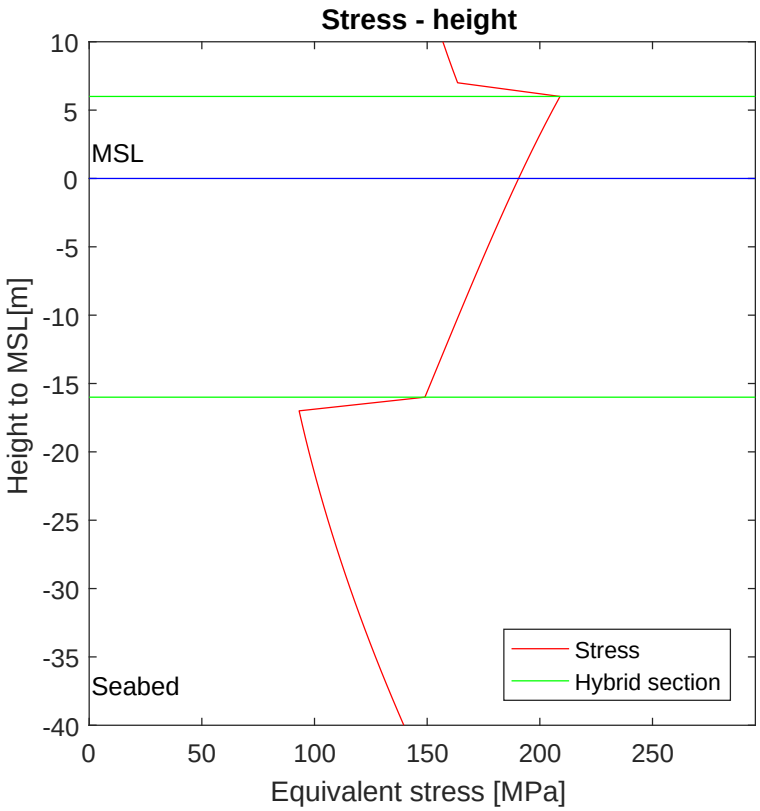

Figure 1.6: Stress in the hybrid monopile with ULS loading

So the main question of the thesis is: *"what does the connection between the CHS profiles and the MP section for a hybrid monopile substructure look like which is strong enough to withstand the ULS, SLS and FLS?"*

This question results in the following sub questions:

- What are possible concept designs of Transition section one and two for the hybrid monopile?
- Can the concept connection design withstand ULS loading?
- Regarding SLS, what is the influence of the connection design on the natural frequencies?
- How should the detailed connection be modeled so the HSS methodology can be used?
- What is the fatigue life of the concept connections?
- How is the fatigue stress range, and thus the fatigue life, influenced by the concept design parameters?

1.6 Approach

How will the questions addressed in previous section be answered? The starting point is the global configuration of the hybrid monopile[3] shown in figure 1.4 The following steps are executed, to answer these questions, shown in the flow chart below. In the calculations Finite Element Analysis, further referred to as FEA, is used.

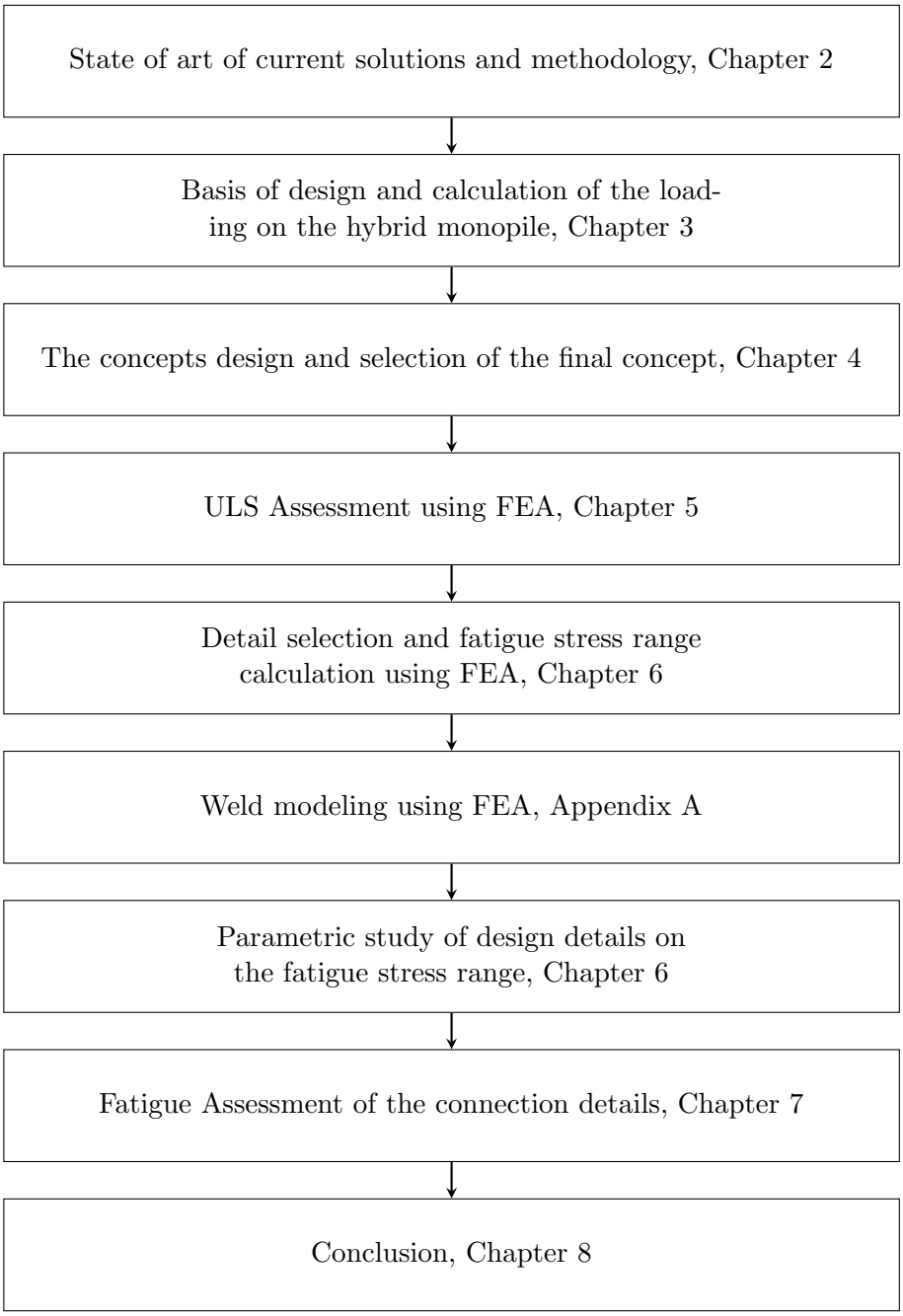

Figure 1.7: Flowchart approach

Chapter 2: State of art

In this chapter is looked into construction with similar properties to the hybrid MP. First looked into existing solutions for offshore substructures which have the same property that there is a transition between a large diameter section to smaller CHS profiles. Secondly the more detailed connection between a hollow profile and a steel plate. Thereafter the Hot Spot Stress, further referred to as HSS, methodology as provided by the DNVGL is explained and the program for the FEM is discussed.

2.1 Lattice structure to tower section

When an offshore wind turbine is founded on a jacket their has to be a construction from the jacket lattice structure to the tubular of the wind turbine. These construction, from 'small' diameter members to one large diameter pile, are somewhat similar to the hybrid monopile principle. In the past several of those jacket foundation with transitions are built. three of those: Block island, Baltic 2 and the Bremerhaven jacket are discussed below. with there main pros and cons regarding the hybrid MP.

2.1.1 Block island

First example is the Block Island Offshore Wind Farm (OWF) started operating early 2017. It is located off the coast of the U.S. state of Rhode Island and consists of six megawatt turbine in 23 meter of water. The four legs of the tower are connected to the tower support by large hollow beams. The four tubular beam transfer the forces onto the jacket legs.

Figure 2.1: Block island jacket

Benefits	Downsides
• Flexible width and angle of the connection between legs and tower due to the horizontal beams.	• Only four legs, thus higher loads at connection compared to hybrid MP. • Large amount of steel due to the beams.

2.1.2 Baltic 2

Baltic 2 is offshore wind farm of Germany in the Baltic Sea and started producing in September 2015. It has three point six megawatt turbine in water depth of 35 meter and above. The three legs of the jacket are directly connected to conical tower support structure. The forces are transfer directly from the conical section onto tower legs. Additional braces are connected to the conical section for increased torsional capacity. This concept could be suitable for the hybrid MP concept.

Figure 2.2: Baltic 2

Benefits	Downsides
• Conical tower section, thus straight slotted connection between tower and legs. • Separate construction of the connection and the jacket.	• Only three legs, thus higher loads at connection compared to hybrid MP. • Large amount of steel due to extra short diagonals at the connection. • Long overlapping length of the slotted legs

2.1.3 Bremerhaven jacket

This six megawatt wind turbine is located onshore in the Bremerhaven in Germany. The four legs of the jacket are directly connected to the conical section by slotting the members and welding. It is built onshore to prove concept of the connection between the jacket and the turbine tower.

Figure 2.3: Bremerhaven jacket

Benefits	Downsides
• Conical tower section, thus straight slotted connection between tower and legs. • Separate construction of the connection and the jacket.	• Only four legs, thus higher loads at connection compared to hybrid MP. • Long overlapping length of the slotted legs

2.2 Detail connection, CHS to plate

Main issue is the connection between the CHS profiles and the steel plate of the MP sections. There are several possibilities which can be used for the Hybrid MP connection detail, a few of those will be discussed in this section.

2.2.1 Directly welded, straight

The CHS is cut open, to create the required overlapping length, and welded to the plate material. Can also be done the other way around by cutting open the plate material and then weld the CHS to it.

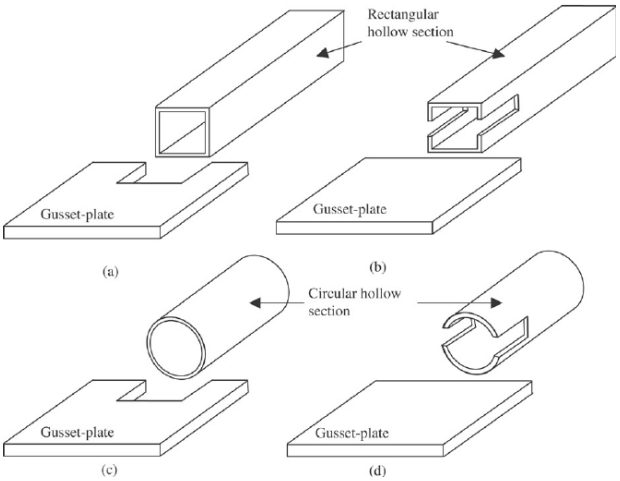

Figure 2.4: Directly welded, straight

Benefits	Downsides
• Direct connection between CHS and MP. • Weld length is easy to adjust.	• nod needed in main CHS or conical MP section to create straight connection

2.2.2 Directly welded, angle

No slot cut out in the CHS or the plate material. The CHS profile is welded, under a angle, directly to the plate material. The angle between the CHS profile and the plate material has to be at least 30 degrees[16] or guaranteed by a fabricator that a good quality weld can still be made.

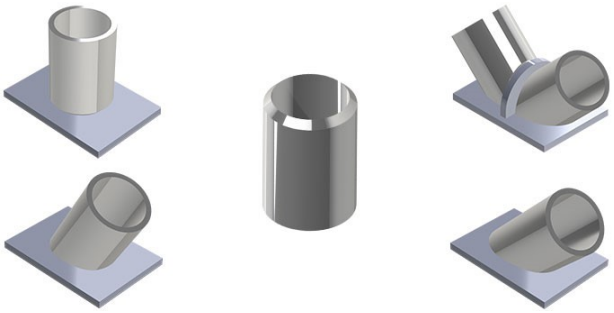

Figure 2.5: Directly welded, angle

Benefits	Downsides
• Direct connection between CHS and MP	• Minimum angle needed between MP section and CHS profile • not possible to increase weld length • difficult to implement in hybrid MP case

2.2.3 End plate

In this case at the the end of the CHS is a steel plate constructed which transfers the load from the member onto the gusset plate. stiffeners are added to provide enough stiffness for the gusset plate and to decrease the stresses in the welds between the gusset plate and endplate.

Figure 2.6: Endplate

Benefits	Downsides
• No nod needed in main CHS endplate could be under angle with MP section. • Relative easy to construct.	• Extra stiffeners needed after endplate. • Not possible to increase weld length. • Endplate in hybrid MP case has certain width and cannot be decreased due to CHS diameter.

2.3 Fatigue

2.3.1 S-N Curves

The behavior of a material under cyclic loading is characterized by the stress versus the cycle or a so called SN curve. Which is also known as a Wohler's curve. The relation between between the stress and cycle is exponential therefor the SN-curves are plotted on a logarithmic scale. SN curves are derived from experiments. Specimens are cyclic loaded under a stress range until failure, this results in an amount of cycle with a corresponding stress range. Doeing this for different stress ranges result in a graph like shown in figure 2.7

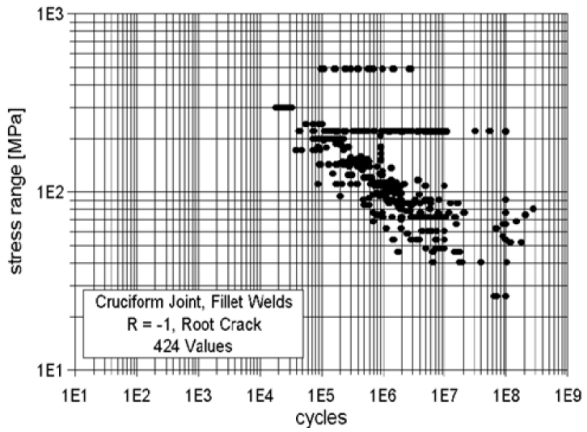

Figure 2.7: Expirimental fatigue data [28]

The large scattering in the data shows how complex the fatigue lifetime prediction is. The strength of the specimen depends on many effects. To use the data a curve is fitted to the data

with an assumed Gaussian log-normal distribution. The characteristic SN-curve represents a confidence level of 95% survival probability and is used as basis for fatigue assessment.

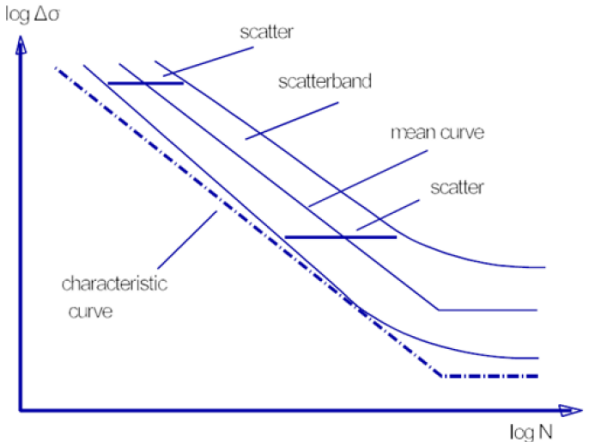

Figure 2.8: SN-curve statistics

The SN-curve used for fatigue assessments is modeled as shown in the equation below.

$$\log N = \log a - m \log \left(\Delta\sigma \left(\frac{t}{t_{ref}} \right)^k \right) \tag{2.1}$$

with

m	=	negative inverse slope of the S - N curve
$\log a$	=	intercept of log N axis
t_{ref}	=	reference thickness, 32 mm for tubular joints 25 mm for other welded connections.
t	=	thickness through which a crack will most likely grow
k	=	thickness exponent on fatigue strength

2.3.2 Hot Spot Stress

Due to welding discontinuity arise at the toe of the weld. It is likely that due to stress oscillations a fatigue cracks occur at the weld toe, see figure 2.9. To compute the stress at these locations, the so called Hot Spots, the HSS methodology is used. The stress is calculated using FEA, but due to the finite elements the computed stress at the weld toe has a non realistic peak. to compute a realistic geometric stress the stress is used at two measuring points. Those points are mostly at a distance of a half t and two-thirds of t from the hot spot. A straight line is drawn between the measuring points and extrapolated to the hot spot, this is the HSS visualized in figure 2.10.

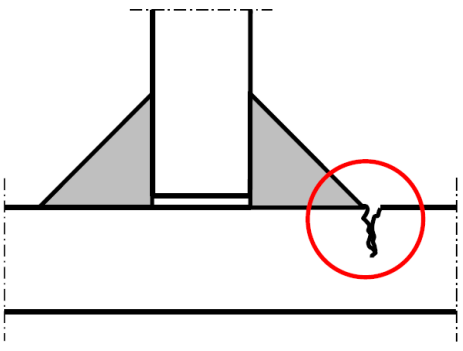

Figure 2.9: Fatigue crack at weld toe

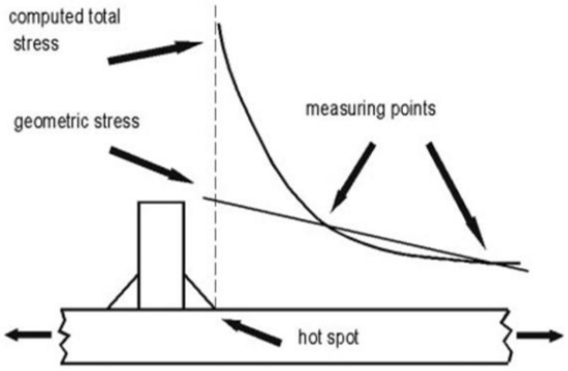

Figure 2.10: Hot Sport Stress methodology

For the connection between the various parts of CHS profiles, the HSS method is 'not used'. Instead the nominal stress with a Stress Concentration Factor (SCF) is used, further explained in chapter 6.

2.4 Guidelines

The hybrid monopile is an offshore structure, therefore the regulations of the DNV GL are used for the fatigue assessment. The DNV GL is an international accredited registration and classification society with there headquarters in Norway.

2.4.1 Stress

For the fatigue assessment the guidelines provided by the DNVGL is used. In the DNV GL[12] the effective hot spot stress range is calculated as follows.

$$\sigma_{eff} = max \begin{cases} \sqrt{\Delta\sigma_{\perp}^2 + 0.81\Delta\tau_{//}^2} \\ \alpha|\Delta\sigma_1| \\ \alpha|\Delta\sigma_2| \end{cases} \tag{2.2}$$

The stress ranges of σ_1, σ_2, $\sigma_\perp$ and $\tau_{//}$ are directly taken out of the FEA. The factor alpha is set to one. This equation 2.2 is used to account for the different directions of the fatigue crack.

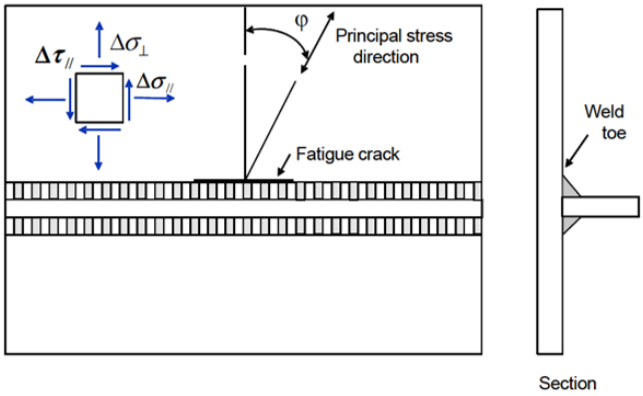

Figure 2.11: Fatigue cracking along weld toe [12]

2.5 ANSYS

The finite element method is used to find a numerical solution, in this case the software package ANSYS Mechanical APDL. This system offers many different element types and allows for parametric geometry design. Only two elements types are used. One for modeling the hybrid MP and one for loading introduction, More information about the elements used can be found in chapter 5.

The hybrid MP detail connection is a linear problem, therefore for most calculations in this thesis linear structural static analysis is executed. The two other analysis that are used are a buckling analysis, for the natural frequency calculation, and a modal analysis, for the natural frequency calculation.

Chapter 3: Basis of design and loading

This chapter discusses the basis of design for the transition sections and explains the methodology for calculation of the loading on the hybrid MP substructure.

3.1 Offshore wind turbines

Offshore wind turbines are complex multi-component systems in which the subsytems interact with each other and the loading environment, see figure 3.1. This makes the design of an offshore wind turbine rather complex. For a more detailed description and technical background of offshore wind turbines see reference [17].

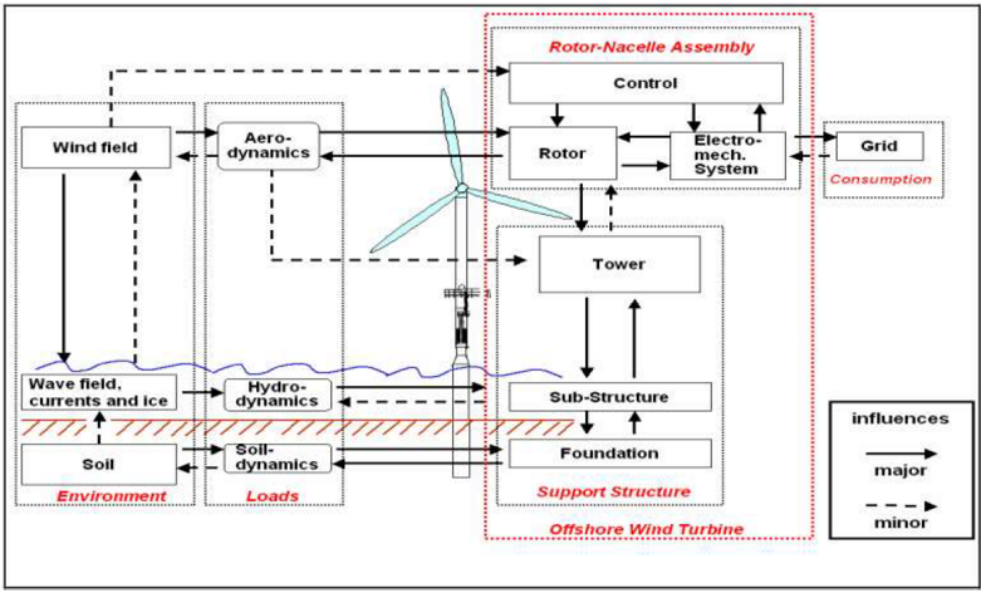

Figure 3.1: Offshore wind turbine components and their interactions [18]

The hybrid monopile consist out of the foundation and the sub-structure. The focus of this thesis is on the two transition sections of the hybrid monopile and therefore only the substructure part of the hybrid monopile are considered. The part below the seabed, the actual foundation, is therefore not taken into account in this thesis.

3.2 Reference Turbine

The hybrid monopile is more suitable for the larger diameter therefore the design is based on an eight MW turbine. The data for this turbine, see table 3.1, is based on a Vestas V164-8.0 MW model. The average life span of offshore wind turbines is 20-25 year. In this case it is assumed to be 25 years, plus 2 years of installation, thus the sub structure should at least have a designed life span of 27 years.

Table 3.1: Vestas wind turbine parameters [3]

Parameter	Value	Unit
Rated power	8.0	MW
Rotor diameter	164	m
Mass of rotor and nacelle	460	tonnes
Tower mass	375	tonnes
Cut-in wind speed	4.0	m/s
Cut-out wind speed	25.0	m/s
Lower bound rotor speed	5.4	rpm
Upper bound rotor speed	11.5	rpm
Nominal rotor speed	10.6	rpm
1P frequency range	0.09 - 0.192	Hz
3P frequency range	0.27 - 0.575	Hz
Nominal operating frequency	0.177 (1P), 0.530 (3P)	Hz

3.3 Location

For a potential location of the hybrid MP the North Sea is selected. Compared to standard monopiles the concept is better suited for the relative deeper waters and therefore water depth of 40 meters is chosen. This is also the water depth for offshore windturbine in the nearby future[9]. In table 3.2 the relevant heights for the hybrid monopile sub-structure. This date is based on North Sea conditions in the 40-meter water depth region, see figure 3.2.

Table 3.2: Relevant heights for the foundation [3]

Parameter	Value	Unit
Mean sea level(MSL)	40	m
Tower bottom	MSL + 20	m
Hub elevation	MSL + 108	m
Max 50-yr level (includes storm surge)	MSL + 2.5	m
Tidal range	+/- 1.25	m
Height hybrid section	22	m
Bottom hybrid section below MSL	16	m

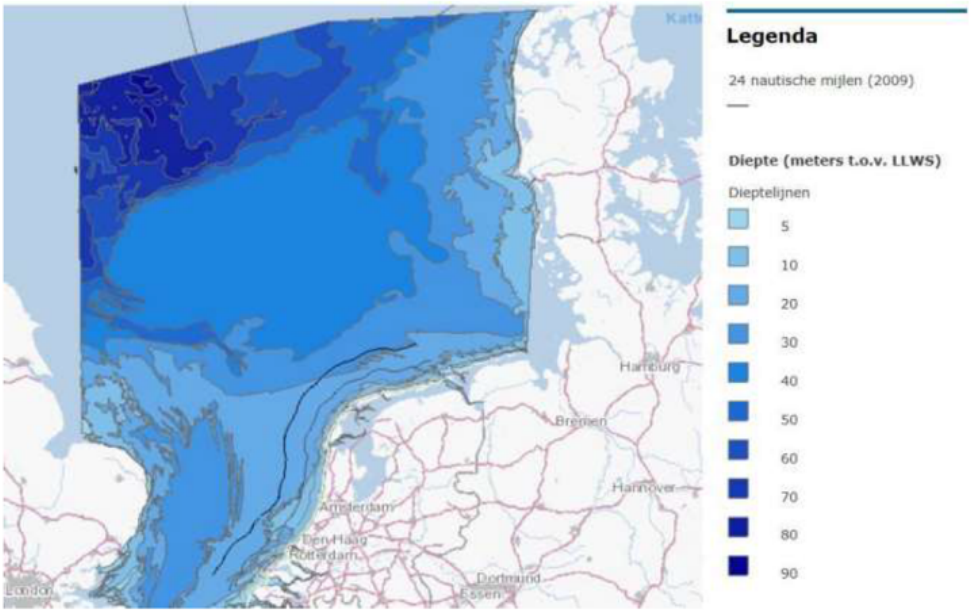

Figure 3.2: North Sea locations with 40 meter water depth []

3.4 Wave data

The wave data used in this project is provided by Enersea, table 3.3 shows the assumed sea state witch occurrences and their corresponding probability. This corresponds with the condition in the North sea at 40 meter water depth.

Table 3.3: Anticipated occurrences of each sea state over a 25-year turbine service life [1]

H_s [-]	T_0 [s]	n cycles (25 yrs.) [-]	Probability [-]
0.5	3.2	103050938	9.608E-02
1	4.3	59092332	5.510E-01
2	5.9	30269367	2.822E-01
3	6.9	5779211	5.388E-02
4	7.8	1326349	1.237E-02
5	8.6	345151	3.218E-03
6	9.2	96626	9.009E-04
7	9.8	28093	2.619E-04
8	10.3	8322	7.759E-05
9	10.8	2498	2.329E-05
10	11.2	762	7.105E-06
11	11.6	238	2.219E-06
12	12.0	76	7.086E-07
13	12.3	25	2.331E-07
14	12.6	8	7.459E-08
15	12.9	3	2.797E-08
16	13.2	1	9.324E-09
17 (ULS)	13.8	0.5	4.662E-09

Using this wave data of significant wave height and peak period wave spectra are calculated

for each seastate using the JONSWAP spectra. JONSWAP is used for not fully developed sea states, for locations close to shore this is often the case [13].

Using the significant wave height H_S and the corresponding peak period T_P the spectrum can be calculated using the following equations [19].

$$S_{JW}(f) = C(\gamma) \cdot 0.3125 \cdot H_s^2 \cdot fp^5 \cdot f^{-5} \cdot exp\Big(-\frac{5}{4} \cdot \big(\frac{f_p}{f}\big)^4 \Big) \cdot \gamma^{exp(\alpha)} \tag{3.1}$$

$$\alpha = \frac{(f - f_p)^2}{2 \cdot \sigma^2 \cdot fp^2} \tag{3.2}$$

$$C(\gamma) = 1 - 0.287 \cdot ln(\gamma) \tag{3.3}$$

$$\sigma = \begin{cases} 0.07 & for f \leq f_p \\ 0.09 & for f > f_p \end{cases} \tag{3.4}$$

with

S	Spectrum	[m^{2}s]
γ	Peak enhancement factor	[-]
H_s	Significant wave height	[m]
f_p	Wave peak frequency	[Hz]
f	Frequency	[Hz]
$C(\gamma)$	Normalizing factor	[-]
σ	Spectral width parameter	[-]

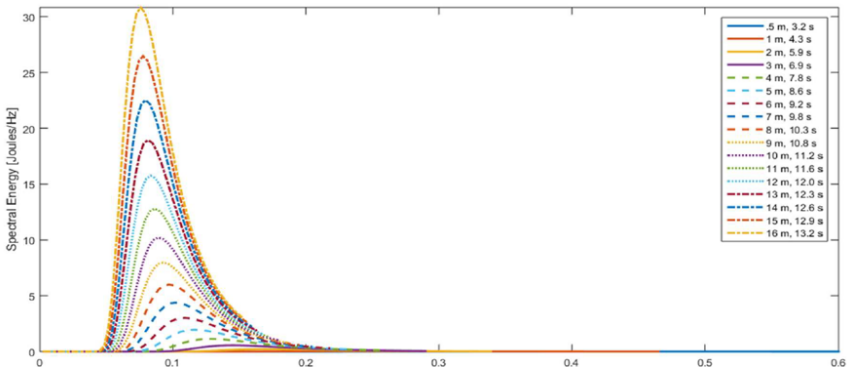

Figure 3.3: JONSWAP spectrum for all the seastates. [18]

From these spectra the wave loading is calculated in either the frequency domain or the time domain. In figure 3.4 a time series produced from a wave spectra with a significant wave height of four meters. These irregular waves are computed by superimposing the individual components of the spectra.

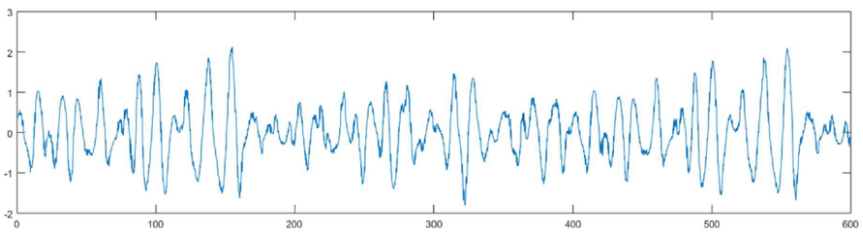

Figure 3.4: The wave height in the time domain for seastate five [18]

Although not all waves fall in the linear/Airy wave theory, larger waves fall in Stokes' 5^{th} order equations, the different in resulting loading on the hybrid monopile was of such small extent that the hydrodynamic loading calculation where only executed with the Airy wave theory[3].

3.5 Breaking waves

Braking waves are not considered. Because, even the largest waves, are well below the wave breaking criteria. [3]. This breaking criteria is 0.78 times the water depth.

3.6 Current

Tidal current is taken as 1.4 m/s at the still water line and decays with depth with a power law function. The current loads on the structure are included in the ULS analysis, but not in the FLS assessment. The time period is (n) times larger than that of the wind and waves[13]. In this power law function h is the water depth and z the negative elevation from the still water surface.

$$U_c(z) = 1.0 * (\frac{h+z}{h})^{\frac{1}{7}} \tag{3.5}$$

3.7 Wind profile

Logarithmic scaling of wind measurements is used to compute the actual wind speed at the hub height of a wind turbine. This results in a logarithmic wind profile of wind speed. These wind measurements correspond to eighteen seastates.

$$V_{hub} = V_{10} \frac{\ln(\frac{10}{z_0})}{\ln(\frac{h_{hub}}{z_0})} \tag{3.6}$$

z_0 represents the surface roughness length, taken as .002 for an offshore environment Germanischer Lloyd [20]. V_{10} indicates the height above the earths surface at which the wind speed measurement is taken, in this case at 10 meters.

In reality a wind profile is never constant and always contains turbulence. The turbulence intensity is a function of the local wind speed and its standard deviation:

$$I_t = \frac{\sigma_{V_w}}{V_w} \tag{3.7}$$

A intensity is of 15% is used [3].

The turbulent wind is approximated with the Kaimal spectrum, see the following formula. In figure 3.5 the theoretical spectrum, the black line is compared to a Fourier transform of time history wind data. This figure shows that direct transformation of the wind data is difficult to use with loading calculations, due to the fact that small changes in the steps can change the resulting signal significantly. Therefore for wind induced fatigue calculations the Kaimal spectrum is used.

$$S_{Kaimal}(f) = \frac{\sigma^2_{V_w} 4 \frac{L_v}{V_w}}{\left(1 + 6 f_v \frac{L_v}{V_w}\right)^{\frac{5}{3}}} \tag{3.8}$$

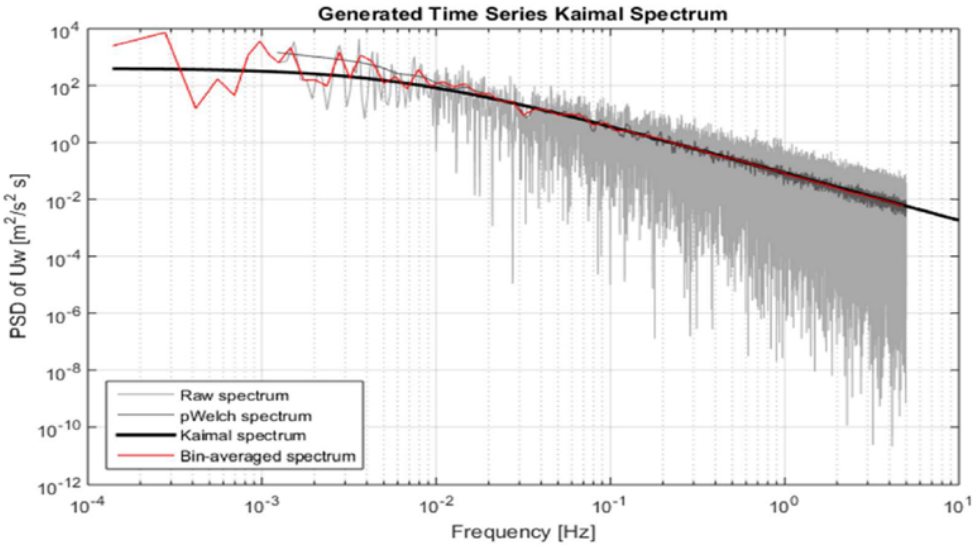

Figure 3.5: Kaimal spectrum

For each sea state, a time series of turbulent wind speeds is generated from the Kaimal spectrum, for more details sea reference [21]. The figure below shows a turbulence wind time series.

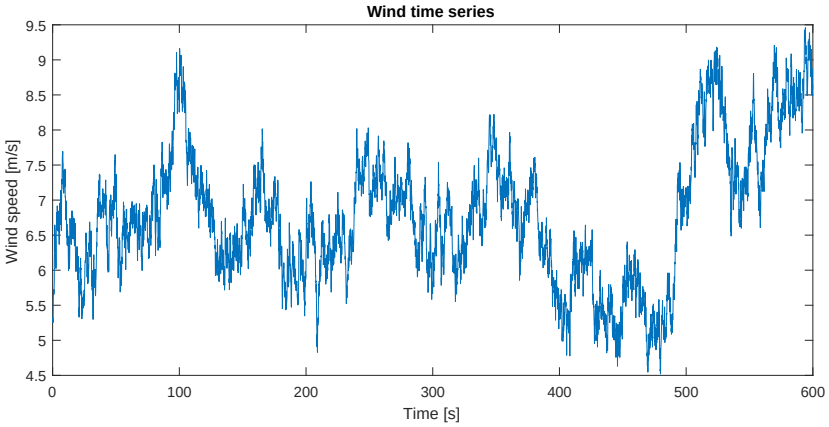

Figure 3.6: Wind time series from Kaimal spectrum

3.8 Loading General

The two most important loads on offshore windturbines are the wind hydrodynamic loading from the current and the waves, and the aerodynamic loading from wind acting on the turbine. Those will be discusses further on in the chapter. To keep an overview over the orientation the individual CHS profiles they are numbered from one to eight like shown in figure 3.7

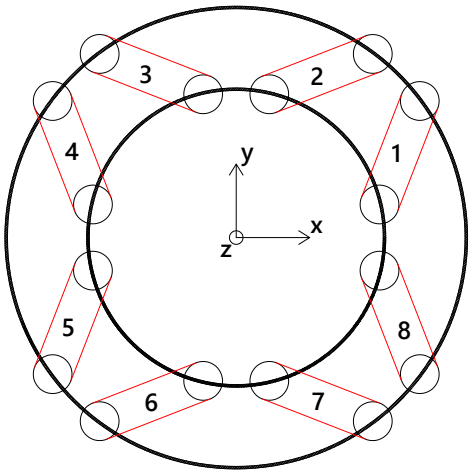

Figure 3.7: CHS profiles numbering

3.9 Hydrodynamic loading

The Hydrodynamic loading on the structure consists of the current loading and the wave loading. For the fatigue assessment only the wave loading is used, the current is assumed to be constant.

3.9.1 Morison equation

For each wave the water particle velocity and acceleration are described by the following linear wave theory equations.

$$u_w(x,z;t) = \alpha\omega \frac{\cosh\big(k(z+d)\big)}{\sinh(kd)} \cos(kx - \omega t + \phi) \tag{3.9}$$

$$\dot{u}_w(x,z;t) = \alpha\omega^2 \frac{\cosh\big(k(z+d)\big)}{\sinh(kd)} \cos(kx - \omega t + \phi) \tag{3.10}$$

with

α	Wave amplitude, (Height/2)	[m]
ω	Wave frequency	[rad]
k	Wave number	[1/m]
z	Height in water column, negative downwards	[m]
d	Water column height	[m]
ϕ	Phase angle	[rad]

These equations only exists until the still water line, therefore Wheeler stretching is applied to model the wave particle kinematics above the still water line.

The Morison equation, for forces exerted on vertical cylinders by waves, is used to calculate the hydrodynamic forces from the wave particle velocity and acceleration. [22]

$$f_M = C_d \frac{1}{2}\rho_w D|u(x,z;t)|u(x,z,t) + C_m \frac{1}{4}\rho_w \pi D^2 \dot{u}(x,z;t) \tag{3.11}$$

The inertia coefficient will be dominating in the loading calculations, therefore it is important to select the right inertia coefficient. The Morison equations are meant for loading calculation on slender structures, this means that the pile diameter should be less than one fifth of the wavelength of the forcing wave. If this is not the case diffraction theory should be used as introduced by MacCamy & Fuchs [23]. The Morison equations can still be used by implementing the MacCamy

& Fuchs theory as a correction on the inertia coefficient C_m. The function for the correction curve equation is showed below.

$$C_m(Z) = -2.5 \cdot \frac{D(z)}{\lambda_0} + 7.53 \cdot \frac{D(z)}{\lambda_0} - 7.9 \cdot \frac{D(z)}{\lambda_0} + 3.2 < 0 \tag{3.12}$$

3.9.2 Shielding factor

In the hybrid section the frontal surface of the CHS profiles depends on the wave loading angle. To correct for this change in frontal surface a shielding factor is used. Created by dividing the frontal diameter by the sum of the total diameter, equation 3.13, and is always lower than one. This factor is applied to the total diameter but is a simplification of the actual wave loading.

$$C_{shield} = \frac{\sum D_{frontal}}{8D} \tag{3.13}$$

The actual wave loading depends on wave length and the spacing between the profiles and can differ relative much from this simplification. This is especially interesting for the fatigue assessment. The waves travel around the profiles up front and thus still apply load in the profiles behind, this depends on the amount of spacing between the profiles. This probably results in a higher wave loading in large waves and a lower wave loading in smaller waves than modeled with the factor. This effect is not taken into account in this thesis because modeling the wave loading this way is rather complex.

3.10 Aerodynamic loading

The wind time series, figure 3.6, is used to calculate the wind loading on the turbine using the following equation. Above a certain wind speed, the cut out wind speed, the pitch controllers feather the blades to let the wind flow past them and the rotor hub is braked. In this way the max wind load is controlled.

$$F = \frac{1}{2} C_t A_{rotor} \rho_{air} V_w^2 \tag{3.14}$$

All wind load is to be assumed fully aligned with the rotor. In figure 3.8 the cut out wind speed is clearly seen in seastate 15 for the windloading is reaching a plateau level.

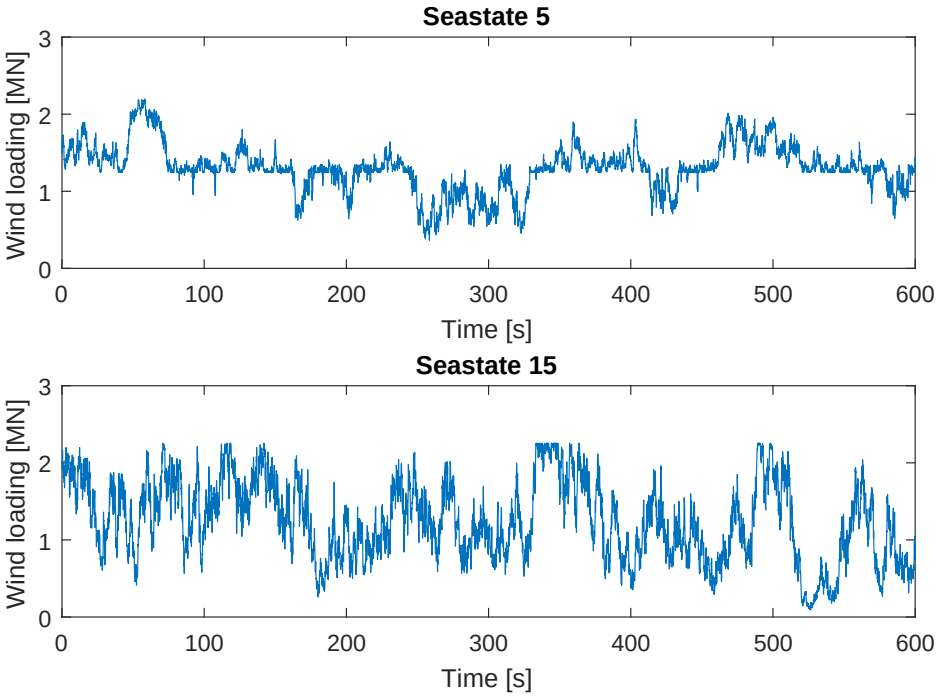

Figure 3.8: Times series of the hub wind load

3.11 Load cases

3.11.1 ULS loading

In the tables below the possible load cases according DNV GL[13] are shown. The values corresponding to these load cases are shown in table 3.5.

Table 3.4: Load combination ULS

Load	Water level	Wind	Waves	Current
1	50-year	50-year	5-year	5-year
2	50-year	5-year	50-year	5-year
3	50-year	cut out	5-year	5-year

The corresponding values are

Table 3.5: ULS values

Load	Water level [m]	Wind [m/s]	Waves [m]	Current [m/s]
1	42.5	36	5-year	5-year
2	42.5	28	50-year	5-year
3	42.5	24	5-year	5-year

From previous studies [3] it is known that load case one is the governing case. This load case will thus be used in the ULS assessment.

Angle

Which loading direction results in the highest member loads/stress. A simple hand calculation was carried out to calculate the stress in the members versus the loading direction, like explained in section 1.5. Figure 3.9 shows the results at transition section one and two for the first four members. the highest loading occurs at transition section one at an angle of 37 degrees and at transition section two at 14 degrees. Those loading directions should therefor be considered in the ULS check.

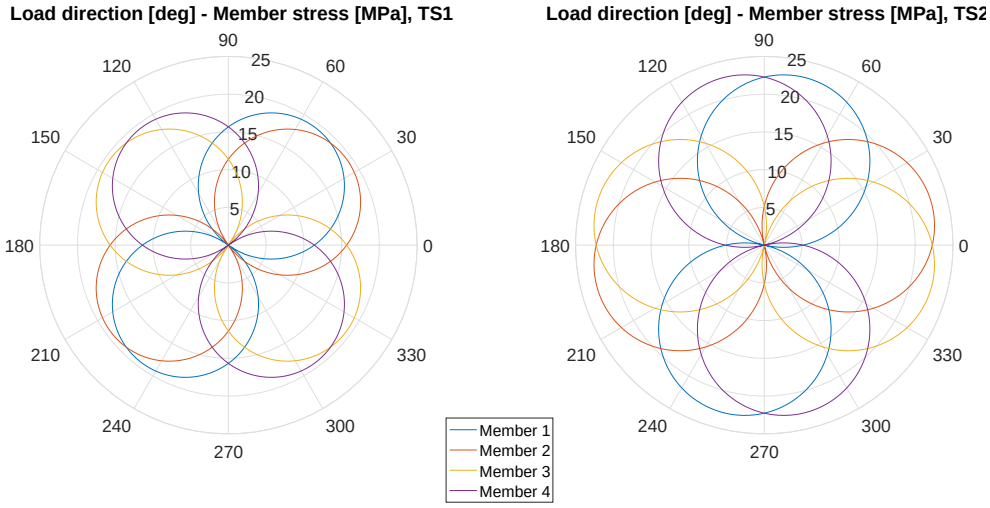

Figure 3.9: Stress versus load direction

3.11.2 FLS loading

Wind

From these time series of the wind loading, the wind loading range, using rain-flow counting is calculated for each of the seastates. For each times series the 5 bins are used. this loading range is used as input in ANSYS. The amount of bins influences the loading range. More bins results in small bins with large loading ranges, and this can influence the fatigue life due to wind loading.

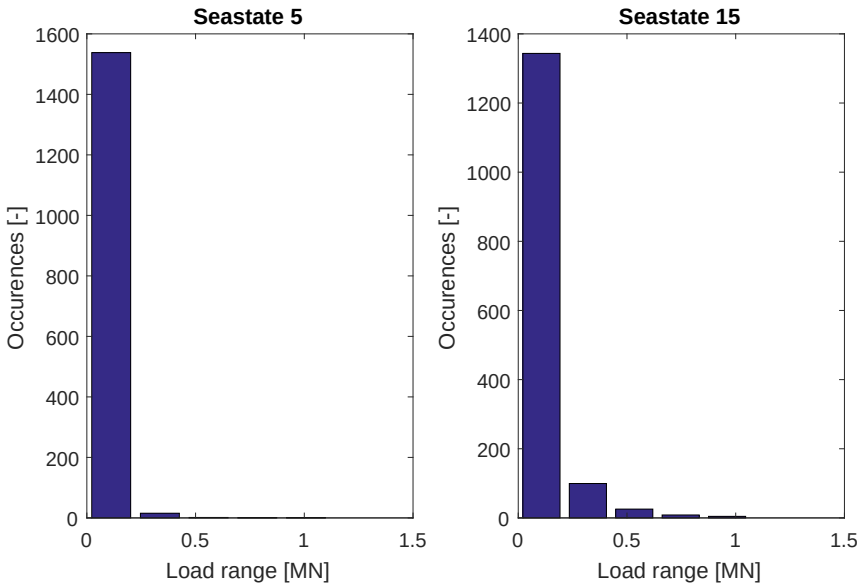

Figure 3.10: Rotor wind loading range for time series of 600 seconds for two seastates

Table 3.6: Histogram results seastate 5, 600s

Loading range MN	Occurrences [-]
0.090	1508
0.271	33
0.451	2
0.631	1
0.812	2

The results of the rainflow counting show a dominance of the small loading ranges. In figure 3.11 a ten second time frame of the time series in figure 3.8. Clearly is seen that there are way more smaller oscillations, which result in the dominance of the smaller loading ranges in the rainflow counting.

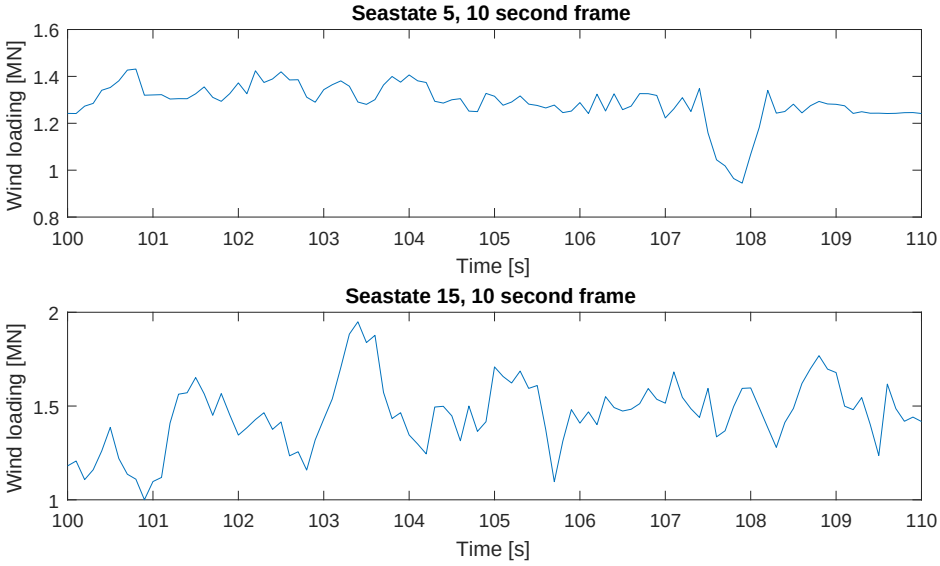

Figure 3.11: Times series zoomed

Wave

The wave load is calculated for each seastate and multiplied with two to create a wave loading range. It is expected that the wave fatigue damage at transition section one will be significant larger than at transition section two because transition section one is always below the still water line and thus always experience wave loading in contrast to transition section two which only experiences wave loading for the higher seastates.

3.12 Additional loading

3.12.1 Marine Growth

Marin growth is also taken in account. Marine growth results in a larger weight of the structure and an increase in diameter and thus wave loading. Marine growth according to the DNV is shown in the table below, with a density of 1325 kg/m3.

Table 3.7: Marin growth

Parameter	Value	Unit
MSL+2 – MSL -10	100	mm
MSL -10 to mudline	50	mm

3.12.2 Corrosion

The first assumption is that the construction is corrosion protected. In the fatigue assessment is checked if this is really necessary.

3.13 Soil

In reality the soil works as rotational spring on the foundation, because this research is focused on the two transition sections of the hybrid monopile the construction is assumed to be rigidly constrained, for all degrees of freedom, at the seabed. In the initial study by Anderson[3] the soil stiffness was already modeled.

3.14 Load and resistance factors

According To DNVGL [11] load factors for offshore steel structures in the table below. These come from the general load resistance factor design and are applied on the ULS load case.

Table 3.8: Load factor for ULS according to DNVGL

Load	Factor
Permanent load	1.0
variable functional load	1.0
environmental load	1.35
deformation load	1.0

3.15 Material

Steel S355 is used with according[11] resistance factor for y_{M0} of 1.15. The following properties for Young's modules, Poisson ratio and density are used:

$$\begin{aligned} E &= 2.1 \quad [GPa] \\ \nu &= 0.3 \quad [-] \\ \rho &= 7850 \quad [\frac{kg}{m^3}] \end{aligned}$$

3.16 SN-curves

The characteristics of the SN-curves used further in this thesis are shown in the table below the curves used in the this fatigue assessment. Like most offshore structures some kind of cathodic protection will be used. In table 3.9 and 3.10 the values of the SN curves relevant for this thesis. In reality transition section two is in most seastates above the maximum wave height, but to be conservative for the fatigue assessment this transition section is assumed to be in the water.

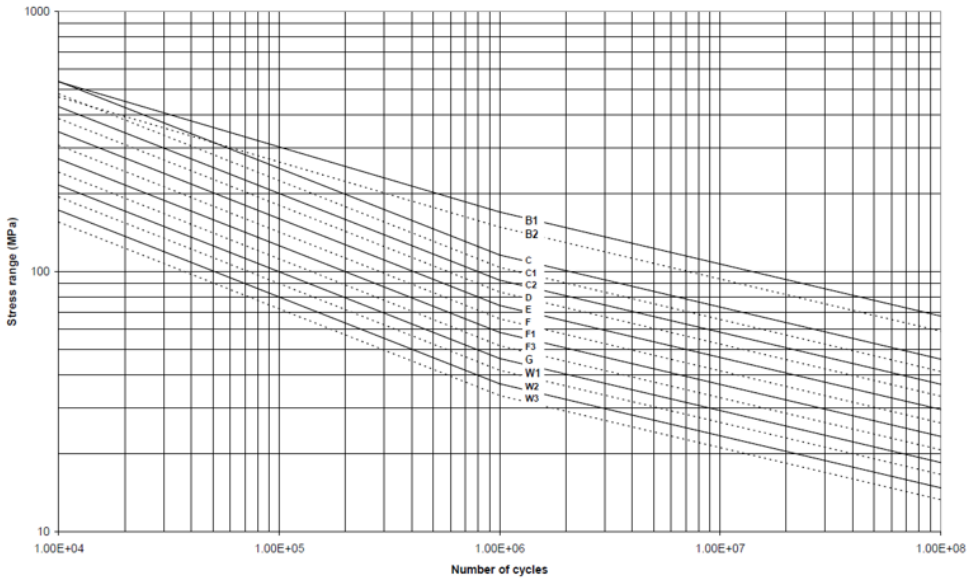

Figure 3.12: S-N curves in seawater with cathodic protection [12]

Table 3.9: S-N curves in seawater with cathodic protection[12]

S-N curve	N< 10^6 cycles		N> 10^6 cycles	Fatigue limit 10^7	k
	m_1	$loga_1$	$loga_2$		
C1	3.0	12.049	16.081	65.50	0.10
D	3.0	11.764	15.606	52.63	0.20
F3	3.0	11.146	14.832	32.75	0.25

Table 3.10: S-N curves in seawater with free corrosion[12]

S-N curve	$loga$ m=3.0 for all cycles	Thickness exponent k
C1	11.972	0.15
D	11.687	0.20
F3	11.068	0.25

3.17 Implementation loading in ANSYS

The aerodynamic wind loading is implemented at the top of the hybrid MP with the corresponding moment, figure 3.13a. The wave load is introduced over these height of the hybrid MP structure, figure 3.13b. The green point load it the own weight of the turbine and the tower, this is only relevant in the ULS and not in the FLS. In chapter 5 the implementation of the wave loading in ANSYS is explained further.

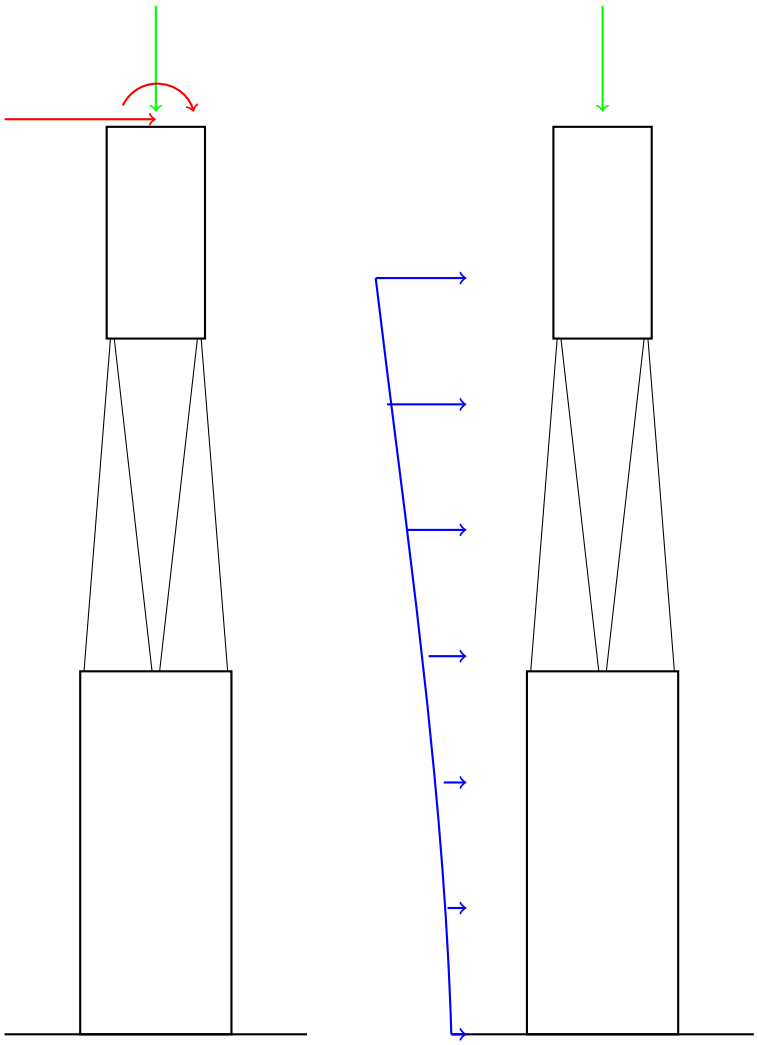

(a) wind (b) wave

Figure 3.13: loading

Chapter 4: Concept design

In this chapter five possible concepts designs for the transition sections are described. Selection criteria for the best concepts are discussed and the five concept are compared with each other. Finally the best concept design is selected for the transition sections which is assessed further in this thesis.

4.1 Concept designs

Based on the state of art of global designs and detail connections five concept connection details where designed, each of them shown in figure 4.1.

(a) Concept 1 (b) Concept 2 (c) Concept 3 (d) Concept 4 (e) Concept 5

Figure 4.1: Hybrid monopile connection detail concept designs

- Concept 1 The members have two nods to provide a straight connection between MP section and the members. The members are slotted and welded to the MP sections. Additional horizontal bracing is added at transition section one to provide stiffness in the horizontal plane.
- Concept 2 A round bended CHS, with diameter of MP sections is welded between the members and the MP section. This CHS provides horizontal stiffness as well. Based on the standard welded connection between CHS profiles.
- Concept 3 A circular endplate/ring, with MP sections diameter, is welded to the members end. This endplate/ring is welded to the MP sections. Below each members circular stiffeners are welded to the MP sections to provide enough horizontal strength. The endplate/ring provides horizontal stiffness as well. Based on figure 2.6.
- Concept 4 Vessel heads at the end of the members. The connection is somewhat similar to a joint, therefor the aligning of the construction is rather easy. Directly below the connection a stiffener ring is welded to the MP sections.
- Concept 5 Members are directly connected to the MP section, therefore the members have to be slotted under an angle. The center of the members are aligned onto a stiffener ring

welded to the inside of the MP sections. This is a combination between the directly welded straight and angular option. Based on figure 2.4c.

The concepts one and five also have a cover plate at the end of the slotted connection to prevent seawater from accessing the inside of the main CHS profiles.

4.2 Concept selection

4.2.1 Feasibility concepts

To verify if the concepts are feasible they where checked if they could withstand ULS loading. All the concepts could withstand the ULS loading, although concept four showed large stresses at the connection between the vessel head and the MP section, results are shown in appendix A. The methodology using ANSYS is further explained in chapter 5. Further the stiffness and steel weight of the concepts have been calculated. Those results are shown in appendix A as well.

4.2.2 Criteria concept selection

For selection of the best concept connection design several criteria were selected like: steel weight, stiffness and resistance. But from appendix A can be concluded that there is no big difference between the concepts in ULS resistance and stiffness. There is a little bit difference in weight, but this is not significant. The global layout of the concepts which determine the main weight are section one, two and three. Because those three sections remain the same for the different concepts, The difference in weight is thus in the transition sections but those differences are small compared to the total weight.

For keeping the hybrid monopile feasible the aim is to keep the fabrication costs as low as possible. therefore the most important criteria is the producability, because this is the main parameter which drives the cost of the hybrid monopile fabrication. This 'conclusion' was supported by specialist at Smulders group and Huisman Equipment. To determine the producability of the concepts there was a focus on two points: The amount of components in the design and the accessibility of the welding locations. Less components is better for the producability, this means less welding and handling.

If welds are easy to access and do not have a complex geometry they are easier to produce, either by hand or automatically, and therefore executed faster and thus cheaper. Below the five concept designs are discussed on the amount of components in the design and the accessibility with fabrication. The minimum amount of components is stated because in reality the design can be cut in more pieces for the continuity of the fabrication process.

- Concept 1:
  - Components: For each CHS profile there are two nods to guarantee a straight slotted fit to the MP sections. Further the horizontal CHS profiles have to be welded to the main CHS profiles. Thus minimum of five components.
  - Accessibility: The welds of the nods between the main CHS profile and the welds between the main CHS and the horizontal CHS profiles can only be accessed from the outside. The weld between the main CHS profile and the MP section could be accessed from two sides if the slotted section is not to long and too small.
- Concept 2:
  - Components: Two 'donut' CHS profile at each transition section, the main CHS profile and for both donuts two circular stiffeners inside. Thus a minimum of seven components.

  - Accessibility: The weld between the donut and the main CHS profile can only be accessed from one side. The stiffeners inside the donut are very hard to fabricate due to the small room for welding and the extra cutting of the donut to even acces the right location.

- Concept 3:
  - Components: Two stiffener rings, one straight CHS profile and two half round circular stiffeners for each transition section. Thus a minimum of seven components.
  - Accessibility: All the main welds can be accessed relative well, only the weld between the main CHS profiles and the stiffener ring can only be accessed from one side.
- Concept 4:
  - Components: Two vessel heads welded to the ends of the main CHS profile and a stiffener ring at the inside of the MP at each transition section. Thus a minimum of five components.
  - Accessibility: All the main welds can be accessed relative well, only the weld between the main CHS profiles and the vessel heads can only be accessed from one side.
- Concept 5:
  - Components: One straight CHS profile welded to the MP section and at stiffener ring at both transition sections. Thus a minimum of three components. A minimum of three components.
  - Accessibility: All the main welds can be accessed relative well, the welds between the main CHS profile and the MP depends on the overlapping part if the inside is still accessible.

4.2.3 Final Concept design

Like described in the previous section the producability is driving in selection of the best concept. Therefore concept five was chosen as the best option because:

- Least amount of components of the concepts.
- All the main weld can be accessed relative easy.
- Bases on fabricators experience, Huisman and Smulders, the concept that is the cheapest to produce.

Concept five has also the benefit that there is room for optimization in the design, like the overlapping length of the slotted section, the height of the stiffener rings inside the MP and the width of stiffener rings.

4.3 Concept connection design

The final connection concept design is thus concept five. This concept is described below in more detail. The two figures below sketch the the connection with the stiffener ring at transition section 1. In figure 4.3 sketch of transition section 2.

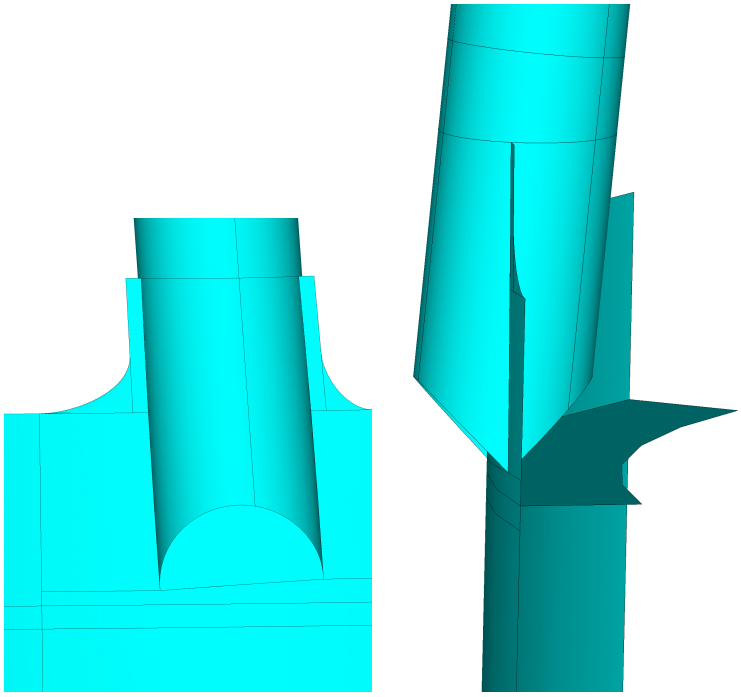

(a) Outside view (b) Side view

Figure 4.2: Concept design TS1

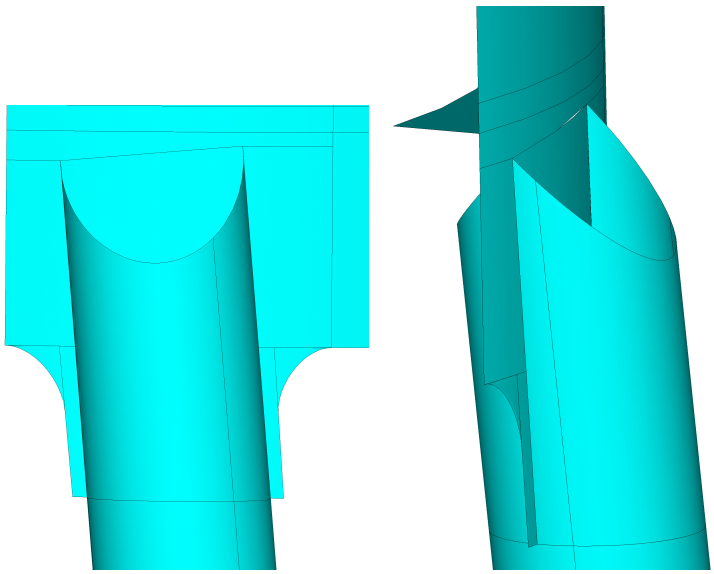

(a) Outside view (b) Side view

Figure 4.3: Concept design TS2

For the introduction of the load from the main CHS profile onto the MP section the so called thumbs, are cut out of the MP section, sketched in the figure below. This is for decreasing the peak stresses at the beginning of the connection due to locally decreasing the stiffness of the MP section by cutting.

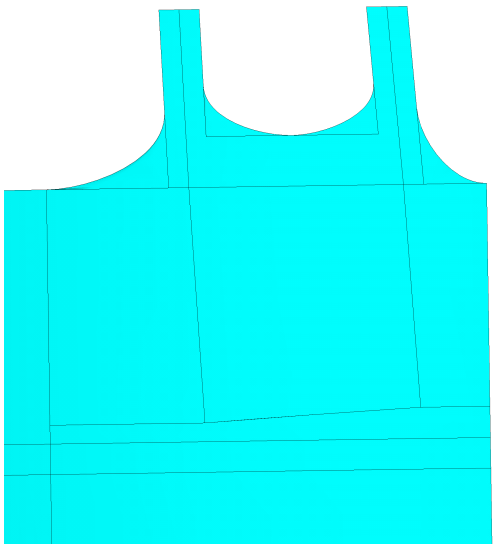

Figure 4.4: Thumbs in the MP section

For an optimized fabrication process, further explained in appendix B, two extra components originated. The main CHS profiles are cut just before the connection at both transition sections. These small CHS profiles are slotted and welded to the MP section. These parts will be further referred to as stubs, sketched in figure 4.5. This cutting of the main CHS profiles results in extra circular welds which can only be accessed from the outside.

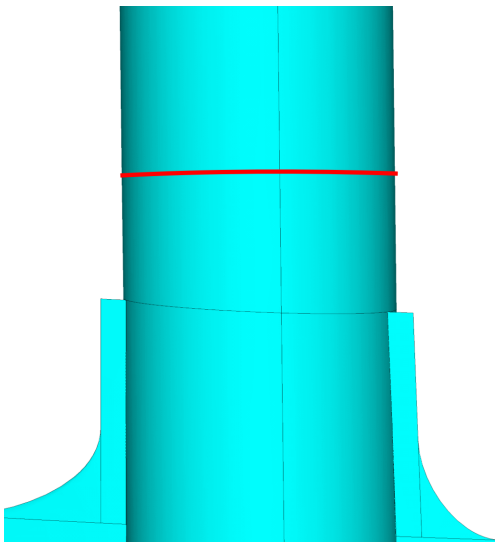

Figure 4.5: Main CHS, above red line, slotted stubs below red line

4.4 Main welds

There are three main welds in the concept design number five. Those main welds are: The weld between the slotted stubs to the MP, the stiffener ring to the MP and the stubs to the main CHS profile. Below follows a description of those three main welds.

The weld between the slotted stubs and the MP section. Automatically welded from the outside. If the inside is reachable the welds can be finished by grinding/smoothing the inside, this is better for the fatigue classification.

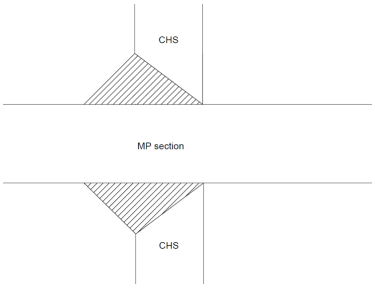

Figure 4.6: sketch of the weld between the slotted stubs and the MP section

The weld between the stiffener ring and the MP section. Automatically welded from both sides.

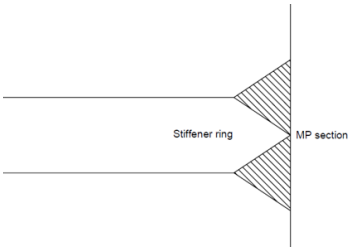

Figure 4.7: sketch of the weld between the stiffener ring and the MP section

The connection between the stubs and the main CHS, figure 4.5 is welded with but welds like in the figure below. There can be a transition in thickness at that location, but the outer diameter of the CHS remains the same. This is the final weld, see appendix B, and can only be accessed from the outside and is thus only welded from the outside.

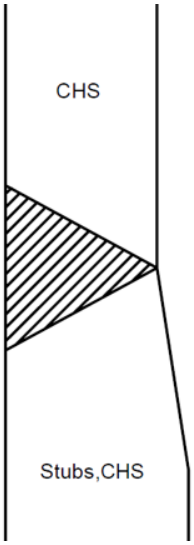

Figure 4.8: sketch of the weld between the CHS with different thickness

Chapter 5: ULS and SLS assessment

In this chapter the hybrid MP substructure is verified against the ultimate limit state and the serviceability limit state. The loading itself consist out wind, wave and current, and is explained in chapter 3. For the ULS two failure modes are analyzed: The exceeding of the maximum allowable Von Mises stress and buckling. For the SLS one of the most critical design parameters is analyzed: The natural frequency of the hybrid MP in combination with the tower and turbine. These natural frequencies should not fall in between the operating frequencies of the wind turbine.

5.1 ANSYS model

To create a 3D model only one eight of the hybrid MP is created using only areas, see figure 5.1. Due to the fact the design is symmetrical the rest of the structure can be copied from this one eight. This section is created using a parametric design script. This means that a script is written from where the model is automatically created using design parameters. This way the design can be changed relative easily without rebuilding the complete model by hand. Parameters are for example width and height of the MP sections, height of the hybrid section, diameter of the CHS profiles and details of the connection, an example of the connection detail parameters of the thumb in figure 5.2.

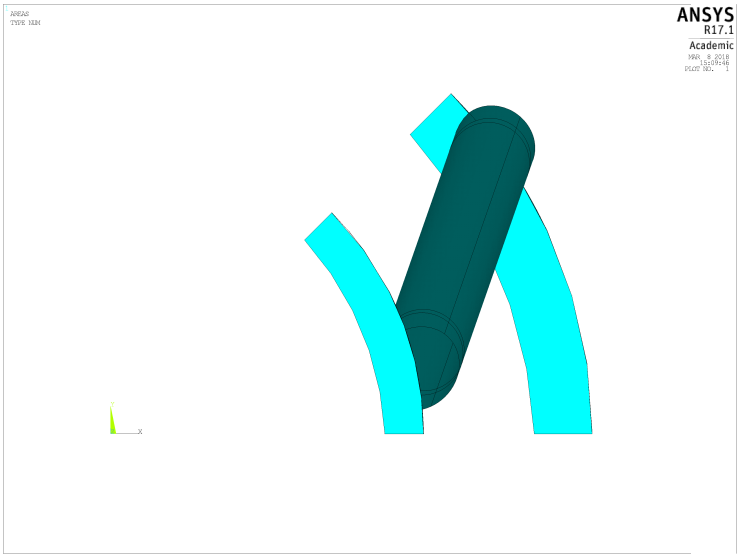

Figure 5.1: modeled one eight of the Hybrid

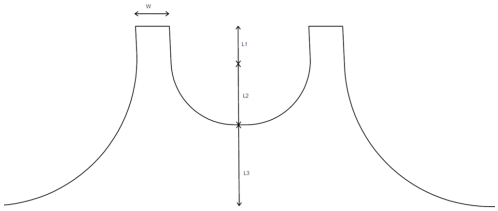

Figure 5.2: detail parameters of the thumb

After modeling one eight the steel plate thickness is assigned to the areas together with the

element type, see next section. Then this one eight of the structure is mirrored three times and glued together. The full model looks like shown in the figure below, the colors stand for the different plate thickness. Therafter the model is ready and is meshed.

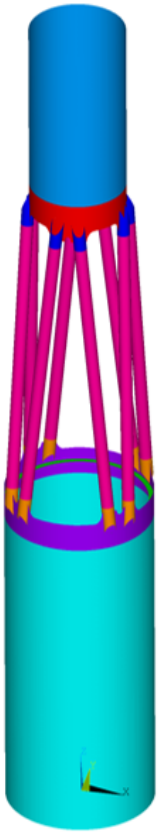

Figure 5.3: ANSYS model without mesh

5.1.1 Elements

For the FEA shell elements are used, this are 2D elements for calculating plate structures. In ANSYS the specific SHELL181 element is used. SHELL181 is suitable for analyzing thin to moderately-thick shell structures. It is a four-node element with six degrees of freedom at each node: translations in the x, y, and z directions, and rotations about the x, y, and z-axes. See the figure below for the element geometry.

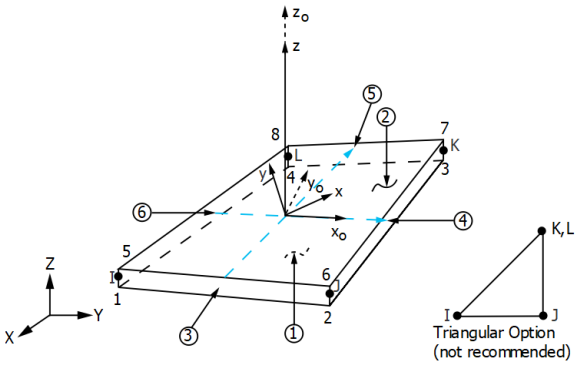

Figure 5.4: Shell181 element geometry[15]

For the introduction of the wind load and turbine weight at the top of the hybrid MP a rigid link element is used. The MPC184 rigid link/beam element can be used to model a rigid constraint between two deformable bodies or as a rigid component used to transmit forces and moments in engineering applications. See the figure below for the element geometry.

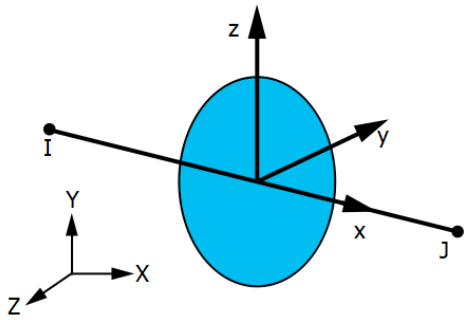

Figure 5.5: MPC184 rigid element geometry[15]

5.1.2 Material model

For the ULS and SLS calculations a linear material model is used with the properties mentioned in chapter 3. This material model is used as well in the FLS calculation further on.

5.2 Loading

The wind load is implemented as a point loads and a moment at top center node, the MPC184 rigid elements are clearly seen as the lines coming from this node in figure 5.6.

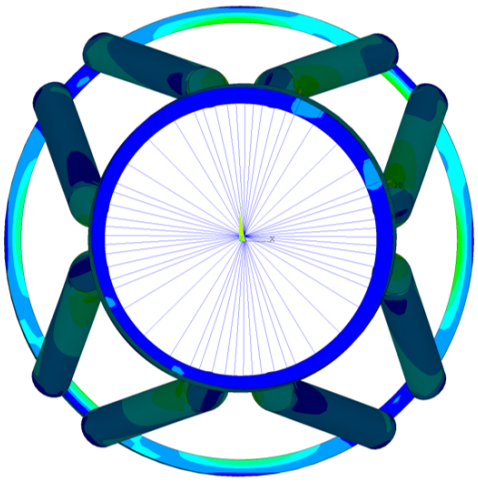

Figure 5.6: MPC184 rigid element used for wind load introduction

The wave loading is introduced as a distributed load divided over the different sections. This is done by summing the wave load over each section height and distribute it equally over that section height, like shown in figure 5.7.In the ANSYS model the load is applied as an acceleration on these sections. Therefore first the mass of the individual section has to be calculated and extracted out of ANSYS, thereafter the corresponding accelerations are calculated and applied in ANSYS.

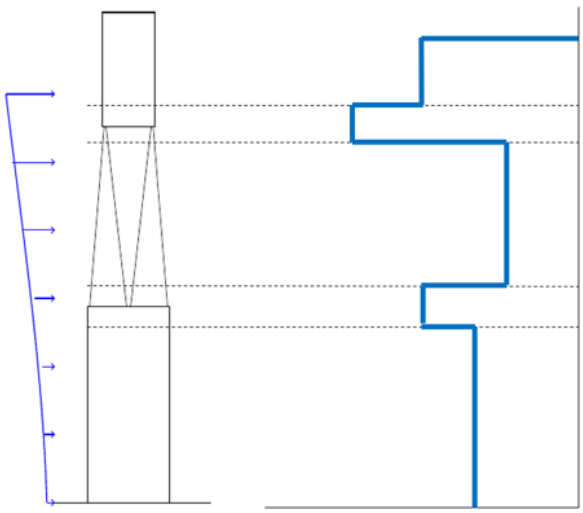

Figure 5.7: Schematic distributed wave loading over the five sections

5.3 Validation

The wave loading is lumped, therefore a check is necessary to validate if it is applied correctly. This is done using the following methods:

- The sum of the loading in x-direction must be equal to minus the sum of the reaction force at the constrained force at the bottom.
- Moment check: the moment around the y-axis at the constrained nodes has to be the same as the total overturning moment out of the hybrid MP tool. The moment at the constrained nodes is calculated by multiplying the distance to the y-axis with the force in z-direction and summed. see table 5.1 for result.

Table 5.1: Overturning moment at seabed comparison Loading versus ANSYS

Loading MNm]	ANSYS [MNm]	Difference [-]
498.2	503.0	1%

5.4 Steel thickness

As already shown in figure 5.3 the different thickness of the main steel, below a summary of the used steel thickness. A detailed drawing with the steel thickness is provided in appendix D.

- main steel of section one and three is 55 mm
- The main part of the hybrid CHS section two is 48 mm
- MP steel of transition section one is 74 mm
- MP steel of transition section two is 74 mm
- Stiffener ring of transition section one is 48 mm
- Stiffener ring of transition section two is 30 mm
- The slotted stubs of transition section one are 65 mm
- The slotted stubs of transition section two are 65 mm

5.5 Mesh size

To selected the right meshsize for the ULS assessment the influence of this on the stress was analyzed. Several computations where run with decreasing the mesh size around the connection. In figure 5.8 the influence of the meshsize on the stress at the the connection between the CHS profile and the MP section. This shows that below a meshsize of 90 millimeter the stress does not change significantly, therefore this meshsize in small enough for the ULS assesment.

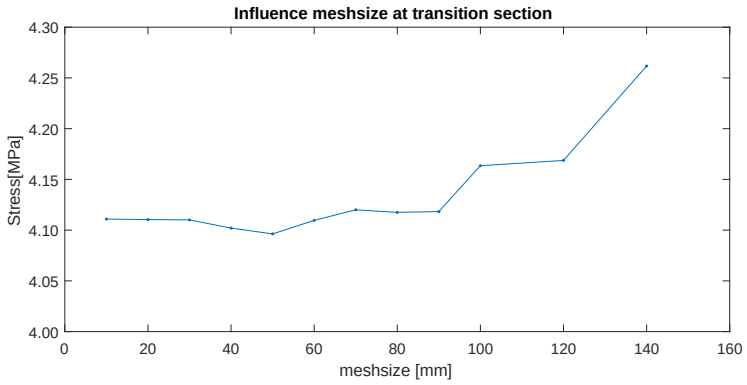

Figure 5.8: Influence meshsize on the stress

5.6 Yield strength

According to DNVGL[10] the maximum allowable stresses of steel depends on the thickness of the plate. The allowable stresses for steel S355 for given plate thickness ranges are given in the table below.

Table 5.2: Allowable stresses of S355 including a safety factor of 1.15[10]

Thickness [mm]	Allowable yield stress [MPa]	Including Safety factor [MPa]
$t \leq 25$	355	309
$25 < t \leq 50$	335	291
$50 < t \leq 75$	320	279
$75 < t \leq 100$	310	270

In the next figures contour plots of the Von Mises stress for the ULS calculation in ANSYS for wind, wave and current loading.

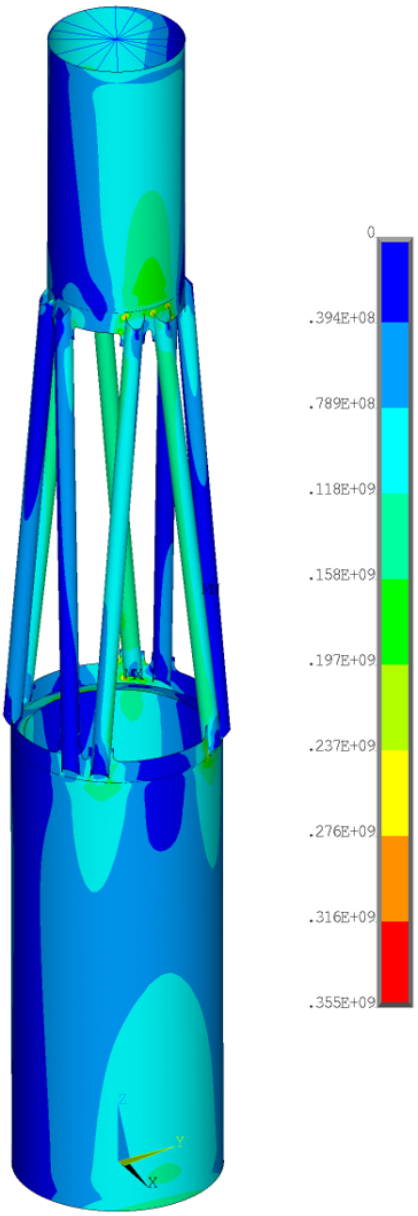

Figure 5.9: ULS, Von Mises stress [Pa], global view

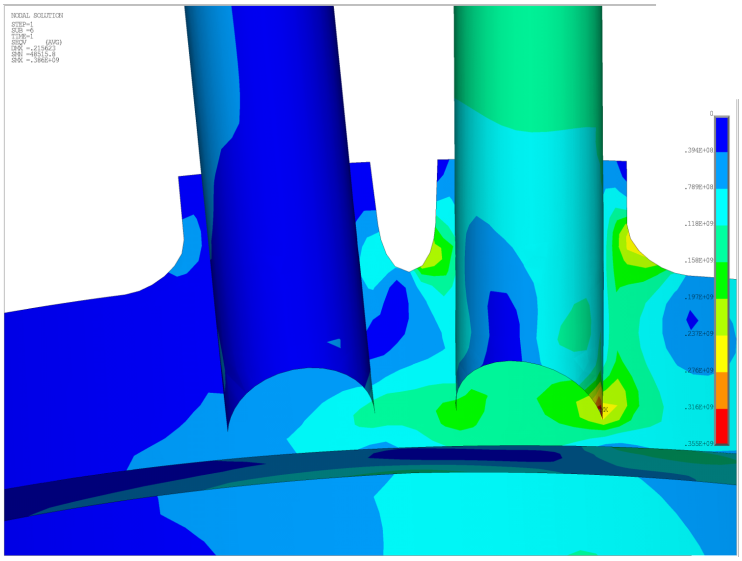

Figure 5.10: ULS, Von Mises [Pa] stress at transitions section 1 inside view

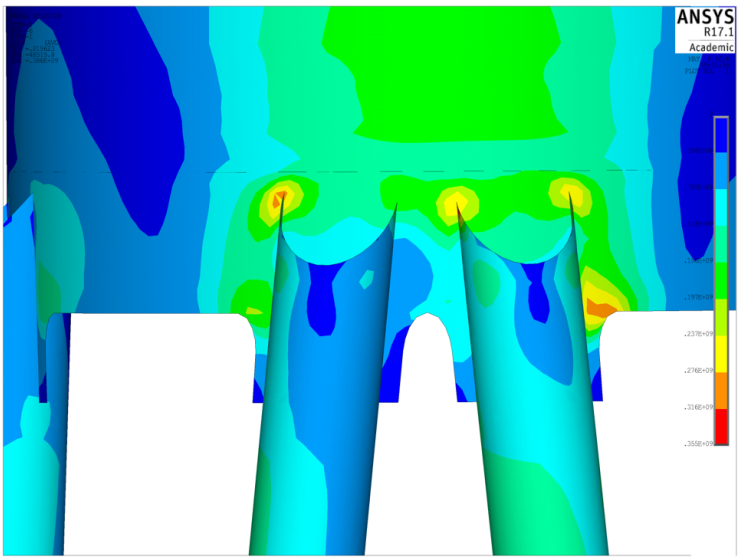

Figure 5.11: ULS, Von Mises [Pa] stress at transitions section 2 outside view

In general the design has enough resistance to withstand the ULS loading, the calculated maximum Von Mises stresses is lower than the maximum allowable stress according to table 5.2. There are some large peak stresses at the transitions sections, but those are due to the finite nature of the calculation. This peak stresses thus come forth of the FEA and can therefore be neglected as a realistic simulation of the stresses.

5.7 Loading direction

In contrast with a traditional MP the maximum stress depends as well on the direction of the loading. If the loading is parallel with the x-axis the overturning moment is largely taken by the two out most profiles, but if the loading direction increases relative to the x-axis the moment is more and more taken by one profile. This is plotted simplified in figure 3.9. Therefore the ULS loading calculation was carried out for two other directions as well. The direction where the

stress according to figure 3.9 is the largest in the CHS member, thus at 14 degrees for TS2 and 37 degrees for TS1, relative to the x-axis.

To compare the influence of the loading direction the stresses at the connection for TS1 and TS2 are compared. The results are shown in table 5.3 where the nodal averaged Von Mises stress is plotted versus the loading direction. It is clearly seen that the loading direction influences the maximum stress, this is because with changing the direction in the two stated directions the loading is not anymore equally divided by two CHS profiles but more one CHS profile and therefor increasing the stresses. For further design the loading direction should be taken into account for the ULS case.

Table 5.3: Von Mises nodal averaged stress versus loading direction

Direction [deg]	TS1 [MPa]	TS2 [MPa]
0	93	55
14	101	77
37	100	88

5.8 Buckling

Because the hybrid monopile is a slender structure the safety against buckling should be checked. First a simplified linear Euler buckling check is performed in ANSYS to look for the buckling mode shapes. The smallest safety factor occurs with the fourth mode, in this mode the CHS profiles of section two buckle, in figure 5.12a this is visualized. This safety factor is a factor applied on the ultimate limit load before this buckling mode occurs. Local buckling of the stiffener ring is also possible see figure 5.12b, but this has a larger safety factor to buckling than the fourth mode. The buckling resistance of the profiles is calculated in the next section.

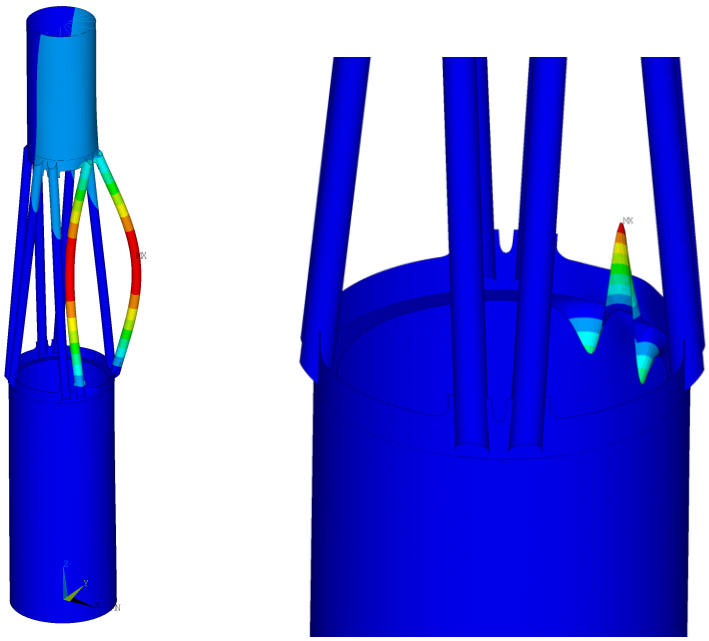

(a) Mode 4 (b) Mode 2

Figure 5.12: Two buckling mode shapes

5.8.1 Buckling resistance

To calculate the restistance against buckling Eurocode 3 for the design of steel structures is used [27]. It is calculated as follows.

$$N_{b,Rd} = \frac{\chi A f_y}{y_{m1}} \tag{5.1}$$

In which A is the area of the CHS profile, f_y the yield strength and y_{m1} the safety factor. The buckling reduction factor χ is

$$\chi = \frac{1}{\Phi + \sqrt{\Phi^2 - \overline{\lambda}^2}} \tag{5.2}$$

in which

$$\Phi = 0.5[1 + \alpha(\overline{\lambda} - 0.2) + \overline{\lambda}^2] \tag{5.3}$$

buckling curve a is used with the according α of 0.21. The non dimensional slenderness is

$$\overline{\lambda} = \frac{A f_y}{N_{cr}} \tag{5.4}$$

The critical Euler buckling load

$$N_{cr} = \frac{\pi^2 EI}{L_{cr}^2} \tag{5.5}$$

In which L_{cr} is the critical buckling length. The boundaries do not function completely as hinges but have resistance against rotation, The connection is thus rigidly fixed but like shown in figure 5.12a the buckling mode shape of the profiles looks somewhate like a hinged connection. Therefore $L_{cr} = 0.9L$ is used, this is common in the design of fixed connections in lattice structures [27]. The resulting buckling resistance is the same for all the CHS profiles and is 19.18 Mega-Newton.

5.8.2 Compression force CHS profiles

The compression loads are extracted out of ANSYS just above the connection of TS1. At the connection between the main CHS profiles and the stubs. This is done for three loading directions, the results are in the table below. The largest compression loads occur with the ULS loading at an angle of fourteen degrees to the x-axis. For the profile numbering see figure 3.7.

Table 5.4: Normal load in CHS profiles

CHS profile [-]	Load 0 deg [MN]	Load 14 deg [MN]	Load 37 deg [MN]
1	17.21	17.27	15.2360
2	1.83	5.72	11.2660
3	-3.50	0.57	6.9718
4	-18.26	-17.23	-13.6420
5	-15.31	-15.43	-13.5370
6	-6.49	-10.35	-15.7800
7	5.23	1.15	-5.1948
8	13.78	12.78	9.1677

The compression load is compared to the buckling resistance of the CHS profiles. If their is tensile loading in the profiles safety to buckling is not relevant and is neglected. If the safety factor is larger than one the yield criteria will be decisive. In table 5.5 the safety factors against buckling of all the profiles for tree loading directions. The safety factor is always larger than one, the minimum is 1.11, thus the yield criteria is decisive.

Table 5.5: Safety factors to buckling for three loading directions

CHS profile [-]	SF 0 deg [-]	x SF 14 deg [-]	SF 37 deg [-]
1	1.11	1.11	1.26
2	10.49	3.35	1.70
3	-	33.38	2.75
4	-	-	-
5	-	-	-
6	-	-	-
7	3.67	16.67	-
8	1.39	1.50	2.09

5.9 Natural frequency check

For the SLS verification the natural frequencies of the hybrid monopile are calculated. Mentioned in table 3.1 are the nominal operating frequency of the reference turbine. The upper limit for the 1P range is 0.192Hz and the lower limit for the 3P range is 0.270Hz. The natural frequency of the combined substructure and turbine must be between those two limit ranges. The range between the 1P upper bound and the 3P lower bound is the so called soft stiff region. In this case a soft stiff range from 0.192 to 0.270 Hz.

The reference wind turbine tower has a diameter at the bottom of 6.5 meter and at the top of 4.5 meter. The steel thickness of the tower is decreasing in thickness from bottom to top, starting at the bottom with 50 millimeter and and ending at the top with 22 millimeter. For modeling the tower in ANSYS Shell elements are used, to assign the corresponding thickness with the tower is divided in twenty-four parts each with each part there corresponding thickness. To model the turbine and TP the own weight of both are added at the corresponding locations.

In figure 5.14 the first six mode shapes are show. The corresponding natural frequencies are plotted in figure 5.13 together with the 1P and 3P region of the turbine. Further modal shapes have eigen frequencies well beyond the 3P range and are therefore not relevant.

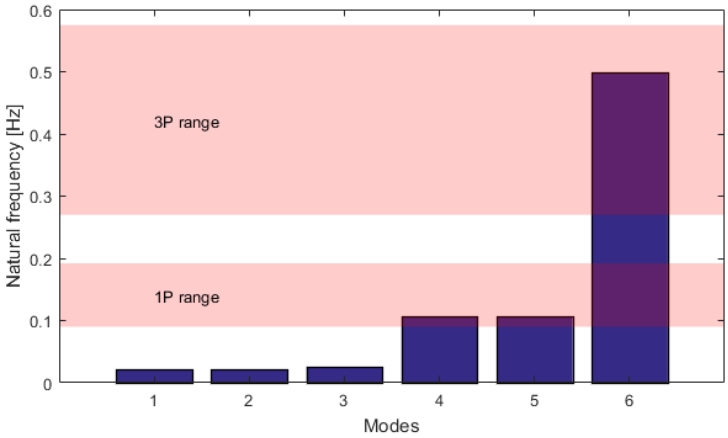

Figure 5.13: Natural frequencies for modal shapes one till six with 1P and 3P ranges

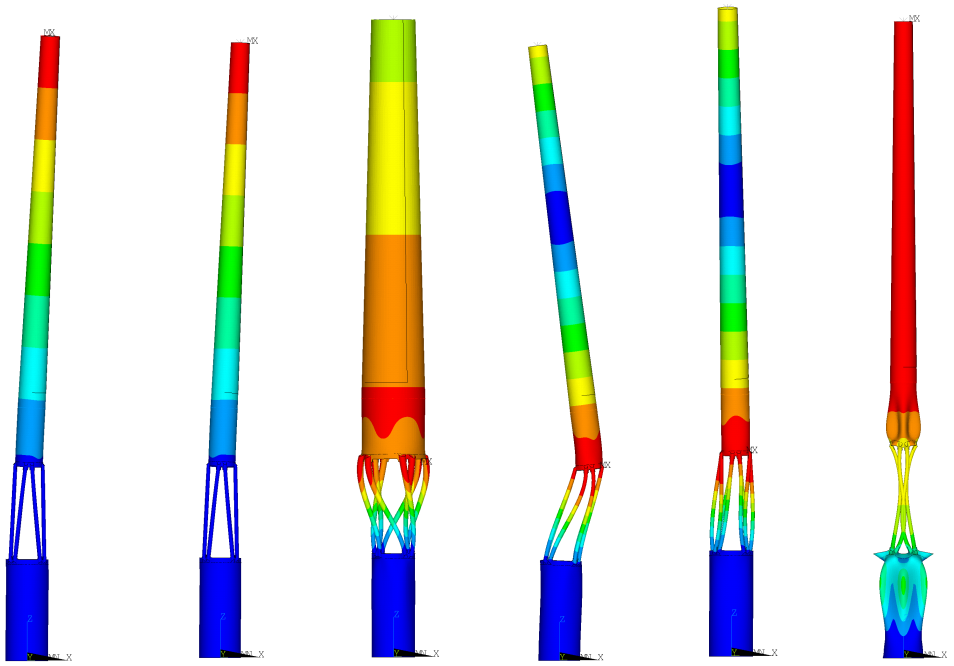

(a) mode 1 (b) mode 2 (c) mode 3 (d) mode 4 (e) mode 5 (f) mode 6

Figure 5.14: Modal shapes, Colors are the total displacement vector sum

Mode shapes one, two, four and five are similar and expected because the tower hybrid MP system functions as a cantilever beam. The third and sixth mode shape are unique for the hybrid MP because in these cases the hybrid section has a significant displacement compared to the rest of the structure. In figure 5.13 it is clearly seen that the natural frequencies four till six are in the operating frequencies of the turbine.

It should be noted that these results are just a approximation because the hybrid MP is constrained in all direction at the seabed, in reality the foundation functions as a spring and therefore influences the natural frequency. Especially the first, second, fourth and fifth natural frequency are influenced by the soil stiffness. In Anderson[3] mode shapes one, two, four and five where modeled more realistic with inclusion of the soil in the calculation. The resulting natural frequencies for those mode shapes are in the safe range and are thus assumed to be safe.

In vertical direction there is almost no influence of the soil stiffness. Thus mode shape three and six are not influenced by the interaction of the soil with the monopile. Therefore the sixth natural frequency, also shown in figure 5.15, could be problematic because is falls into the 3P region of the turbine. It is questionable if this mode shape occurs in reality. It is mostly a displacement of the tower in vertical direction and a rotation around the z-axis. It requires thus no displacement in horizontal direction, but during operating this horizontal load with its according displacement always exists. Thus it is doubtful that this natural frequencies and mode shape occur during operation.

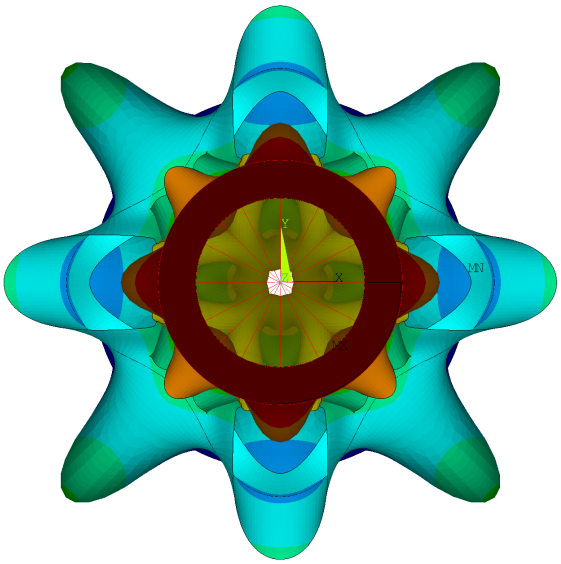

Figure 5.15: Modal shape six, figure 5.14f, top view

Thus in conclusion the dynamic behavior of the hybrid monopile can be assumed to be safe. Only further study should be executed on mode shape six. Detailed finite element analysis of the wind loading in the time domain could conclude if mode shape six can occur in reality.

Chapter 6: HSS calculation

In this chapter the selection of the Hot Spot, further referred to as HS, and the calculation of the HSS is discussed. For calculating the HSS two methods are used in this chapter. The HSS methodology and the nominal stress multiplied with a stress concentration factor. Further in this chapter the modeling in ANSYS is described, and the post processing of the ANSYS calculations is described. Thereafter the different methods for modeling welds in FEA are discussed. In the end a parametric study is carried out on the influence of design parameters on the HSS. This is useful for future optimization of the design.

6.1 Fatigue detail locations

The fatigue design of slotted pipes to a plate material, also called gusset joints, is a complex process. Therefore DNVGL provides an example[12] of such a connection with the according HS locations and read out direction, see the figure below.

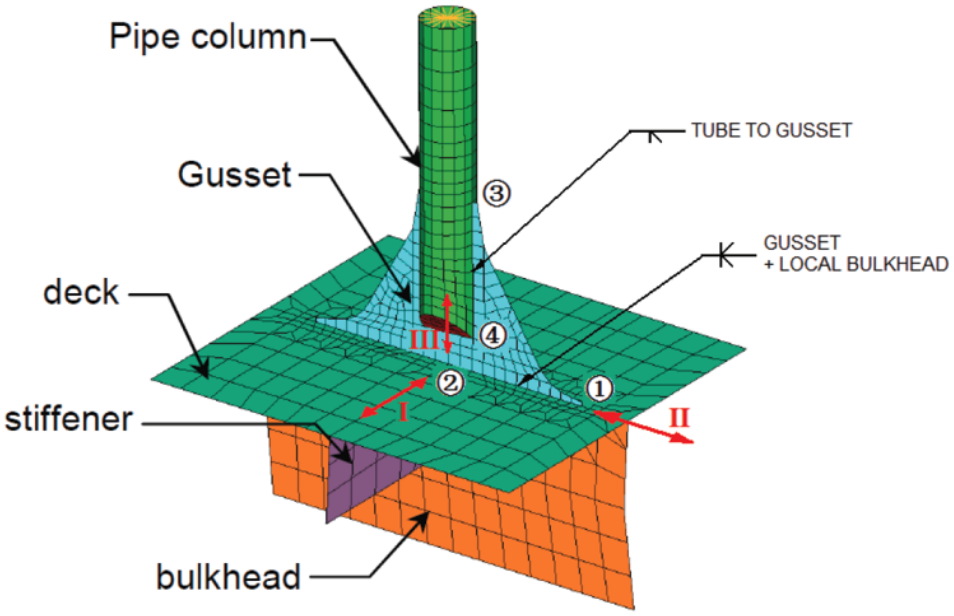

Figure 6.1: HS positions according to DNVGL [12]

From the above provided example and further information in DNVGl[12] four positions are selected in the concept design where the HSS is extracted. These positions are shown in figure 6.2.

- Position I: The start of the slotted connection between the CHS stubs and the MP thumbs.
- Position II: The end of the connection between the stubs and the MP section.
- Position III: The connection of the stiffener ring to the MP section.
- Position IV: The connection of the CHS stubs to the the main CHS.

For the first three positions the HSS methodology is used, at position four the HSS is calculated using the nominal stress with a stress concentration factor. In the figure only the positions at transition one are shown, but these positions are the same for transition section two, only mirrored in the horizontal plane. The connection between the MP sections is not taken into account because the focus of this thesis is on the transition sections.

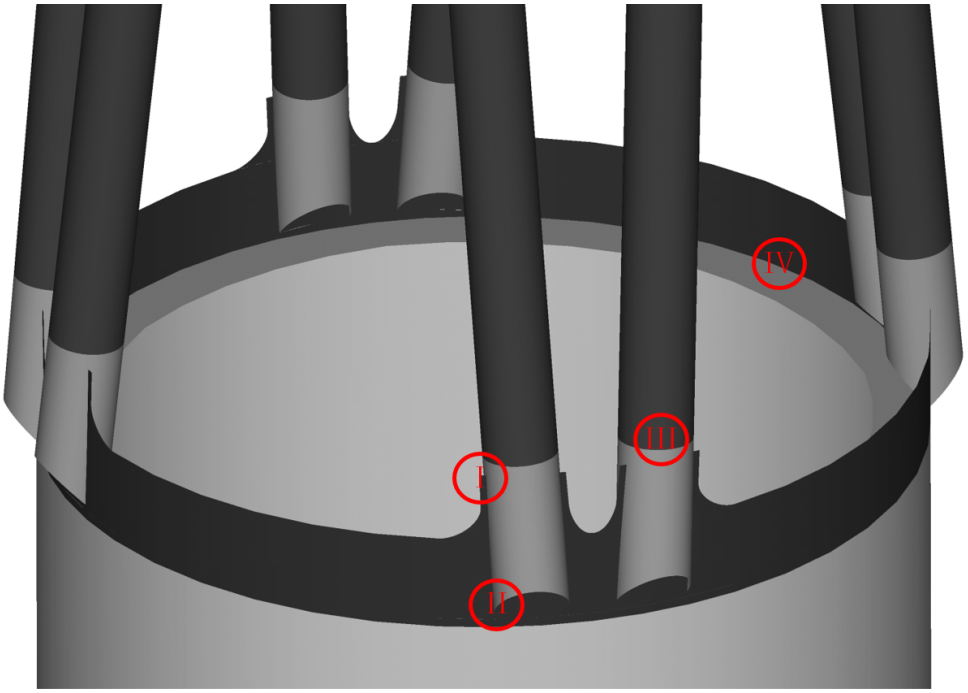

Figure 6.2: HSS detail positions

In figure 6.3 the locations are shown in ANSYS with the arrows indicating the direction, and in figure 6.2 the details are sketched with welds and the read out direction of the HSS. At location four the HSS method will not be used instead the nominal stress will be used, explained further on in this chapter.

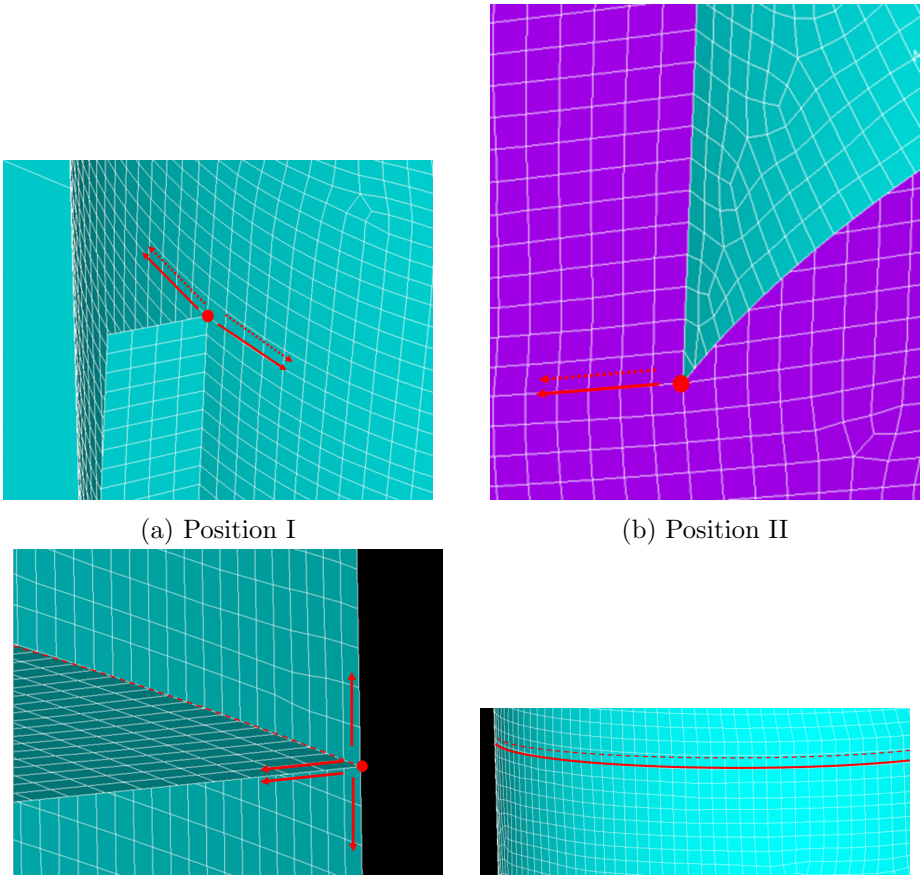

(a) Position I

(b) Position II

(c) Position III

(d) Position IV

Figure 6.3: Location of the details in ANSYS

At position one the stress is read out horizontally from the stubs, both on the inside and outside of the CHS stubs and on both sides of the thumbs. For position two the stress is read out horizontally on the MP section and only outside the stubs due to the presence of a cover plate. Position three the HSS is calculated using both the stresses on the stiffener ring and the MP section. At position four the averaged nominal stress, over both sides of the shell elements, is used.

The location of the maximum HSS at position three and four depends on the loading direction and the local parameters of the connection. With detail three it can be anywhere along the welds of the stiffener ring, and with detail three can be anywhere around the circumference of the CHS profiles. Therefore the HSS has to be calculated along the length of those welds to locate the maximum.

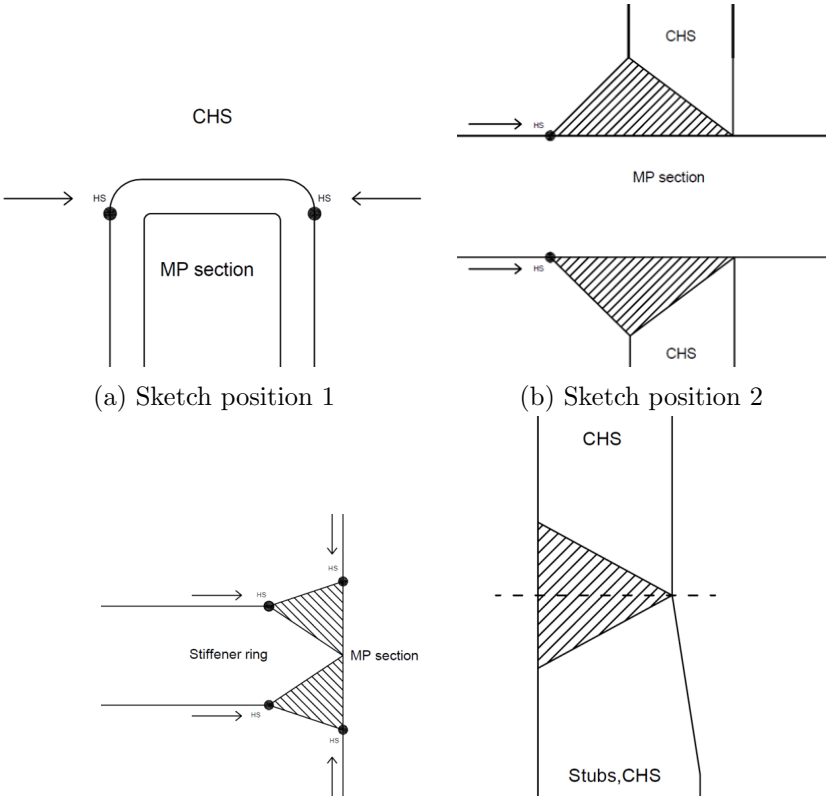

(a) Sketch position 1 (b) Sketch position 2

(c) Sketch position 3 (d) Sketch position 4

Figure 6.4: Sketch of the welded position 1 to 4 with the HSS read out direction

Thus in the end this result in sixteen HS locations where the HSS methodology is used and two locations where the nominal stress is used. This results in eighteen fatigue HS locations per transition section and thus a total of thirty-two. In the table below they are summarized and visualized in figure 6.5.

Table 6.1: HS location description

Location	position	Description
1	position I-1:	Left thumb, Outside MP, Outside stub
2	position I-2:	Left thumb, Inside MP, Outside stub
3	position I-3:	Right thumb, Outside MP, Outside stub
4	position I-4:	Right thumb, Inside MP, Outside stub
5	position I-5:	Left thumb, Outside MP, Inside stub
6	position I-6:	Left thumb, Inside MP, Inside stub
7	position I-7:	Right thumb, Outside MP, Inside stub
8	position I-8:	Right thumb, Inside MP, Inside stub
9	position II-1:	Left side of the bottom of the stubs, inside of the MP section
10	position II-2:	Right side of the bottom of the stubs, inside of the MP section
11	position II-3:	Left side of the bottom of the stubs, outside of the MP section
12	position II-4:	Right side of the bottom of the stubs, outside of the MP section
13	position III-1:	Above Stiffener, MP stress
14	position III-2:	Stress stiffener top
15	position III-3:	Stress stiffener bottom
16	position III-4:	Below stiffener MP stress
17	position IV-1:	maximum nominal stress times SCF_i
18	position IV-2:	maximum nominal stress times SCF_o

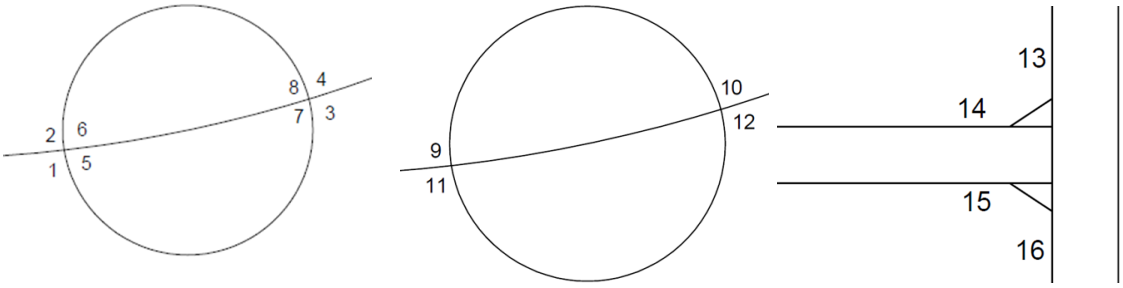

(a) Position I (b) Position II (c) Position III

Figure 6.5: Sketch of the HS location numbering for position I, II and III

6.2 Connection stubs with main CHS profiles

At the connection between the stubs and the main CHS profile there is a transition in thickness. At this weld a stress concentration occurs on the inside or the outside of the CHS. This stress concentration can be increased by misalignment, center eccentricity and out of roundness but those will be neglected in this calculation. The connection is assumed to be a butt welds from the outside, like sketched in figure 6.4d. If the inside is reachable and can be grinded after welding a better detail class can be chosen for the fatigue assessment. This is discusses in chapter 7. The HSS is calculated by extracting the nominal stress out of ANSYS and multiplied with a Stress Concentration Factor, further mentioned as SCF. The calculation of the SCF is described in the following figure and equations 6.1 and 6.2.

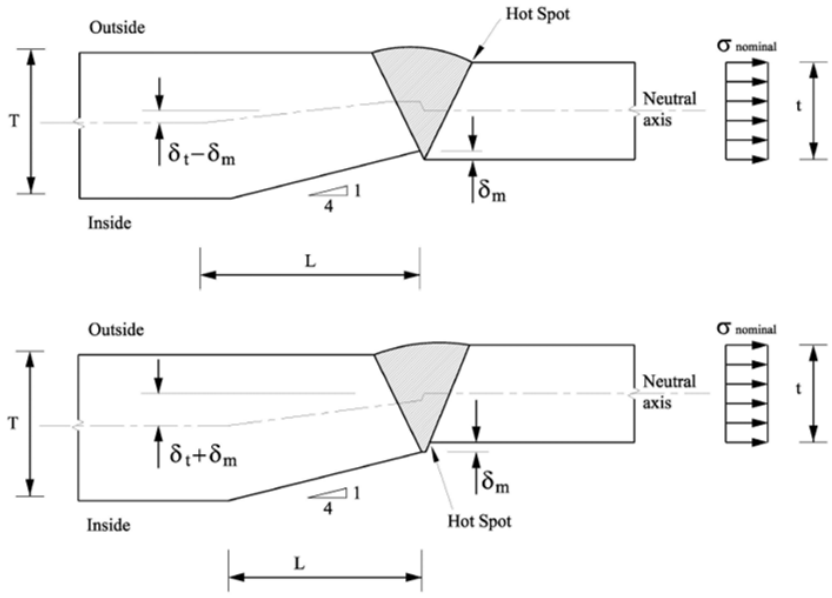

Figure 6.6: Hot spot for tubular but welds with transition in thickness[12]

$$SCF_i = 1 + \frac{6(\delta_t - \delta_m - \delta_0)}{t} \frac{1}{1 + \left(\frac{T}{t}\right)^{\beta}} e^{-\alpha} \tag{6.1}$$

$$SCF_0 = 1 - \frac{6(\delta_t - \delta_m)}{t} \frac{1}{1 + \left(\frac{T}{t}\right)^{\beta}} e^{-\alpha} \tag{6.2}$$

6.3 ANSYS model

For fatigue assessments using FEA a detailed mesh is necessary of the selected part. In the case of the hybrid monopile this is thus the transition section one and two. To decrease unnecessary computational time only one eight is meshed with a fine mesh. This is enough because of the symmetry of the hybrid monopile. How this looks like in ANSYS is shown in figure 6.7 where the mesh is plotted for one eight of transition section one.

The same elements are used for the HSS calculation as used for the ULS assesment, shown in figure 5.4. With the only difference that there is more attention to the mesh of the critical areas for the HSS calculation.

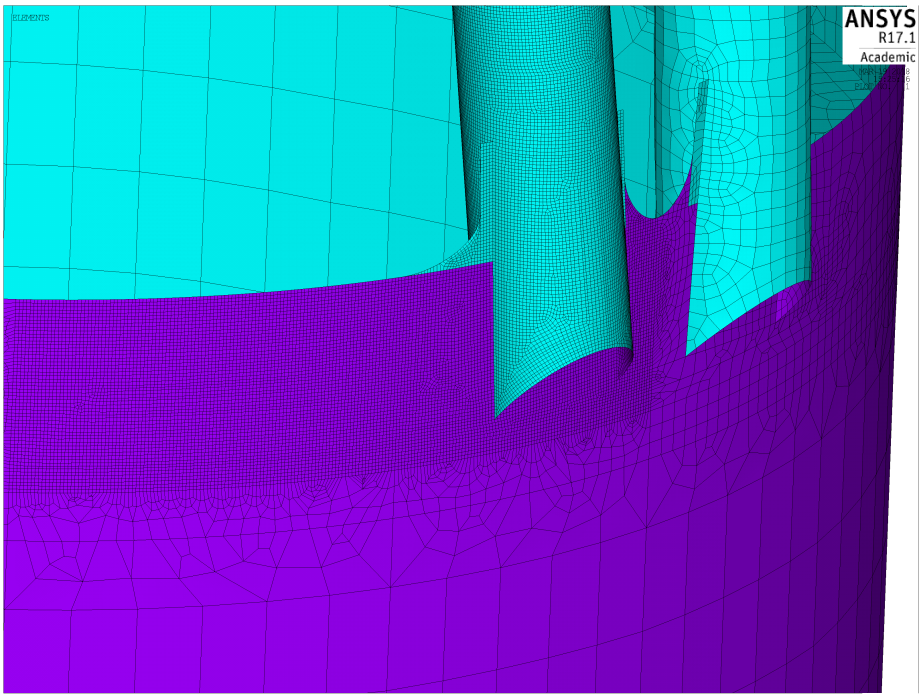

Figure 6.7: Example of the mesh around on of the connections at transition section one

6.4 Processing ANSYS results

The following steps are taken to go from the ANSYS result to the HSS range, this is done for each selected HSS location. The nodal averaged stress from the ANSYS is used.

- First a local coordinate system is defined at the HSS location. In this way the result can be transferred to the local coordinate system and the stresses to be used for the HSS calculation are in the right direction. (Perform stress transformation to obtain equivalent surface stress at the nodes)
- Thereafter the nodes are selected in the read out direction of the details.
- The nodal averaged results are written to a text file.

For location four, the connection between the main CHS and the stubs, the line defining the connection between those part is selected, thereafter a local coordinate system is created and the nodal nominal stresses at all the nodes on that line are extracted and written to a text file.

6.5 Determining HSS using Matlab

After the stress calculation using ANSYS APDL further processing is done using Matlab. The following steps are taken to come from the stress data at the locations to the HSS.

- Import the results from the text file into Matlab.
- The distance to the HS, the weld toe, is calculated.
- The effective stress range is calculated according DNVGl, see equation 2.2.
- The stress range is calculated using linear interpolation at t/2 and t*2/3 from the weld toe.
- The HSS is calculated using those two read out points.

In figure 6.8 an example of the calculation of the stress range using the HSS methodoly with read out point t/2 and t*2/3.

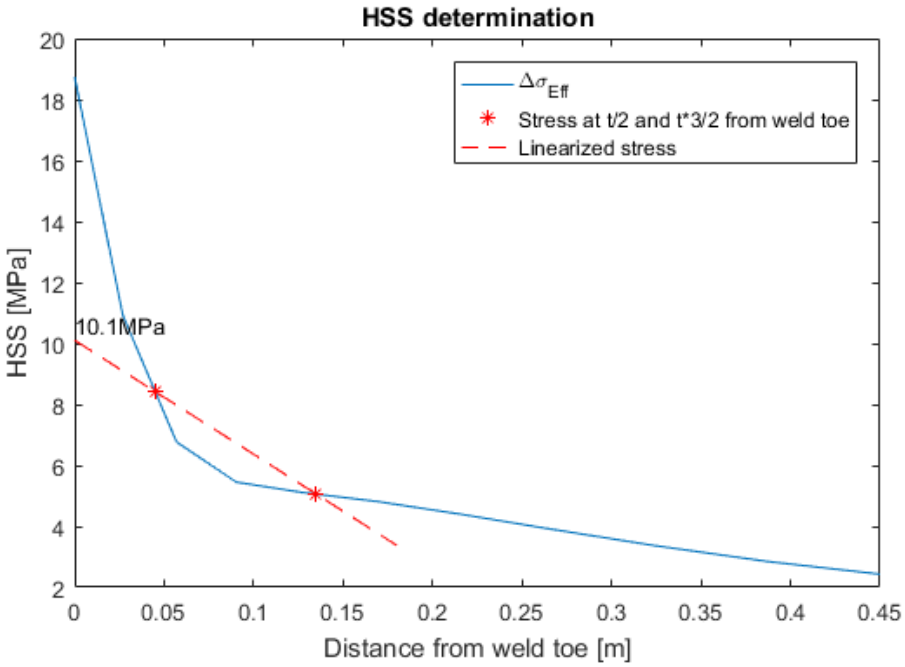

Figure 6.8: Example result of the HSS calculation

6.6 Weld modeling

There are several ways to model welded connections for fatigue assignments using FEA. The tree main options are: Only shell elements without modeling the weld and assume the weld in the postprocesing. A shell model where the weld is modeled using shell elements with the same thickness as the weld throat size. A model with solid elements where the connection and the weld are modeled completely. In this section and appendix C the first two options are discussed. The third option, the solid modeling, was also studied but due to severe modeling problems with 'brick' elements in the complex geometry this is not further taken into account in this thesis.

The problem that weld nodes are before the HS and therefor create an extra peak which influence the HSS. In figure C.5b it is seen that the peak stress at the plate connection is lower with the weld model, but due to the extra fluctuation around the weld node the HSS is larger than the model without the shell weld. This larger HSS is not realistic, therefore in the final fatigue assessment the model without the shell welds is used.

From the conclusion for the mesh size in appendixC is concluded that for the final fatigue assessment a mesh size of t/2 will be sufficient.

6.7 Parametric study

Study the influence of different parameters on the HSS. Useful for future detailed design and construction purposes of the Hybrid MP.

6.7.1 Parameters

The influence of the parameters below on the HSS is studied. the last two parameter are sketched in figure 6.9. These parameters, except the loading direction, are chosen because they can change for construction purposes and it is therefore useful to know how they influence the HSS. Therefore parameters like CHS diameter and width of the MP sections are not studied.

- Loading direction
- Width stiffener ring

- Distance end of stubs and stiffener ring
- Cutting of inside MP section inside stubs

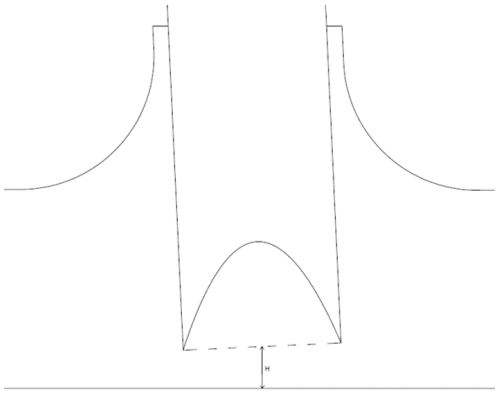

(a) Distance end stubs and stiffener ring

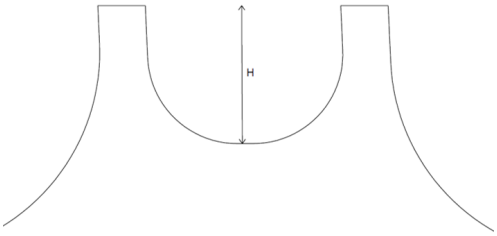

(b) Cutting of inside MP section inside stubs

Figure 6.9: Sketch of the parameters three and four

6.7.2 Modeling

Parametric modeling like discussed in chapter 5 is used. For the loading direction the model does not have to change, but for the other three parameters the hybrid MP model has to be rebuild and re-meshed. Only one load is applied at the model. At hub height a load of 1 MN is used which is transferred to a height of sixty meter from the seabed thus resulting in an applied moment en horizontal load.

6.7.3 Results

Direction

The HSS depends logically on the loading direction. In the FLS assessment the loading is conservatively assumed to be in one direction only, for further designing and placement of the hybrid MP it is useful to know the influence of the loading direction on the HSS. To do study this the loading direction is adjusted from zero to forty-five degrees relative to the x-axis while the load remains the same. The results of the calculation for locations one to twelve of transition section one are shown in figures 6.10 and 6.11, and for the locations of transition section two in figure 6.12 and 6.13.

Although the hybrid MP is symmetrical with the one eight where the HSS are calculated the maximum HSS, for some locations, is still exceeding with increasing loading direction.

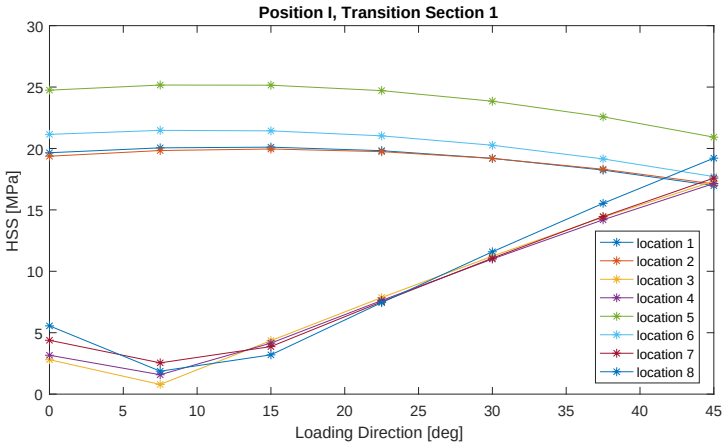

Figure 6.10: HSS versus direction wind load at hub height, location 1 to 8, TS 1

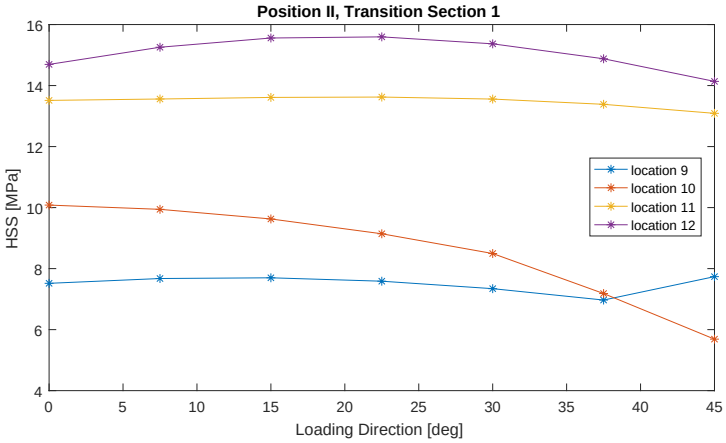

Figure 6.11: HSS versus direction wind load at hub height, location 9 to 12, TS 1

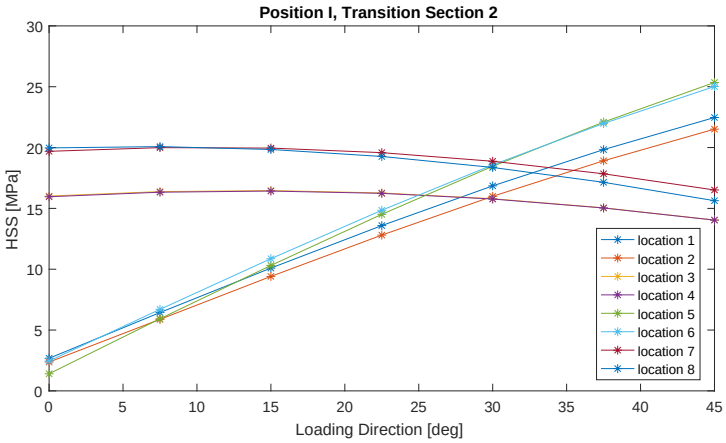

Figure 6.12: HSS versus direction wind load at hub height, location 1 to 8, TS 2

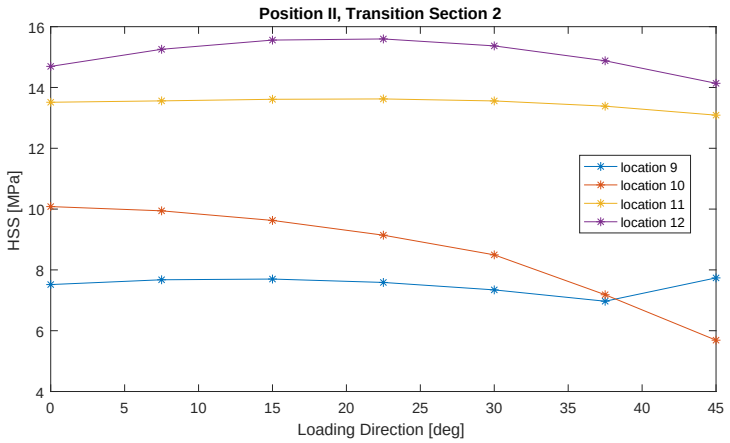

Figure 6.13: HSS versus direction wind load at hub height, location 9 to 12, TS2

Stiffener ring

The HSS for location fourteen and fifteen are plotted in figure 6.15. These are the maximum occurring HSS along the stiffener ring. In figure 6.14 the HSS of location nine till twelve. The increasing of the width thus stiffness of the ring has a positive effect on the HSS, it decreases. Except for location nine where there is a slight increase in HSS.

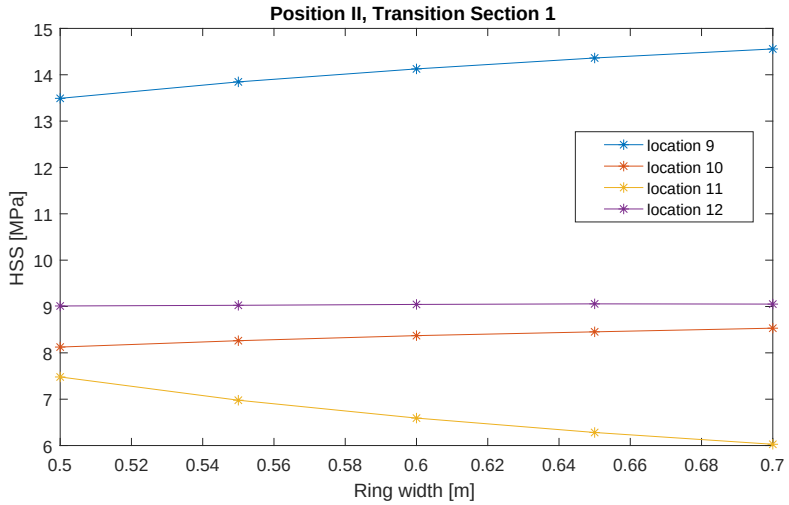

Figure 6.14: HSS versus ring stiffener width for location nine to twelve

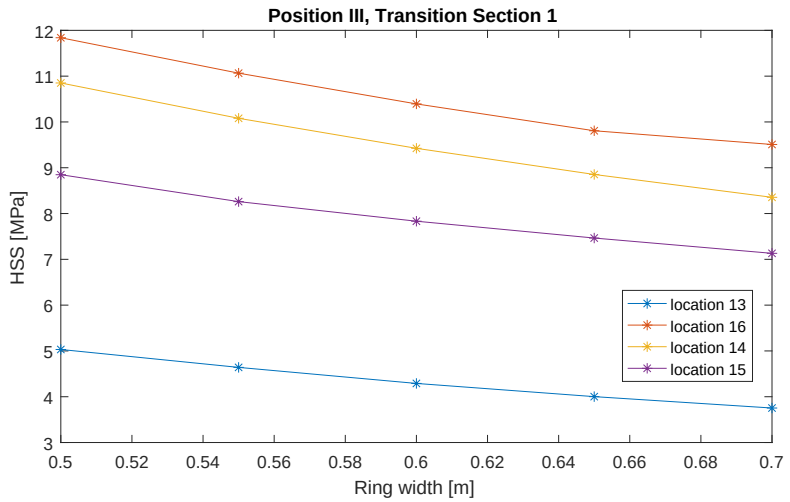

Figure 6.15: HSS versus ring stiffener width for location fourteen and fifteen

Distance end of stubs and stiffener ring

The results of location nine till twelve are plotted in figure 6.16 because those locations are the nearest to the stiffener ring. There is almost no influence at all on the HSS, little bit on location nine but these can be neglected.

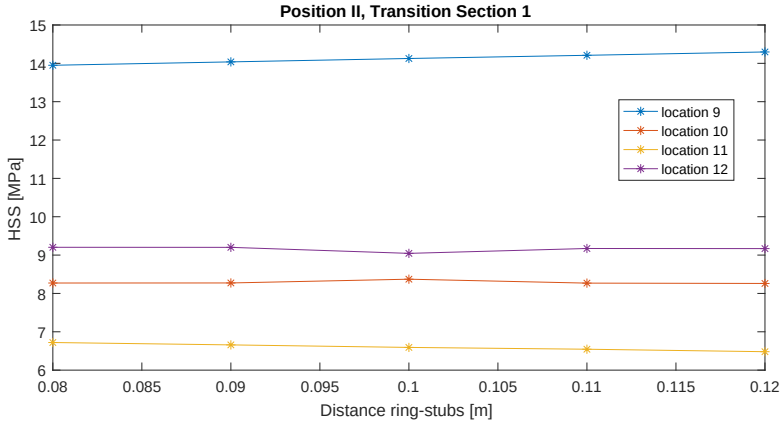

Figure 6.16: HSS versus distance end of stubs and stiffener ring

Cutting MP inside stubs

The HSS inside, location five to eight, is going up will the stress on the outside, location one till four is going down with increasing free height inside the stubs. This is the same for both transition sections

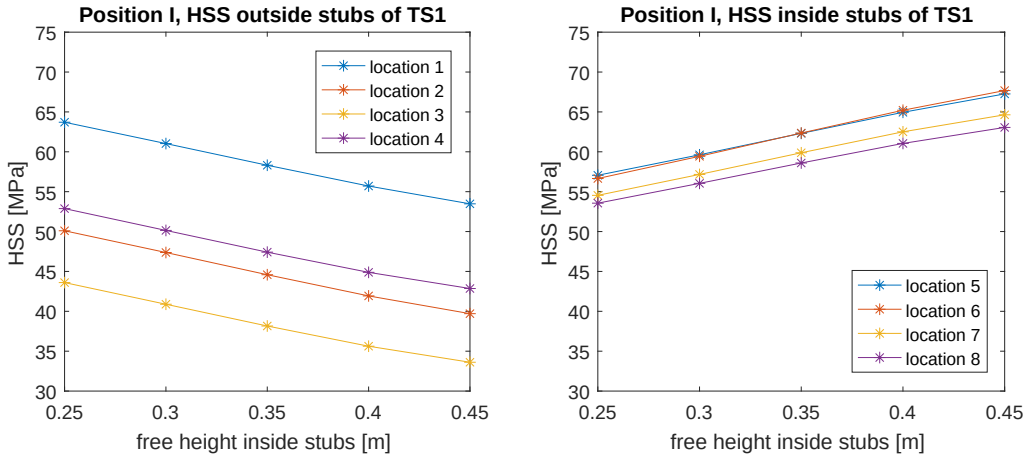

Figure 6.17: HSS versus cutted MP inside stubs TS1

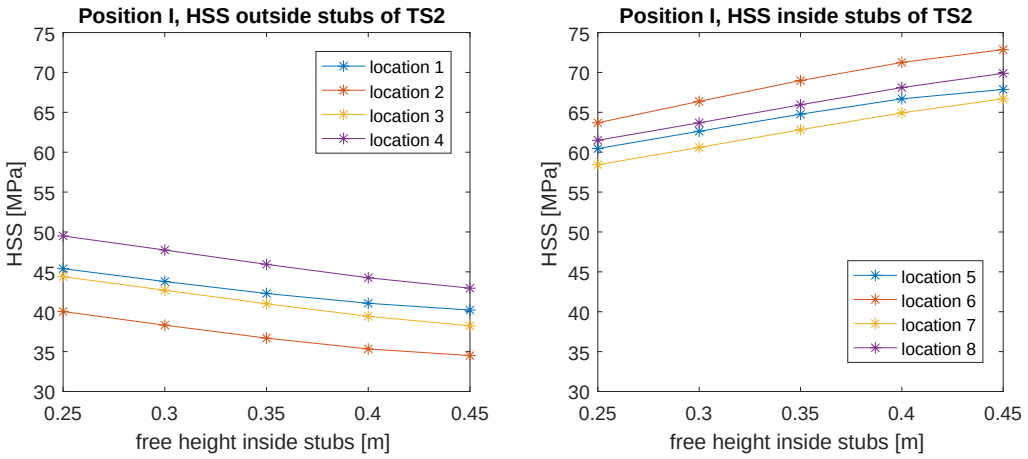

Figure 6.18: HSS versus cutted MP inside stubs TS2

6.7.4 Conclusion

The loading direction influences the HSS. Changing it even forty-five degrees can double the HSS at some details, therefore with the final orientation of the hybrid MP the HSS of the critical details should be as low as possible. In reality the loading comes from several directions during the lifetime, but there is always a direction which occurs the most.

Increasing the width and stiffness of the stiffener ring is reducing the HSS around the stiffener ring. When designing is should be taken into account that the HSS of detail nine is slightly increasing.

Varying the distance a little bit between the stubs and the stiffener ring has no influence on the HSS. Therefore the distance can be optimized for construction purposes so the welds are reachable and easy to produce.

For construction purposes it is useful to have a low as possible HSS on the insight of the stubs because post-treatment of the welds is difficult there. Therefore the cutting of the MP inside the stubs should as low as possible or even no cutting at all. Only if the HSS on the outside becomes critical it could be useful to cut some of the MP section inside the stubs away.

Chapter 7: FLS assessment

In this chapter the methodology for the FLS assessment is discussed together with the final calculation of the fatigue life. The Fatigue Limit state is not really a limit state but in the offshore industry this expressions is generally used to indicate the calculation of the fatigue life. In the fatigue calculation the loading is assumed to be from one direction only. This is conservative because wind and wave loading come from different directions over the lifetime, and mostly wind and wave loading are not fully aligned. But this calculation is a feasibility check of the design therefore only one direction is used to reduce computational time.

7.1 Fatigue calculation

The following flowcharts describes the process to come from the input of the wind load, wave load and concept properties to the final design life of the transition section one and two. This flowchart is based on van der Tempel[26]

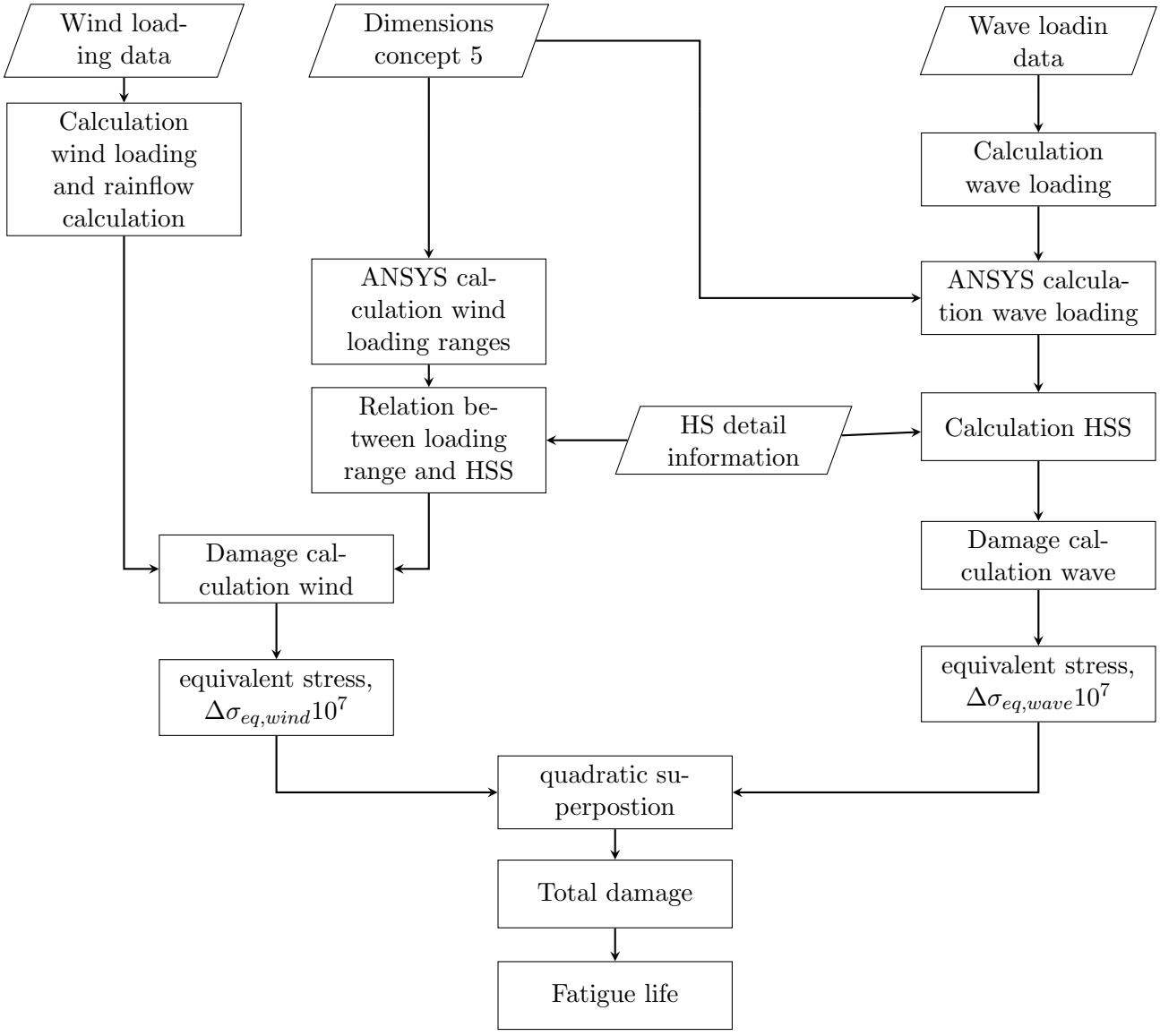

Figure 7.1: Flowchart fatigue calculation

7.2 Damage calculation

The allowable numbers is calculated using the corresponding SN curve discussed further on. The damage is calculated using Palmer-Miner's rule [12], see the following equation.

$$Damage = \sum_{i=1}^{k} \frac{n_i}{N_i} \tag{7.1}$$

with

$Damage$	Total damage	[-]
n_i	Number of occurrences	[-]
N_i	Allowable number of occurrences, based on SN curve	[-]

With this total damage the fatigue life is calculated using the formula below. Normally the design life of an offshore wind turbine is twenty-five years including two years for installation and service this result in a design life for the fatigue assessment of twenty-seven years.

$$Fatiguelife = \frac{Designlife}{DFF \cdot Damage} \tag{7.2}$$

In this equation DFF stand for the Design Fatigue Factor, it is applied to reduce the probability for fatigue failures. This is a safety factor applied to the total damage and depends on the accessibility and location of the detail. A DFF of tree will be used based on DNVGL C203 [12]. This high DFF is applied because, especially transition section one, falls below the still water level and is thus always below sea water, and according to the DNVGL, non-accessible areas, areas not planned to be accessible for inspection and repair during operation should have a DFF of three.

7.3 Damage equivalent stress

For combining the wind and wave damage the damage calculation is reversed to a 1-Hz damage equivalent stress, this is done using the inverse of the SN curve in equation 7.3.

$$\Delta\sigma_{eq} = \frac{10^{\left(\frac{\log a \log N}{m}\right)}}{\left(\frac{t}{t_{ref}}\right)} \tag{7.3}$$

After applying this equation to the total wind and wave damage two decoupled 1-Hz DES remain for the wind and wave loading. These are summed but are combined using quadratic superposition, an extensive on why using quadratic superposition is used for combining wind an wave loading can be found in Kühn[14].

$$DES_{tot} = \sqrt{DES_{wind}^2 + DES_{wave}^2} \tag{7.4}$$

Once the combined DES is calculated the 1-Hz damage is calculated and the damage is calculated.

7.4 SN-Curve detail classification

Each detail has a corresponding SN curve, these curves are selected based on the DNVGL standard [12]. Table 7.1 gives the details with their corresponding category. These details are used together with the corresponding values of the used SN-curve given in table 3.9.

The example from the DNVGL in figure 6.1 provides the applicable SN curves for the details ate position I and II as well. In figure 7.2 the SN curves for the details at position III and IV.

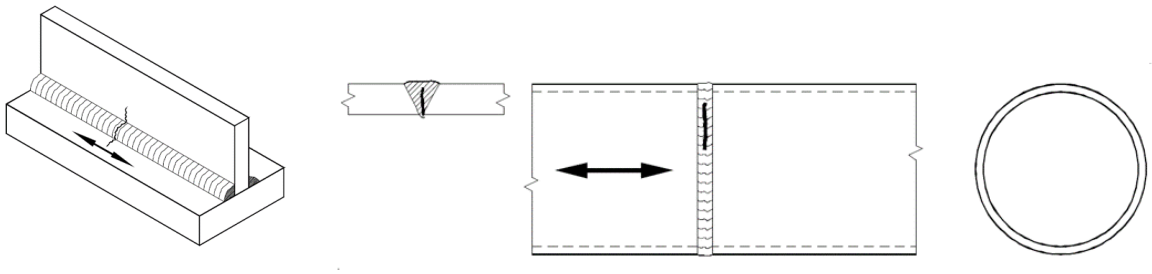

(a) SN curve classification position III

(b) SN curve classification position IV

Figure 7.2: SN curve classification stress direction [12]

Table 7.1: Fatigue positions with corresponding DNVGL detail category

Position	Detail Category	Description
I	D Outside CHS	End of the MP thumb and end of slotted stubs. Stress read out of the outside of the CHS
	D/F3 inside CHS	End of the MP thumb and end of slotted stubs. Stress read out of the inside of the CHS.
II	F3	End of the CHS stubs
III	C1	Connection of the stiffener ring to the MP section.
IV	D Outside CHS	Connection of the stubs to the main CHS profiles.
	F3 inside CHS	Connection of the stubs to the main CHS profiles.

7.5 Relation between wind load and HSS

The damage due to wind loading is calculated using the results of the rain-flow counting discussed in chapter 3. Running an ANSYS simulation for every possible bin would consume to much computational time therefore a different method is used. The wind load is assumed to only act at one location on the offshore wind turbine, this is as a point load at hub height. In the ANSYS model a linear material model is used as well, see chapter 5 ,therefore there is a linear relation between the loading range at hub height and the HSS. In 7.3 this linear relation is plotted for HS location one at both transition sections.

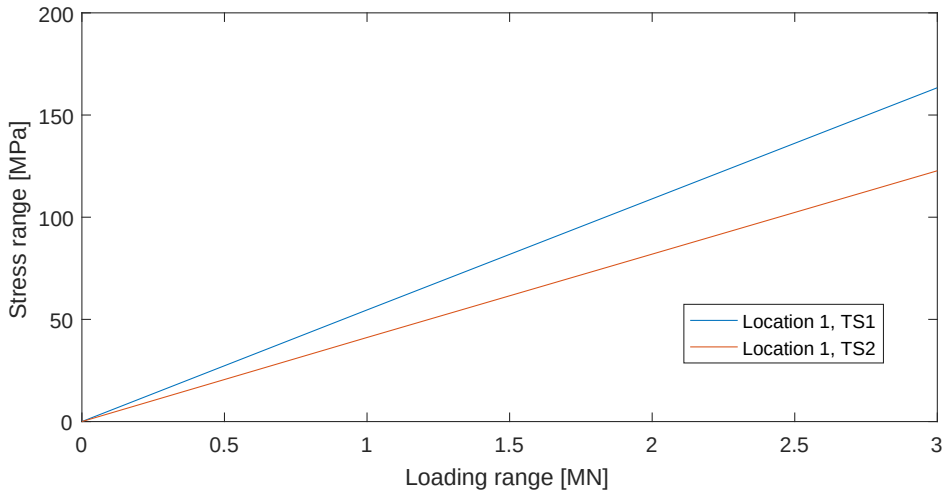

Figure 7.3: Relation between wind loading range at hub height and HSS range

This linear relation is calculated for all the HS locations using several wind loading ranges in the ANSYS model. With this relation and the data from the rainflow counting the wind damage is calculated using Matlab.

7.6 Influence bin numbers rain-flow counting wind loading

Since a rainflow counting algorithm is used for the wind loading not every wind loading range is taken into account. The algorithm averages the loading ranges to a certain number of bins with a corresponding width. This bin width depends on the amount of bins, increasing the number of bins means that there are more smaller bins width larger loading ranges. The question remains then what is the influence of the amount of bins in the rainflow counting on the total damage due to wind.

To analyze the influence of the number of bins on the wind damage. the wind damage is calculated for calculated for several numbers of bins. In figure 7.4 the result for HS location number nine of transition section one and HS location eleven of transition section two. This result shows that the damage is decreasing with increasing bin numbers. This is probably because the bins with the smaller loading ranges have the largest amount of occurrences, see figure 3.10, when there are less bins the average loading range of these bins increases as well as the total amount of occurrences. Therefore the amount of bins in the rain-flow counting algorithm should be above eight to count for effect of bin numbers.

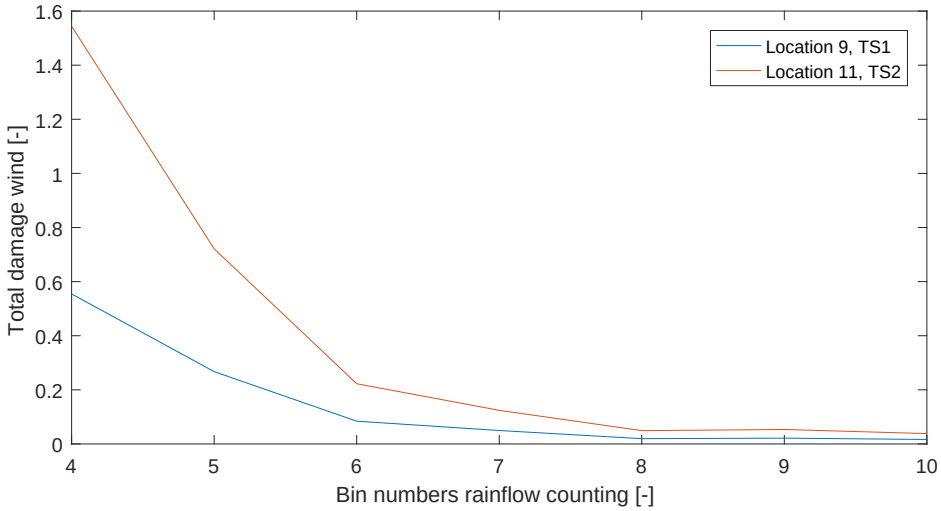

Figure 7.4: Relation between the number of bins and the total wind damage of location 9 and 11

7.7 Damage due to wind loading

In figure 7.5 the damage versus the seastate is plotted for two details. Most of the damage is done in the lower seastates, the possibility of these sea state are higher and therefore the amount of oscillations of this sea states during the life time is larger which result in more damage. The distribution of the sea states are stated in table 3.3.

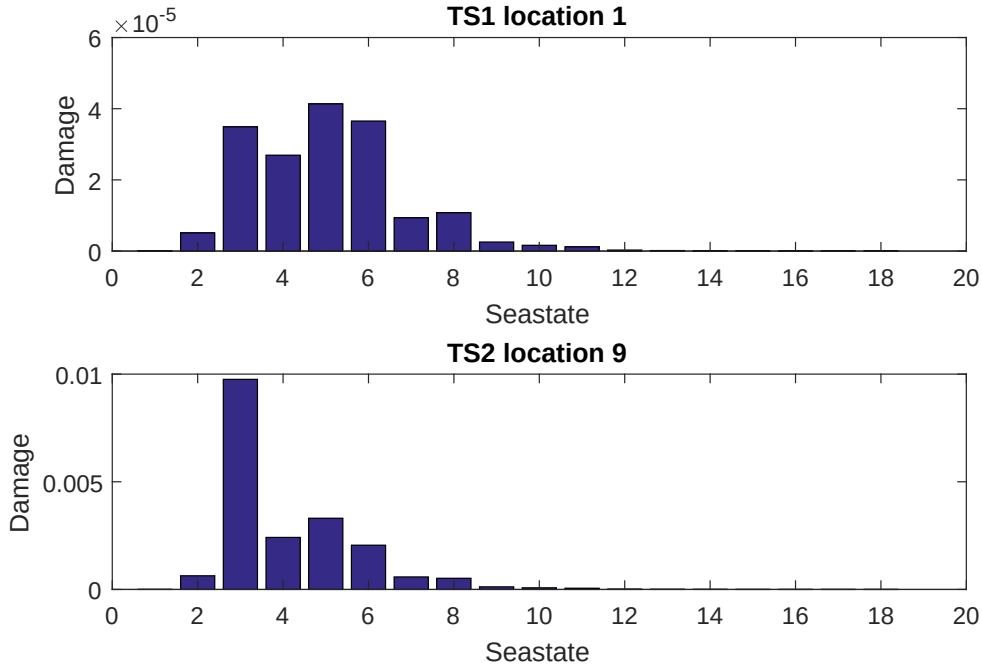

Figure 7.5: Damage wind

Most of the damage due wind is done to location nine of transition section one and location eleven of transition section two. In the figure below the total damage due to wind loading.

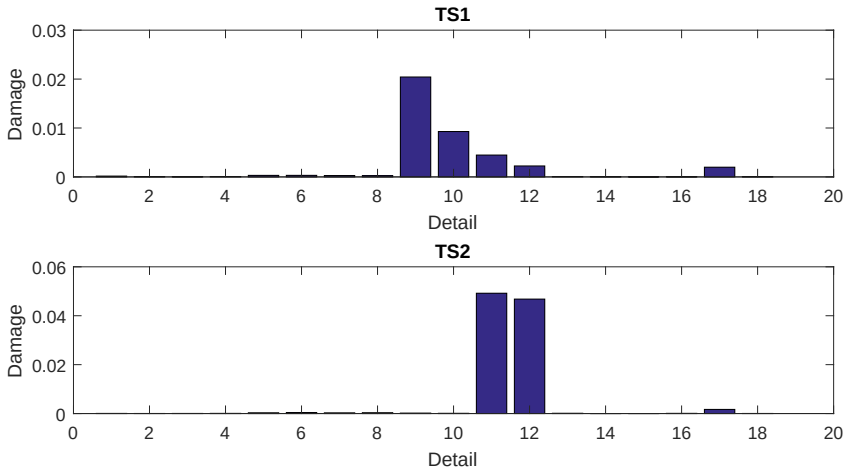

Figure 7.6: Total damage due wind

7.8 Damage due to wave loading

The wave loading is applied and verified like described in chapter 5, only multiplied with a factor two. When a wave passes by the loading is first positive then negative, resulting in a wave loading range which is two times the maximum fatigue wave load. In figure 7.7 and 7.8 the resulting stresses and damage for location seventeen. The increasing wave loading results in higher stress.

The difference in stresses between transition section one and two is clearly seen. Larger stresses occur in transition section one because this is always below the water level in contrast to transition section two which is only below the top of the wave for the larger waves.

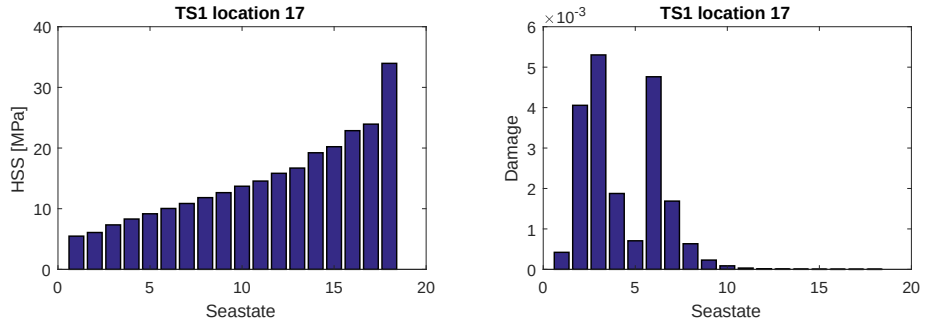

Figure 7.7: Damage wave transition section 1

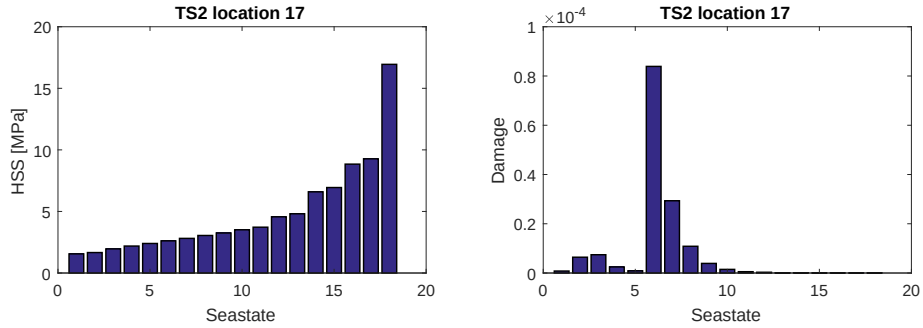

Figure 7.8: Damage wave transition section 2

In figure 7.9 the total damage due to wave loading. Location seventeen is the governing detail for the wave loading.

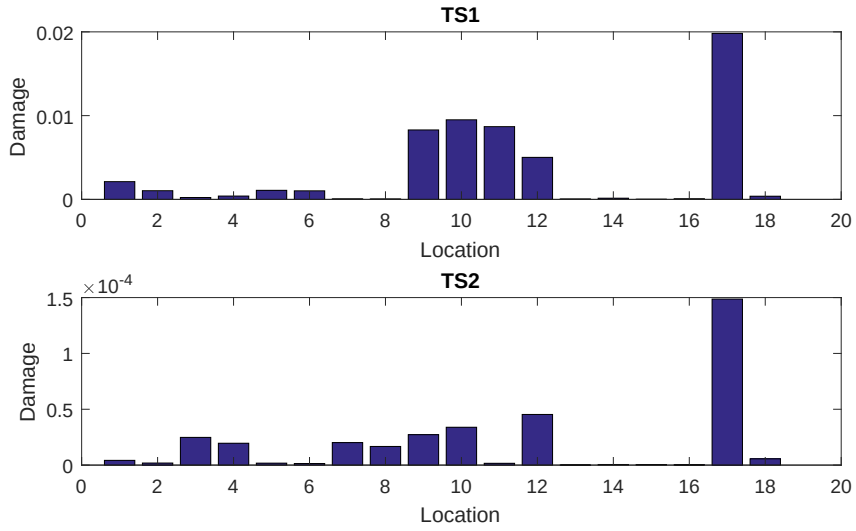

Figure 7.9: Total damage due wave

7.9 Distribution wind and wave

To investigate the influence of the wind and wave loading on the fatigue life the DES of both transition sections are compared with each other. In the figures below all the DES due to wind and wave loading are plotted.

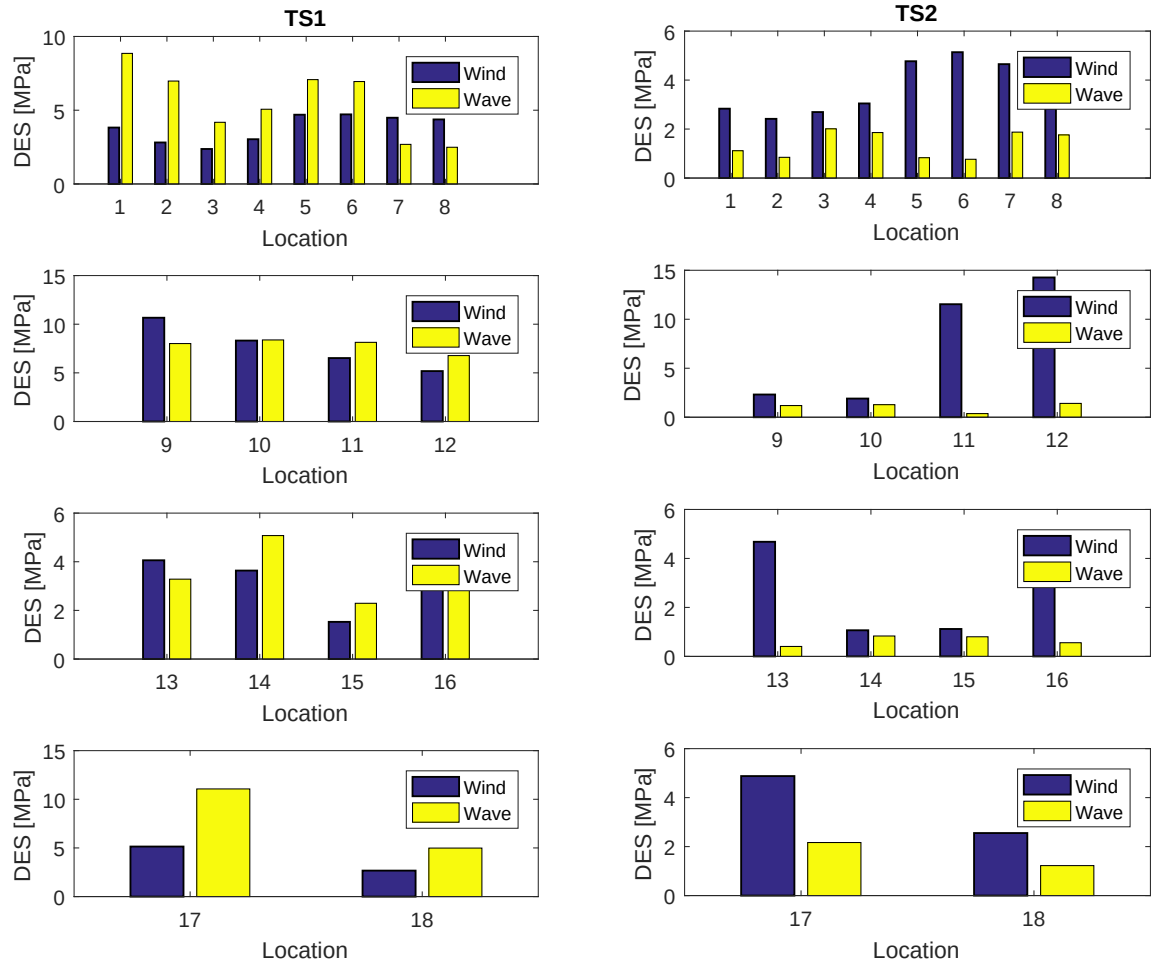

(a) Transition section 1

(b) Transition section 2

Figure 7.10: DES comparison wind and wave loading

The HS DES of he wave loading at transition section two are in all cases smaller than the wind DES. At transition section one this is not the case, the influence of the wave loading on the DES is significantly larger. Here is seen that the influence of the wave loading is smaller at transition section one.

7.10 Fatigue life

In table 7.2 the final governing fatigue life of the critical HS locations. The most critical locations have the lowest fatigue life. These locations are at the end of the stubs at position II, see figure 7.11, where they are circled in red. To demonstrate the difference in fatigue life between steel with and steel without corrosion protection in seawater they are both calculated. In the table SCP stands for Seawater Cathodic Protection and SFC stands for Seawater free corrosion which refers to the SN curve used.

Table 7.2: Fatigue life in seawater

TS [-]	Location [-]	Fatigue life SCP [year]	Fatigue life SFC [year]
1	9	235.2	3.8
1	10	338.9	5.3
1	11	492.3	10.9
1	12	899.3	22.2
1	17	338.7	8.6
2	9	31561.7	156.8
2	10	46150.7	232.1
2	11	182.6	3.5
2	12	189.5	3.6
2	17	4043.7	35.5

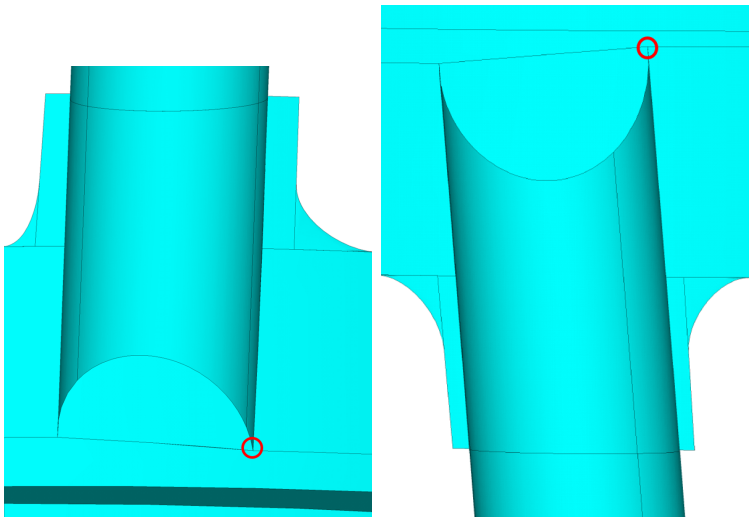

(a) TS1, inside MP (b) TS2, outside MP

Figure 7.11: Critical location of the fatigue life assessment circled in red

The critical location arise not necessarily due to the largest HSS at those HS but also due to the lower classification of the detail, namely F3. which is that low due to difficulty welding at that location and the present of a cover plate.

The conclusion of the fatigue assessment is that hybrid MP has sufficient strength for a design life of twenty-seven years. Table 7.2 shows that there is still a lot of room for optimization in the case of corrosion protection. The fatigue life of the governing HS location is still more than ten times larger than the assumed design life.

Chapter 8: Conclusion

8.1 Conclusion

To come to the final conclusion of this thesis we return to the questions stated in the introduction.

What are possible concept designs of Transition section one and two for the hybrid monopile? In chapter 4 five concepts are designed and elaborated. The concepts are discussed, and the best concept, concept five, is selected. Concluded was that fabrication is leading in selection of the concept design.

Can the concept connection design withstand ULS loading? In chapter 5 the ULS assessment is discussed including the modeling and load implementation into ANSYS. The concept is strong enough to withstand ULS loading, there are some peak stresses but they arise from the finite element size at those locations and can be neglected. In the SLS case the natural frequencies of the hybrid MP are investigated, but those result need to be studied further with inclusion of the soil model for the first two mode shapes. For the third mode shape the natural frequency calculation is reliable but it is questionable if that shape can occur in reality.

How should the detailed connection be modeled so that the HSS method can be used? In chapter 6 and appendix C the modeling, HS selection and the HSS calculation are discussed. Two different methods for including the weld in the model are discussed in appendix C and is concluded to use the model without the shell weld for the fatigue assessment because it has more accurate and consistent results.

What is the fatigue life of the concept connections? In chapter 7 the calculations and results of the fatigue assessment are presented. The conclusion is that the concept connection has a long enough design life to withstand fatigue failure when cathodic protection is used. without cathodic protection the fatigue life is significant smaller and will fail during the estimated lifetime. When using cathodic protection the resistance against fatigue failure is high and therefore there is room for optimization of the connections in the transition sections.

How is the HSS, and thus the fatigue life, influenced by the concept design parameters? In chapter 6 the results are shown and discussed. The parameters studied are the loading direction and three parameters which can change with final the final design or due to optimization for fabrication.

To come back to the main question of the thesis: *"what does the connection between the CHS profiles and the MP section for a hybrid monopile substructure look like which is strong enough to withstand the ULS, SLS and FLS?"* The final concept design looks like described in chapter 4 with a detailed drawing in appendix D. This design is verified on feasibility for the ULS and the FLS cases. The current concept connection design is thus feasible for a lifetime of twenty-seven years with a water depth of 40 meters in the North Sea. It shows enough resistance to the simplified ULS assessment and can withstand failure due to fatigue. There is still room for optimizing the plate thickness of the steel and detailed parameters of the connection design. Thus this concept connection design is a feasible option for the hybrid MP concept without bringing down the gained advantages of the hybrid MP. In the end a toolbox is created, using both the FEA ANSYS and Matlab, for a feasibility check of the hybrid MP connection details regarding ULS and fatigue life.

8.2 Recommendations

For further investigation of the hybrid monopile substructure there are several subjects to focus on.

The wave load interaction between the individual CHS profiles is simplified by a shielding factor. In reality this interaction is more complex, it depends on the distance between the profiles,

the diameter, current velocity and the wave height and length. For some sea-states it may the reduce the wave loading and for other sea-states it can increase the wave loading. Therefore it is recommended to invest the effects of a detailed wave loading model on the hybrid monopile design.

Wind loading for the fatigue assessment is calculated statically. With the actual wave loading there is interaction between the loading and the displacement of the turbine which can result in different HSS ranges than calculated with the static model. This can influence the fatigue life.

Dynamic behavior of the the whole structure, including the foundation. The natural frequencies should be calculated including the stiffness of the soil.

3D modeling of the connection. In this thesis only two models where considered. for a complete understanding of the stress behavior, and a more realistic HSS the connection should be modeled in 3D with solid elements. The difficulty modeling this connection lays in the creating the correct block mesh for the HSS stress methodology.

The influence of the direction of the wind and wave loading should be investigated. In this thesis only one direction for the FLS assessment is used for the sake of computational time, otherwise for each direction a complete new set of calculation should be executed.

At last the additional load load cases should be calculated. Like the critical loading during the handling and installation of the pile, and the impact of an accidental load on the hybrid MP.

Bibliography

[1] Rolf Groen. *Concept feasibility of 10 m Hybrid monopile.* Project/MEMO No. 16023-MEM-RG-002. Enersea, 2016.

[2] Huisman. *Hybrid monopile feasibility study.* Document No. A16-11690-C0-001. Huisman, 2016.

[3] Mary Carol Anderson. *The hybrid monopile.* August 2017.

[4] Marc Seidel. *Substructures for offshore wind turbines: Current trends and developments.* Festchrift Petern Schaumann. Hannover 2014.

[5] Wind Europe, *The offshore wind industry: key trends and statistics 2016.* January 2017.

[6] European Union. 2020 climate & energy package, *https://ec.europa.eu/clima/policies/strategies/2020*

[7] Det Norske Veritas Germanischer Lloyd (DNV GL), *Offshore wind: A manifest for cost reduction.* 2014.

[8] IRENA, *Renewable energy technologies: Cost analysis series, Wind power.* June 2012.

[9] EWEA, *Deep water: The next step for offshore wind energy.* July 2013.

[10] Det Norske Veritas Germanischer Lloyd (DNV GL), *Metallic materials* DNVGL-OS-B101, July 2015

[11] Det Norske Veritas Germanischer Lloyd (DNV GL), *Design of offshore steel structures, general - LRFD method* DNVGL-OS-C101, July 2015.

[12] Det Norske Veritas Germanischer Lloyd (DNV GL), *Fatigue design of offshore steel structures* DNVGL-RP-C203, June 2014.

[13] Det Norske Veritas Germanischer Lloyd (DNV GL), *Design of Offshore Wind Turbine Structures* DNVGL-OS-J101, 2013.

[14] Martin Kühn. *Dynamics and design optimization of offshore wind energy conversion systems,* Delft 2001

[15] ANSYS, Inc. *ANSYS mechanical APDL modeling and meshing guide* 2017.

[16] CIDECT. *Design guid for structural hollow sections in mechanical applications.* Köln 1995.

[17] Twidell, J., Gaudiosi, G. *Offshore wind power. Multi-Science Publishing Company.* 2009

[18] Arany, L., Bhattacharya S., Macdonald, J.H.G., Hogan, S.J. *Closed form solution of Eigen frequency of monopile supported offshore wind turbines in deeper waters incorporating stiffness of substructure and SSI.* Soil Dynamics and Earthquake Engineering 83, 2016

[19] Pierson, W.J. Moskowitz, L. *A proposed spectral form for fully developed wind seas based on similarity theory of S.A. Kitaigorodskij*, Journal of Geophysical Research, 1964

[20] Germanischer Lloyd. *Rules and Guidelines: 4 Non-marine Technology, Regulations for the Certification of Wind Energy Conversion Systems.* 2000

[21] Branlard, E. *Generation of time series from a spectrum.* Technical University Denmark. National Laboratory for Sustainable Energy. February 2010.

[22] Morison, J.R. et al *The fore exerted by surface waves on piles. Petroleum Transactions,* AIME 1950

[23] MacCamy, R. and Fuchs, R. *Wave forces on piles: A diffraction theory.* US Army Corps of Engineering, Beach Erosion Board: Technical Memorandum No. 69. 1954

[24] Deutscher Ausschluss für Stahlbau, *DAST-Richtlinie 012 198* 1980

[25] BSI Standards Publications, *Cranes. General design. General principles and requirements.* EN 13001-3-1:2012+A1:2013 2013

[26] Jan van der Tempel, *Design of Support Structures for Offshore Wind Turbines.* Technical University Delft, 2006

[27] Eurocode 3 part 1-1, *Design of steel structures, General rules and rules for buildings.* 2005

[28] Hobbacher A.F. *Recommendations for fatigue design of welded joints and components, Doc. IIW-1823-07 (ex-doc. XIII-2151r4-07/XV-1254r4-07),* WRC Bulletin 520, Welding Research Council, Inc., New York 2008.

[29] Fistuca B.V. *http://fistuca.com/products/*

Appendices

Appendix A: Concept comparison

The maximum Von Mises stress and the stiffness of the concepts are calculated using FEA in ANSYS APDL. The weight is calculated with a hand calculation.

A.1 Stiffness comparison

Force in x direction of one mega-Newton is applied at 60 meter from the seabed. The displacements are at the same location as the applied load. The results are shown in the table below.

Table A.1: Stiffness in x-direction of the concepts at 60 meter above the seabed

Concept [-]	Displacement [m]	Stiffness [MN/m]
1	0.0285	35.09
2	0.0343	29.17
3	0.0318	31.42
4	0.0314	31.82
5	0.0340	29.45

A.2 Von Mises stress comparison

Maximum Von Mises stress of the concepts is compared. the results of the stiffness calculations are used, only now the maximum Von Mises stress is extracted. These are all some peak stresses at intersections of steel plates, those can be neglected in reality, but still gives a good indication of the maximum stresses to expected in the concept. The results are shown in the table below.

Table A.2: Weight concepts

Concept [-]	max Von Mises [MPa]
1	43.9
2	58.4
3	39.7
4	57.9
5	49.3

A.3 Weight comparison

the total weight of the hybrid MP concepts from the seabed till 60 meter above the seabed is shown in the table below. The weight of the separate parts for each concept are calculated and added together.

Table A.3: Weight concepts

Concept [-]	Weight [mT]
1	649
2	677
3	640
4	607
5	639

A.4 Conclusion

In figure A.1 the normalized results of the concept comparison.

Concept one has the largest stiffness. Concept three the minimum Von Mises stress. Concept four has the lowest mass. Like discussed in chapter 4 the driving parameter of the concept selection is the cost, thus the weight and the fabrication time.

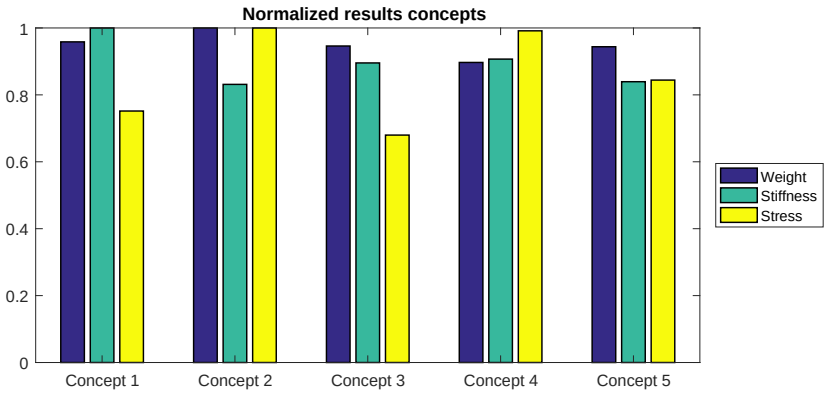

Figure A.1: Normalized results concept comparison

Appendix B: Fabrication

In the following figures a possible fabrication process of the hybrid monopile is described.

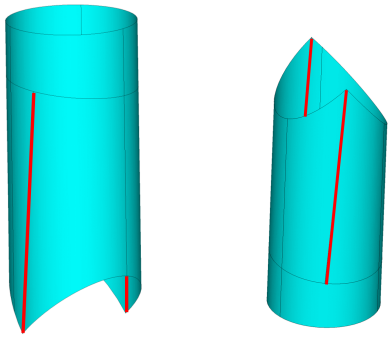

(a) transition section 1

(b) transition section 2

Figure B.1: Stubs of both transition sections with the slotted section in red

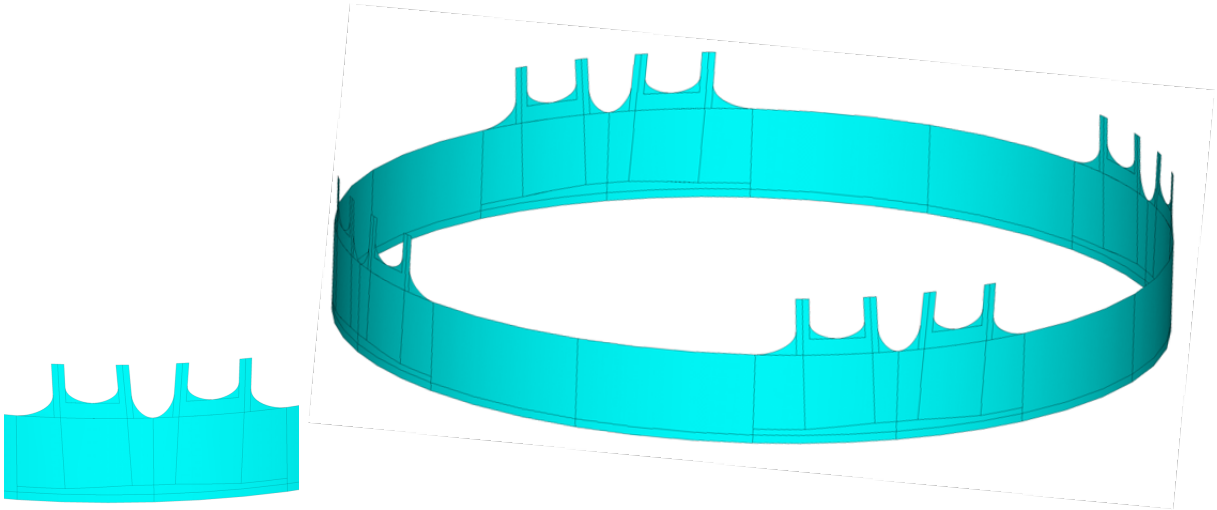

(a) detail

(b) Cutted MP section

Figure B.2: Cutted MP section of TS1 for load introduction en reducing peak stresses

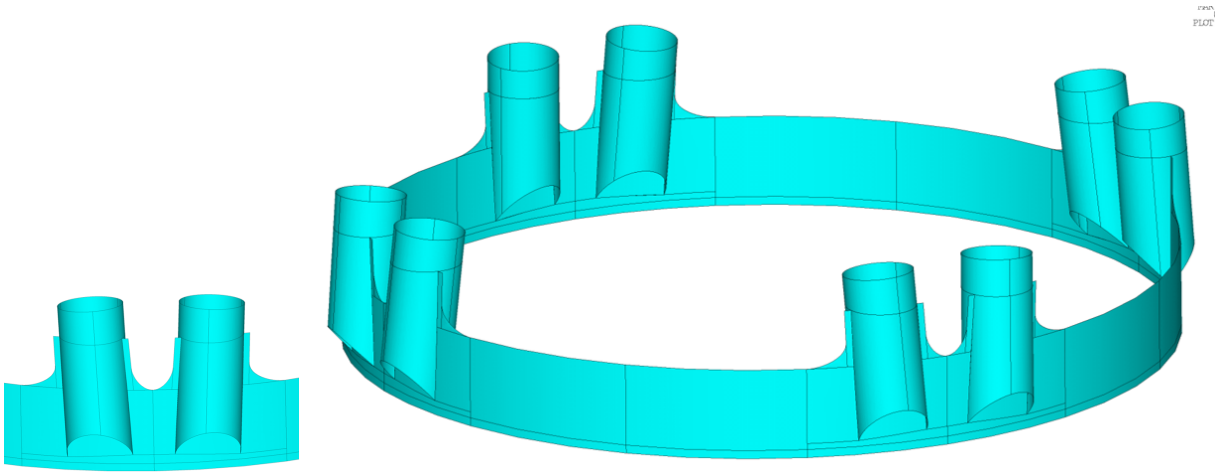

(a) Welded stubs detail (b) Welded stubs

Figure B.3: Welded stubs to the MP section the welds are applied using automatic welding procedure

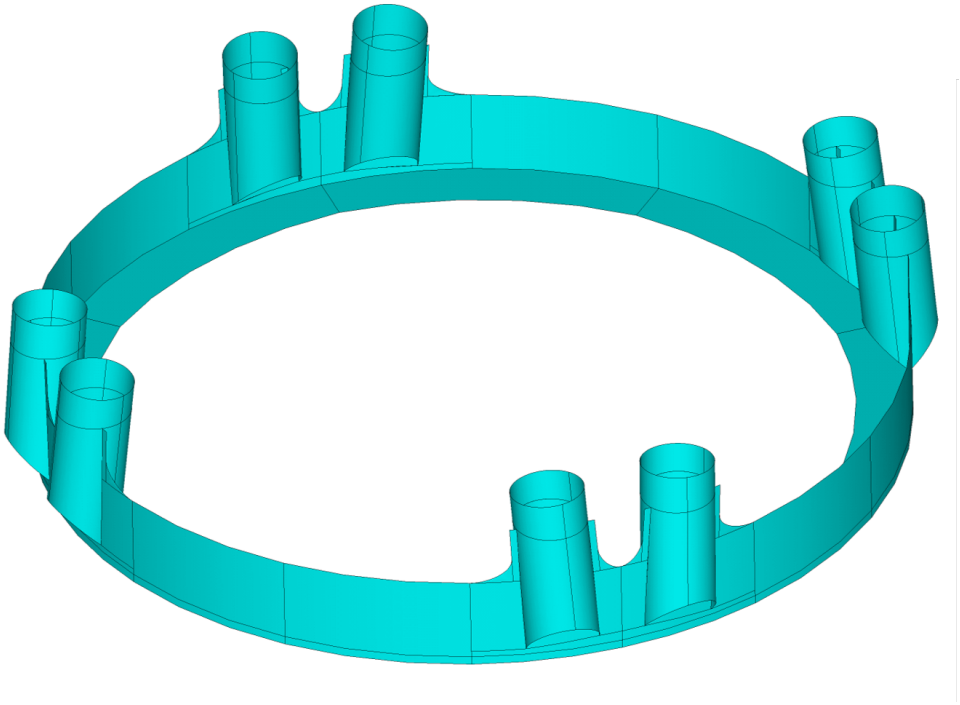

Figure B.4: The stiffener ring is welded on the inside to the MP section below the stubs using an automatic welding procedure

(a) Both TS1 and TS2 are positioned towards eacht other using manipulators

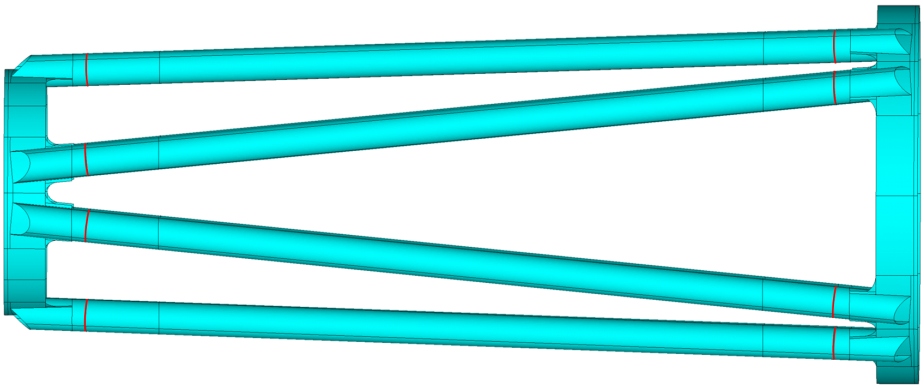

(b) Welded stubs

Figure B.5: The CHS of section 2 are welded between the transition sections, the welds are made from the outside

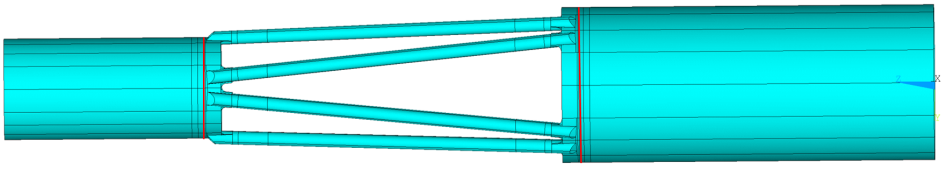

Figure B.6: The section one and three are welded to the rest

Appendix C: Weld modeling in FEA

What is the influence on of increasing the stiffness of the welding on the HSS? To study this a ANSYS model of the connection is made in which the welds are modeled using Shell elements. The two question which have to answerd are:

- What is the difference in HSS between the modeling with and without weld?
- Which model is best to use for further fatigue assessment of the hybrid monopile?

To answer this question the following items will be looked at:

- HSS with and without shell modeling
- Weld size
- Mesh size

The result of the mesh size can also be used to select the mesh size for the final fatigue life calculation.

C.1 ANSYS model without weld

In the ANSYS model without weld itself nothing changes fundamentally. The only thing that has to be taken into account is the distance to the HS. This is done by calculating the distance from the center of the connection to the weld toe, which is half the thickness of the plate plus the with of the weld. visualized in the figure below.

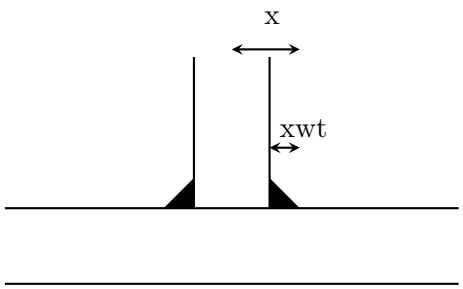

(a) Schematic weld model

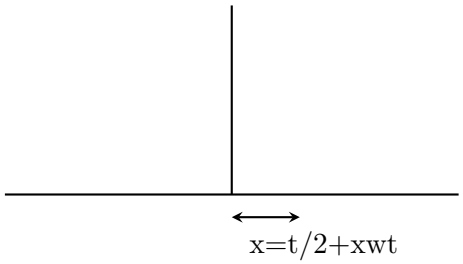

(b) Shell finite element model

C.2 ANSYS model with weld

To model the weld with shell element a new element has to be created with the same thickness as the weld throat size. With the information about the weld throat size and the thickness of the two adjacent steel plates the offset from the center connection can be calculated. With this offset distance a new line is created on the existing areas and the shell weld element can be created, in figure C.2 this is visualized. The throat size of the weld is initially set to thirty millimeter. The

issue with this kind of shell weld modeling is that the weld toe is after the weld node, and with the HSS method this can influence the final result.

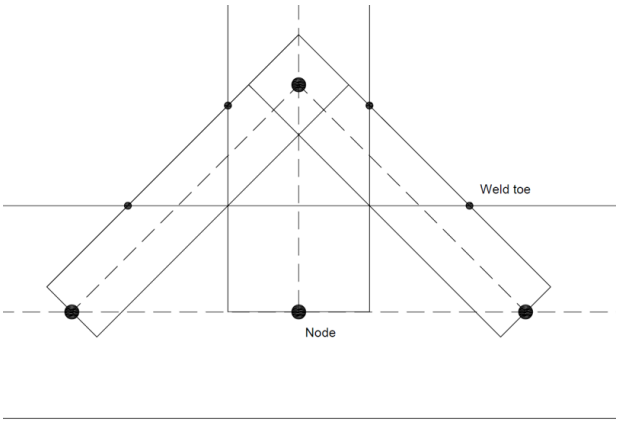

Figure C.2: Shell welds sketch

The shell element weld will look in ANSYS like shown in figure C.2. In these figures the shell elements are plotted with there according element thickness.

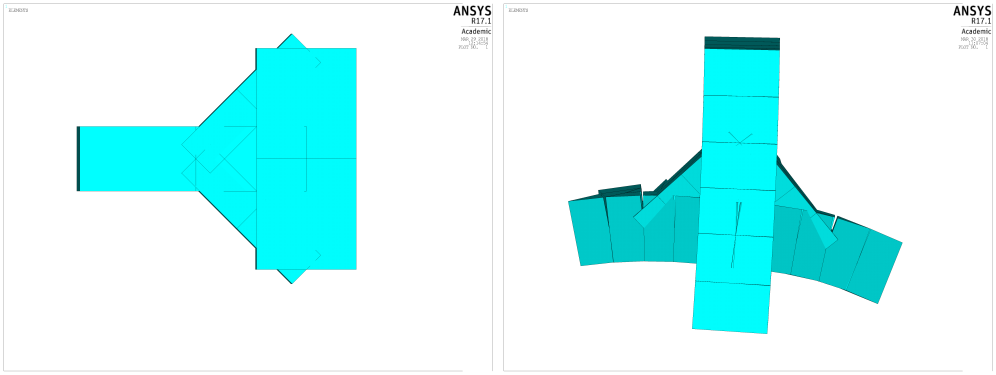

(a) Shell welds stiffener ring

(b) Shell weld stubs

C.3 Results

C.3.1 Model comparison

In the figure below the stress range is plotted versus the distance from the weld toe for detail five and nine of transition section one. In both cases the influence of connection node for the weld is clearly visible by the large discontinuity in the stress. The remarkable effect of this discontinuity is that for detail nine the HSS is larger than compared to the model without weld despite having a lower final peak stress.

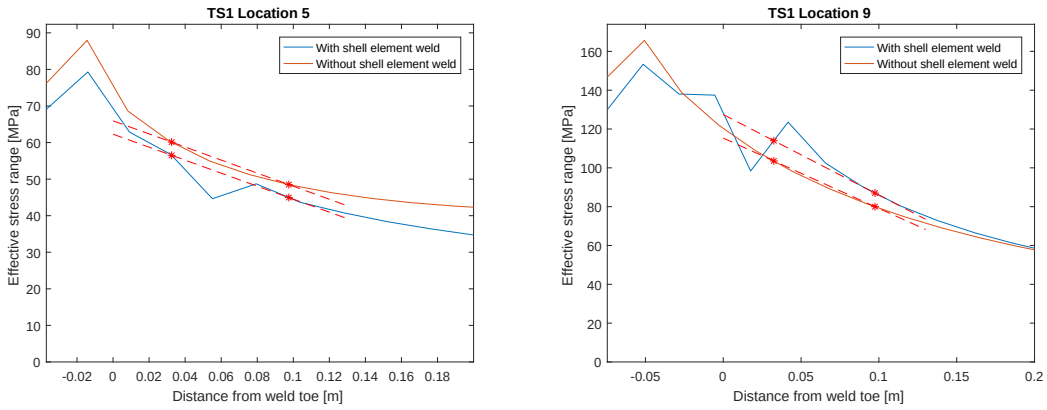

(a) (b)

Figure C.4: With and without shell welds

C.3.2 Weld size

Three weld throat sizes are calculated with the shell weld model: twenty-five, thirty and thirty-five millimeter. Below the results are plotted for detail five and nine of transition section one. The influence of the weld node is again clearly visible. The influence of the weld size is minimal and the peak stresses are almost the same.

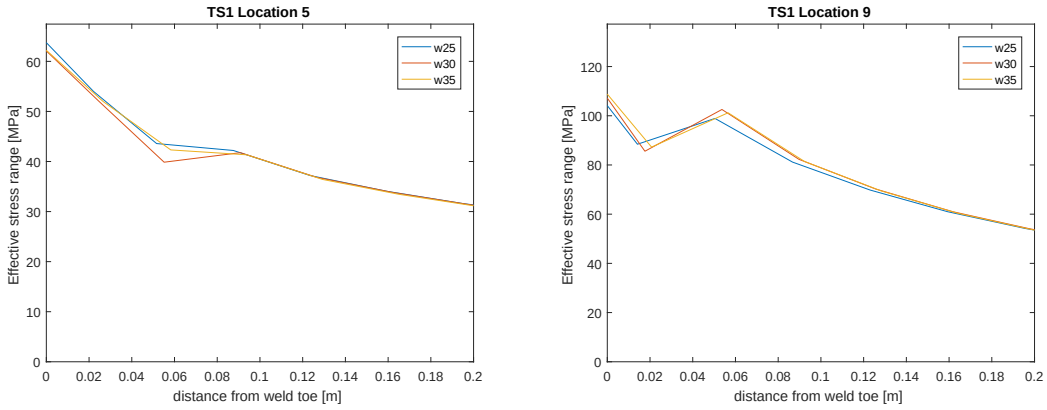

(a) detail 5 (b) detail 9

Figure C.5: Influence weld size

C.3.3 Mesh size

For both models the influence of the mesh size is calculated in the figures C.6 and C.7 the results.

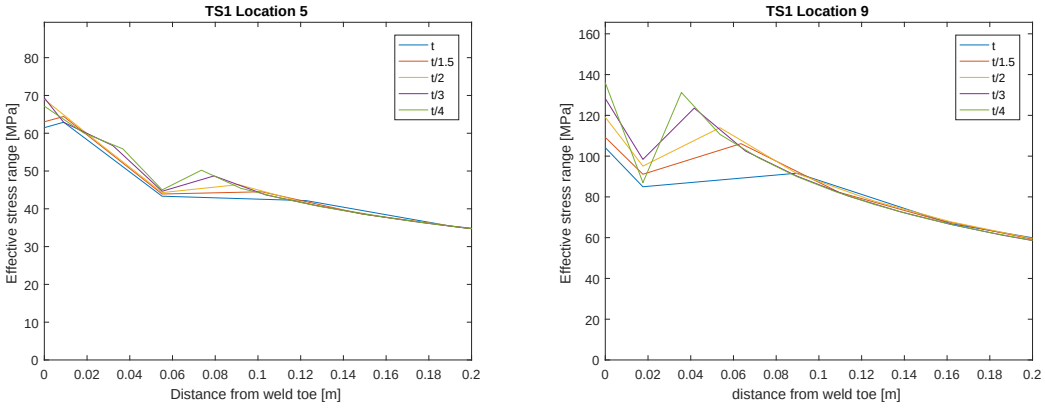

(a) detail 5 (b) detail 9

Figure C.6: influence mesh size with shell weld

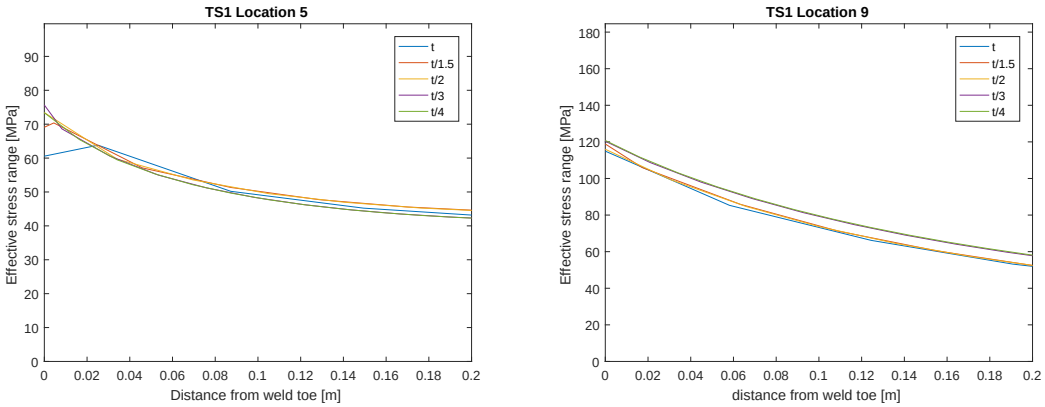

(a) detail 5 (b) detail 9

Figure C.7: influence mesh size without shell weld

C.4 Conclusion

Influence of the weld node after the HSS is clearly visible with the shell weld model. The problem that weld nodes are before the HS and therefor create an extra peak which influence the HSS. In figure C.4 it is seen that the peak stress at the plate connection is lower with the weld model, but due to the extra fluctuation around the weld node the HSS is larger than the model without the shell weld. This larger HSS is not realistic, some reference, therefore in the final fatigue assessment the model without the shell welds is used. For the final fatigue assessment a mesh size of t/2 will be used. In figure C.7 it is shown that the HSS does not change significantly with a smaller mesh size.

Appendix D: Detailed drawing connection

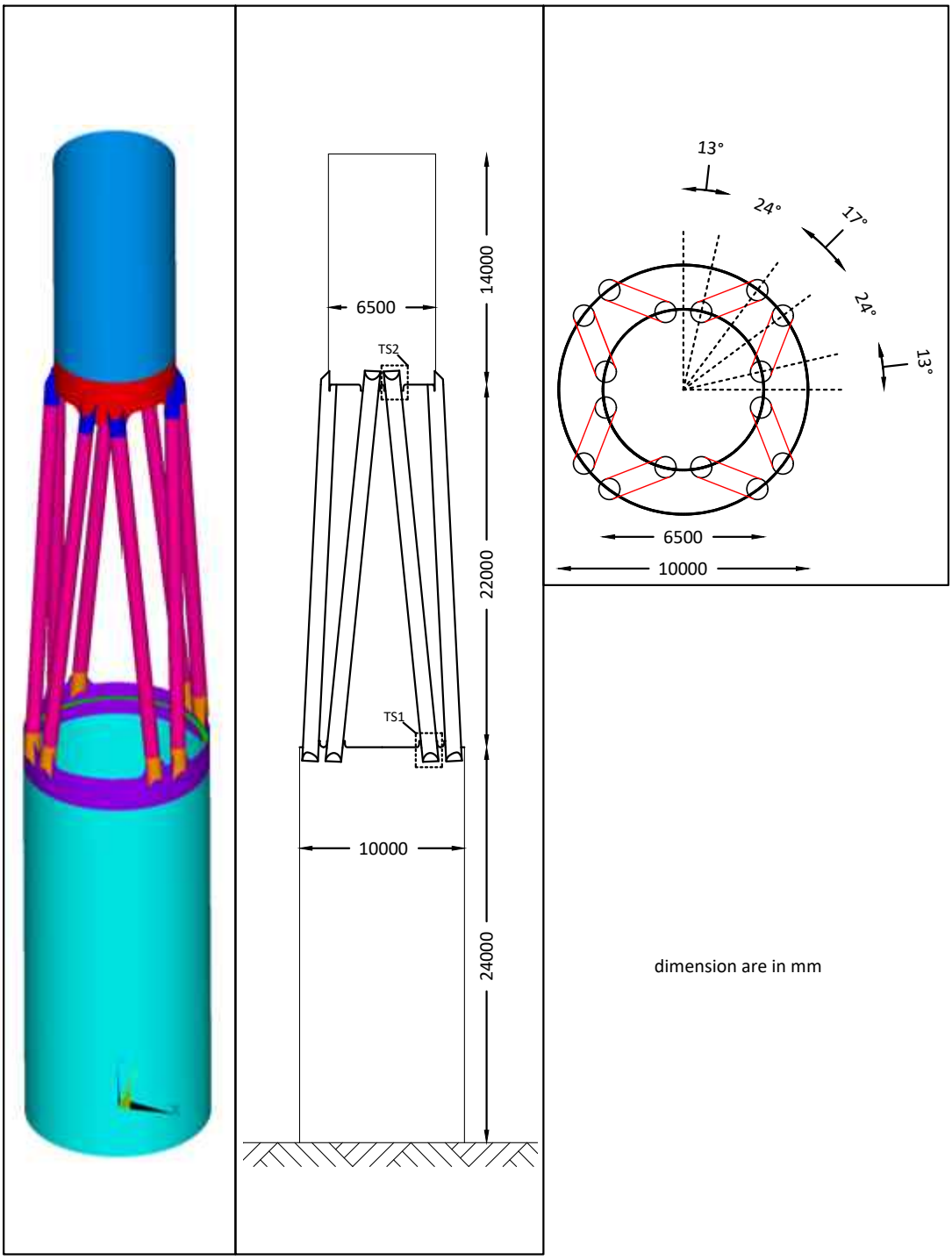

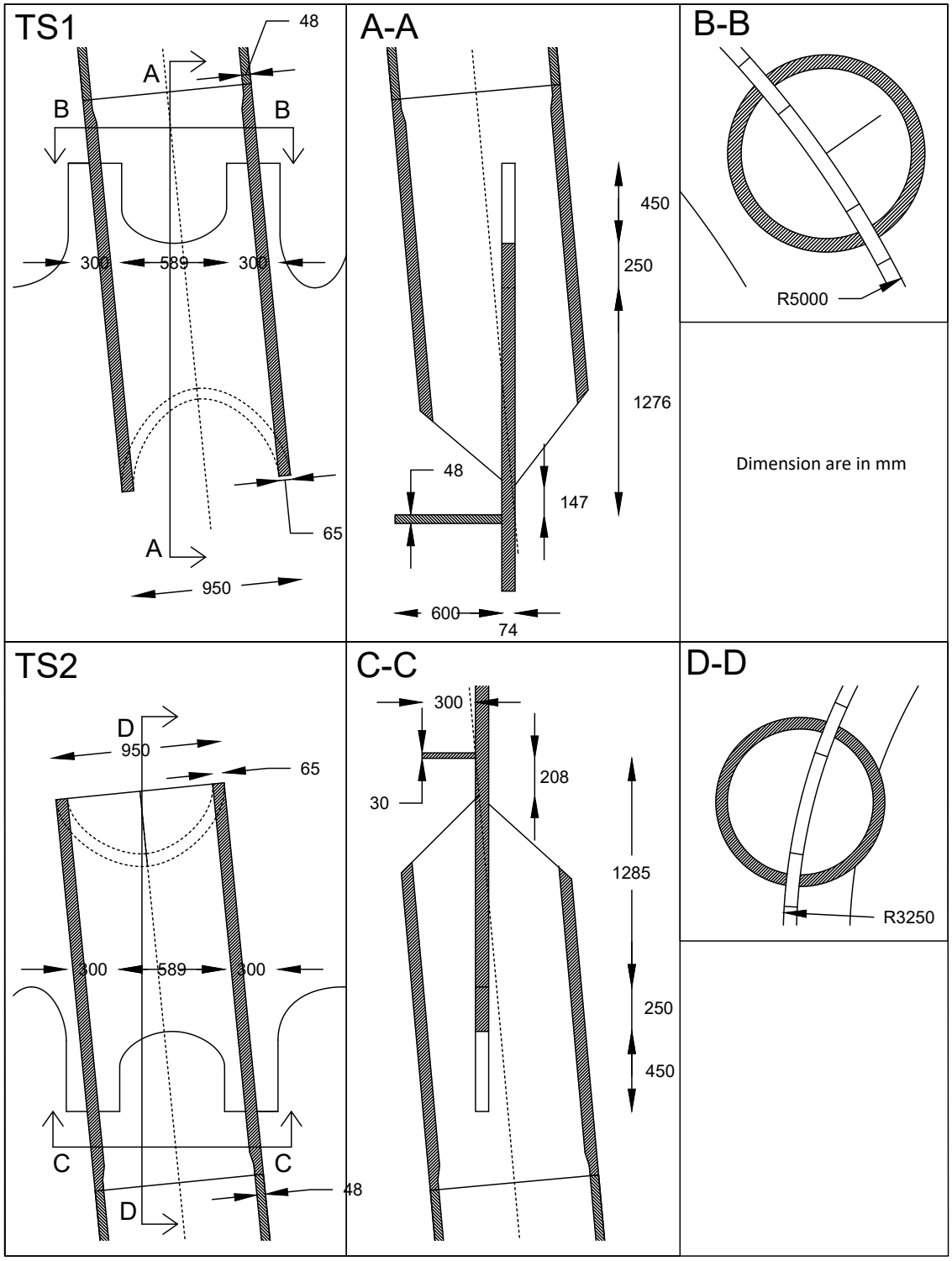
TS1
48
A
B
B
300
589
300
65
A
950
A-A
450
250
1276
48
147
600
74
B-B
R5000
Dimension are in mm
TS2
D
950
65
300
589
300
C
C
48
D
C-C
300
208
30
1285
250
450
D-D
R3250